Study on the calcium carbonate precipitation and anion diffusion in compacted bentonite for performance assessment of engineered barrier in the geological disposal

by

Jaka Rachmadetin

A dissertation submitted in partial fulfilment of the requirements for the degree of Doctor of Philosophy in Engineering

Division of Energy and Environmental Systems

Graduate School of Engineering

Hokkaido University

Sapporo, Japan

2019

Abstract

Compacted bentonite is expected to be used as one of engineered barriers in geological disposal of high-level radioactive waste. For the safety assessment of the geological disposal, it is important to understand fate and transport of radionuclides in compacted bentonite in order to predict long term migration behavior of radionuclides at the radioactive waste repository. Although extensive studies have been conducted to improve the knowledge regarding the performance of bentonite as the engineered barrier, the widely accepted model which can predict long-term transport of radionuclides in bentonite has not been established due to its complexities. Therefore, this thesis intends to improve our understanding in this context in terms of three factors which affects the fate and transport of radionuclides in bentonite; the porewater chemistry, the precipitation processes, and the diffusion mechanism of ions in bentonite.

The porewater chemistry of bentonite was studied from the view of activity coefficient of dissolved ions in the porewater. In this study, the mean activity coefficient of Ca^{2+} and CO_3^{2-} ions was obtained from the estimated concentrations of each ion in the porewater in which $CaCO_3$ precipitation occurred. The $CaCO_3$ precipitation was enhanced by electromigration method in which Ca^{2+} and HCO_3^-/CO_3^{2-} ions were introduced from the opposite sides of the compacted Na-bentonite under electrical potential gradient. A sequential extraction method using radioisotopes as tracer and saturated $CaCO_3$ solution as extractant was developed to distinctly determine the concentrations in the porewater as free ions and in solid phase in bentonite. The results show that the exchangeable Na^+ ions were progressively replaced by the incoming Ca^{2+} ions. The compacted bentonite sample can be divided into three zones: Ca-bentonite, a

mixture of Ca-/Na- bentonite, and Na-bentonite zones, depending on the degree of replacement of the exchangeable Na^+ by Ca^{2+} ions. Precipitates of $CaCO_3$ were observed both in Ca-bentonite and Ca/Na-bentonite zones. The experimentally determined mean activity coefficients were at least smaller by a factor of three compared to the theoretical approximation calculated using PHREEQC code assuming dilute-solution conditions with no electrostatic interactions between ions and bentonite surface.

The precipitation processes were studied for $CaCO_3$ which was enhanced to form in bentonite by the same electromigration method at different experimental periods of time. Electromigration experiments with thin layer source were also carried out to obtain the electromigration parameters of Ca^{2+} and HCO_3^-/CO_3^{2-} in compacted bentonite. The results showed that the reaction front of $CaCO_3$ precipitation under the experimental conditions moved from the anode side towards the cathode side. This advancing reaction front can be attributed to the faster mobility of Ca^{2+} compared to HCO_3^-/CO_3^{2-} ions. The $CaCO_3$ precipitates which were formed during the electromigration were found to have negligible effect on the transport of Ca^{2+} and HCO_3^-/CO_3^{2-} ions.

The anions diffusion mechanism was studied for $^{35}SO_4^{2-}$ ions in Na-bentonite at different dry densities and NaCl concentrations using back-to-back diffusion method. The results showed that the E_a values were smaller than that in free water in bentonite at dry density of 1 kg/dm^3 with NaCl concentration up to 0.3 M. When the NaCl concentrations increased above 0.3 M, the E_a value increased and be equal to that in free water. This indicate that diffusion in porewater is predominant for SO_4^{2-} ions in compacted bentonite at dry density of 1 kg/dm^3 with NaCl concentration higher than 0.3 M. However, lower E_a values than that in free water at NaCl concentration lower than 0.3 M cannot be

explained by the diffusion in porewater, suggesting the presence of different diffusion path than porewater for anions in compacted bentonite.

The results of this study have important sequences in defining solubility, chemical reaction and mass transport in bentonite which are important for safety assessment of disposal of high-level radioactive waste.

Table of Contents

Table of Figures

1. Introduction

1.1. Generation and classification of radioactive waste

Nuclear energy is an important source for present and future energy supply, even after re-evaluation of national nuclear energy policies throughout the world after the Fukushima nuclear accident. While some countries, such as Germany, Belgium and Switzerland, are going to phase out nuclear power generation, other countries, such as UAE, Belarus, Turkey, and Bangladesh have started constructing their first nuclear power plants (NPP). In 2017, the global share of nuclear in total electricity generation was approximately 10.4%. The nuclear share in Japan is 6.2% due to late re-operation of NPPs, but it is projected to be increased to about 20% by 2030 [1].

One of the major issues in the utilization of nuclear for power generation is the generation of radioactive waste [2]. NPPs are not the only source of radioactive waste. Radioactive waste is also generated from other applications, such as medical, research, agricultural and industrial. In principle, this radioactive waste must be managed in such a way as to ensure no burdens on future generations [3]. However, there are various radioactive waste with wide variety of physical, chemical, and radioactive properties. Therefore, the proper classification of radioactive waste is necessary to establish a safe and structured radioactive waste management [4,5].

International Atomic Energy Agency (IAEA) has provided general classification scheme in which radioactive waste is classified into six categories: exempt waste, very short-lived waste (VSLW), very low-level waste (VLLW), low-level waste (LLW), intermediate-level waste (ILW), and high-level waste (HLW) [4,5]. The classification of radioactive waste, however, varies among countries. For example, the types of HLW

depend on national policies on the nuclear fuel cycle. In countries which adopt a once-through fuel cycle policy, the HLW is the spent nuclear fuel (SNF) generated from nuclear reactor operation. In contrast, the SNF is not considered as a waste in countries which adopt a closed cycle, most notably Japan, France, Russia, and China. The SNF in these countries is reprocessed to retrieve the fissile products, resulting in vitrified waste as HLW [2].

The classification of radioactive waste in Japan based on the Reactor Regulation Law is shown in Table 1-1. Radioactive waste is classified into two categories: LLW and HLW. The LLW is further classified into six sub-categories based on the origin of the waste, which may limit kinds of radionuclides, and their levels of radioactivity in the waste. The LLW generated from NPP is classified into three sub-categories: very low-level radioactive waste, relatively lower radioactive waste, and relatively higher radioactive waste. The other sub-categories of LLW are: waste containing transuranic (TRU) nuclides, uranium waste, and radioactive waste from medical and research facilities [6]. In addition to this classification, the waste generated from nuclear facilities which has radioactivity below the clearance level is not considered as radioactive waste and is manage as general waste. The method to determine this clearance level has been approved in 2011 [7].

As of 2013, the worldwide inventory of solid radioactive waste which has been disposed of, and in storage is approximately 21.4 and 6.3 million m^3, respectively. ILW and HLW contribute only small portions of this volume, which are 567,000 and 22,000 m^3, respectively. The majority of ILW and all HLW are currently in storage waiting for disposal facilities. In addition, there are an estimated 370,000 tHM of the SNF discharged from NPP and 3,193 tHM of the SNF from research and other reactors in the world. Note

that the characteristics of the SNF from NPP and research reactor may differ because of the difference in the fuel quantities and the enrichment of uranium [8]. In Japan, there are 2,485 containers of vitrified HLW which have been processed, about 88% of which are stored in the HLW interim storage facilities at the Japan Nuclear Fuel Limited (JNFL) and the remaining are at Japan Nuclear Energy Agency (JAEA). Additionally, there are SNF temporary stored in the NPPs throughout the country. The total amount of vitrified waste and SNF is approximately equivalent to 25,000 containers [9].

The classified radioactive waste will be disposed of in the way which is suitable for each of radioactive waste classes. In Japan, basically radioactive waste disposal facilities are classified into four types based on their burial concepts. Near surface disposal, the unlined trench type, is used to dispose of very low-level radioactive waste. Shallow depth disposal, constructed in 4 to 9 m depth underground, is used to dispose of relatively lower activity LLW. Intermediate-depth disposal, constructed in 50-100 m underground, will be used to dispose of relatively higher low-level radioactive waste. Geological disposal, constructed at deeper than 300 m underground, is to be used to dispose of TRU waste and HLW [10].

Table 1-1. Classification of radioactive waste in Japan.

Category		Origin of waste	Example
1. High-level radioactive waste		Reprocessing facilities	Vitrified waste
2. Low-level radioactive waste	2.1. Relatively Higher Radioactive Waste	Power reactors	Spent control rods, reactor core internals, channel boxes
	2.2. Relatively Lower Radioactive Waste		Spent ion exchange resin, filters, incineration ash
	2.3. Very Low-Level Radioactive Waste		Concrete, metals
	2.4. Waste Containing Transuranic Nuclides (TRU)	Reprocessing Facilities and MOX Fuel Manufacturing Facilities	Parts of fuel elements, liquid waste, filters
	2.5. Uranium Waste	Enrichment and Fuel Manufacturing Facilities	Consumables, sludge
	2.6. Radioisotope and Waste from Research Facilities, etc	Medical or research institutions	Radioisotope waste from medical and other institutions, laboratory waste from test reactors and facilities using nuclear fuel

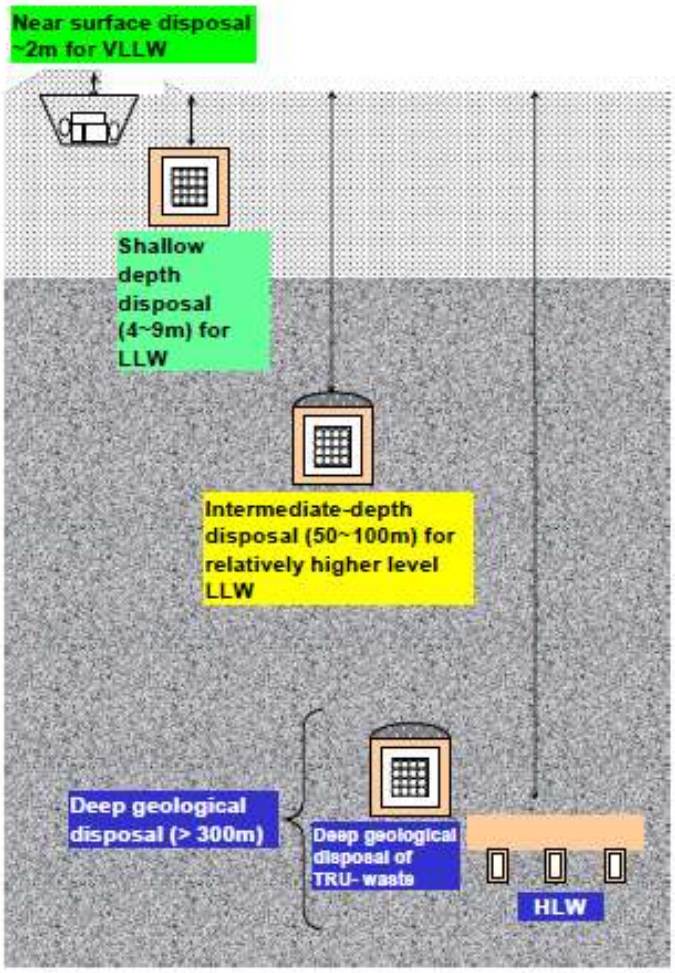

Figure 1-1. Illustration of disposal types in Japan [10,11].

1.2. Bentonite in geological disposal of high-level waste

Despite the relatively small volume, SNF and HLW typically contain over 95% of the total radioactivity in the radioactive waste generated from NPP operation [8,12]. The inventory of radionuclides in the SNF depends on the nuclear fuel type, burn up and the time after used in the reactor. The SNF primarily composed of UO_2, which account for about 96% of the SNF. The remaining balance consists of fission products (for example ^{131}I, ^{137}Cs and ^{90}Sr), transuranium elements (for example ^{239}Pu, ^{237}Np, and ^{241}Am), and activation products (for example ^{60}Co and ^{63}Ni) [13–15]. In countries with

once-through fuel cycle policy, this SNF is considered as HLW and is destined for final disposal. However, the thermal output from radioactive decay in SNF is very high after discharge from reactors. The SNF must be stored in water pools on reactor sites prior to disposal. In some cases, temporary storage in dry cask after the SNF is cooled in the water pool is necessary because no repository facilities are available to dispose of the SNF [15,16].

In countries adopting closed fuel cycle policy, chemical process is applied to recover the ^{235}U and ^{239}Pu from SNF. The recovered materials can be used as a mixed-oxide fuel. This process generates high-level liquid waste, which contains most of the fission products that were in the SNF, unrecovered uranium, and TRU nuclides. Vitrification is adopted by many countries which have SNF reprocessing program as the best method for treatment and immobilization of the high-level liquid waste because of the durability of glass and its ability to provide host-phase containment for wide range of radionuclides [17,18]. In this method, the high-level liquid waste is mixed with glass materials and melted together into the molten glass phase. Borosilicate glass has been universally selected except for alumino-phosphate glass used in Russia. The molten glass is then placed in a container typically made of steel, copper, or corrosion resistant alloys, and solidified [19]. The container used in Japan is made of stainless steel with the dimensions of 1340 mm in height, 430 mm in outer diameter, and 6 mm in wall thickness.

The initial inventory of radionuclides in the vitrified waste depends on the inventory of radionuclides in the SNF subjected to reprocessing and the reprocessing method. This inventory changes over time due to radioactive decay. Figure 1-2 shows an example of inventory of radionuclides in typical vitrified waste from reprocessing. Initially, the total radioactivity of HLW is dominated by radionuclides with relatively

short half-lives, such as ^{137}Cs and ^{90}Sr. After a few hundreds of years, the radioactivity is dominated by radionuclides with long-half-lives [20]. Although the radioactivity of vitrified waste is smaller than SNF, it still requires several hundred thousand years to reach the level of radioactivity of natural uranium [21]. Therefore, disposal facility of HLW must be ensured to contain radionuclides for this long period of time.

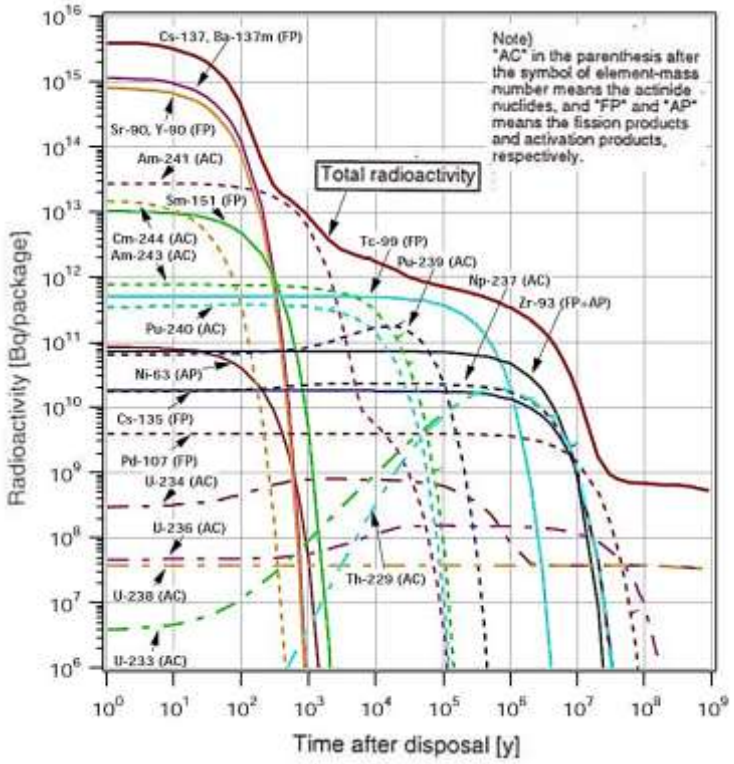

Figure 1-2 Inventory of radionuclides in a typical vitrified waste. The waste is assumed to be generated from reprocessing of spent fuel at a 45000 MWd/ton burn-up, 38 MW/MTU specific output, 1184.2 days operation time in a pressurized water reactor, and 4 years cooling period. Each canister loading is 0.8 MTU/canister. The ratios of U and Pu transferred from the spent fuel to the vitrified waste trough reprocessing are 0.442 and 0.548%, respectively. The cooling period after reprocessing is 50 years [20].

Geological disposal has been a preferred method for HLW since it is expected to have long-term safety for waste isolation [12,22]. A concept of multiple safety functions is required to isolate the radioactive waste from geosphere for long period of time [23]. A multi barrier approach with a series of engineered barriers and natural barriers is adopted. The engineered barriers consist of waste form, waste package, and backfill materials, whereas natural barriers are the rocks surrounding the repository [24]. The potential host rock that widely recognized for geological disposal are granite [25], clay [26], and rock salt [27]. The basic concept of geological disposal in Japan is depicted in Figure 1-3. As previously mentioned, the waste form for HLW is borosilicate glass while the container is made of stainless steel. This waste is placed inside a thick metal container called "overpack". The HLW in the overpack is then surrounded by compacted bentonite as buffer material. The repository will be located in stable formation of granite or sedimentary rock at 300 m or deeper from the surface [10,28].

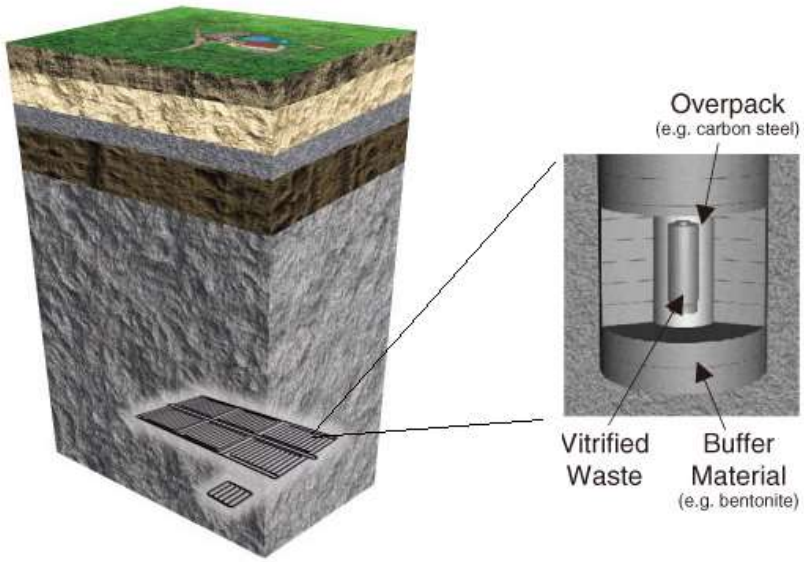

Figure 1-3. The concept of geological disposal of high-level waste in Japan [28].

Compacted bentonite as a engineered barrier is considered not only in Japan, but also in many other countries [20,29,30] due to its characteristics, such as high sorption capacity for radionuclides, high swelling ability, and good durability [26,31–35]. Compacted bentonite barriers may also protect the integrity of HLW canisters by retarding the corrosion rate [36, 37] and by inhibiting growth of bacteria which can induce corrosion [38].

In the safety assessment of geological disposal, the performance analyses of each of those barriers is necessary. The migration of radionuclides in geological disposal can be affected by various processes, such as radioactive decay and growth, glass dissolution from the vitrified waste surface, diffusion in the buffer materials, and release to the host rock [20,39]. Figure 1-4 shows the possible processes in each of barriers for migration of radionuclides from HLW to geosphere in a geological disposal repository. In the scenarios of glass dissolution of the vitrified waste after the failure of the container, radionuclides will be released to compacted bentonite. Therefore, the ability of compacted bentonite to retard the migration of the radionuclides from the HLW to the host rock is critical in the long-term performance of geological disposal.

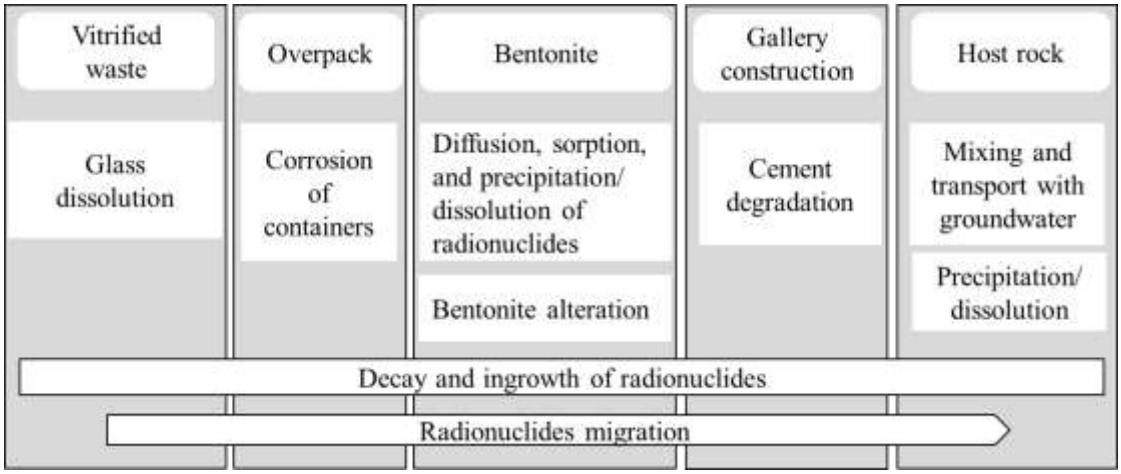

Figure 1-4 Processes describing model for migration of radionuclides in geological disposal [20].

1.3. Properties of bentonite

1.3.1. Crystal and micro- structure of bentonite

Bentonite is a kind of clay consisting of montmorillonite together with other minor minerals such as quartz, feldspar, calcite and pyrite [40,41]. Layers of montmorillonite are composed of an octahedral sheet sandwiched between two opposing tetrahedral sheets as shown in Figure 1-5. Common tetrahedral cations are Si^{4+}, Al^{3+}, and Fe^{3+}, whereas common octahedral cations are Al^{3+}, Fe^{3+}, Mg^{2+}, and Fe^{2+} [42]. The tetrahedral and octahedral sheets have permanent negative charge due to isomorphic substitutions of Si and Al with cations of lower valence. This negative layer charge is balanced primarily by the presence of alkali and alkaline earth metal ions (Na^{+}, K^{+}, Ca^{2+}, Mg^{2+}) on the clay mineral basal surface. The quantity of those cations which is available for ionic exchange with other ions corresponds to the cation exchange capacity (CEC).

The bentonite used in the following chapters of this dissertation is Kunipia F (Kunimine Industries Co., Ltd, Tokyo, Japan). The mineralogical composition of Kunipia F is shown in Table 1-2.

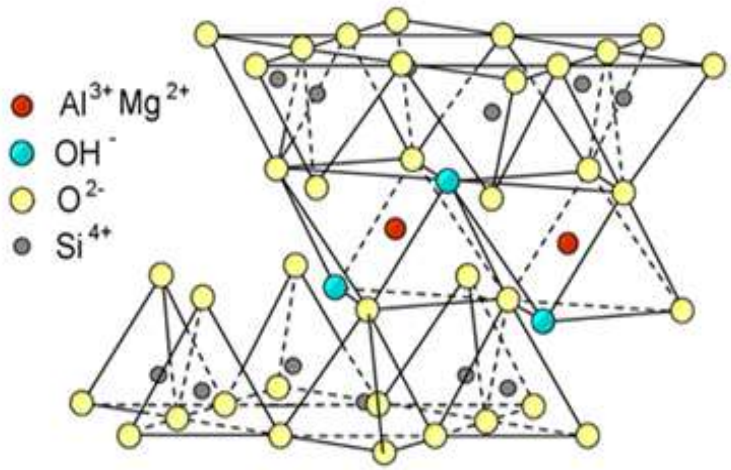

Figure 1-5. Structure of montmorillonite layer and conceptual model of a montmorillonite particle and aggregate.

Table 1-2. Mineralogical composition of Kunipia F [43]

Minerals	Composition (% by weight)
SiO_2	58.0
TiO_2	0.2
Al_2O_3	21.9
Fe_2O_3	1.9
MnO	0.2
MgO	3.4
CaO	0.5
Na_2O	3.0
K_2O	0.1
H_2O	10.8

Montmorillonite in bentonite stacks to form particles. Therefore, two types of pore spaces conceptually exist: the spaces between internal surfaces of parallel montmorillonite layers (interlayer spaces) and the spaces between external surfaces of montmorillonite layers on different montmorillonite particles (interparticle spaces). The total surface area of bentonite can be determined EGME measurement method while the external surface area by BET method. Their respective values for Kunipia-F bentonite were reported to be 750 and 45 m^2/g, respectively [44]. The internal surface area of bentonite was estimated by substracting the total with the external surface area for dry powder of bentonite [45].

1.3.2. Cation exchange reaction in bentonite

In a bentonite-water system, water fills the interlayer and interparticle spaces of bentonite. The cations in the interlayer water and in the interparticle water (hereafter porewater) can be exchanged (cation exchange reaction). The exchange reaction between cation *i* (C_i) and *j* (C_j) can be described by the following equilibrium [46]:

$$C_j^{z_j+} + z_j\, C_i X_{z_i} \leftrightarrow C_j X_{z_j} + z_j\, C_i^{z_i+}$$

where *X* represents one mole of bentonite, and *z* is the charge number of ions. The equilibrium coefficient for this reaction can be described using the Gaines and Thomas convention:

$$K_{GT}^{i/j} = \frac{{\gamma_i}^2\left[C_i^{z_i+}\right]^2}{\gamma_j\left[C_j^{z_j+}\right]} \times \frac{\left(E_{C_j X_{z_j}}\right)^{z_i}}{\left(E_{C_i X_{z_i}}\right)^{z_j}} \qquad (1\text{-}1)$$

where $K_{GT}^{i/j}$ is the Gaines and Thomas ion exchange selectivity coefficient, γ is the activity coefficient of dissolved ions, $E_{C_i X_{z_i}}$ and $E_{C_j X_{z_j}}$ are the equivalent fraction of C_i- and C_j-bentonite, respectively, and square brackets denote the concentration of dissolved ions in the porewater.

The activity coefficient of individual dissolved ions is often calculated using extended Debye and Hückel equation:

$$log\,\gamma_i = -\frac{Az_i^2\sqrt{I}}{1+Ba_i\sqrt{I}} + b_i I \qquad (1\text{-}2)$$

where a_i is the size of hydrated ion *i*, *A* and *B* is the Debye-Hückel constant depending on density, the dielectric constant of water, and temperature, *b* is an empirical ion specific

parameter, and *I* is the ionic strength of the solution which can be calculated with the following expression:

$$I = 0.5 \sum c_i z_i^2 \qquad (1\text{-}3)$$

The activity coefficient of individual ions, however, cannot be measured experimentally. The term of mean activity coefficients of dissolved ions ($\gamma_{\pm}$) is then used to describe the property of the electrolyte solution as given with the following expression:

$$\gamma_{\pm} = (\gamma_{+}^{z+}\gamma_{-}^{z-})^{\frac{1}{z+z-}} \qquad (1\text{-}4)$$

1.3.3. Porewater of Bentonite

The porewater chemistry in compacted bentonite is an important issue to be studied for long-term assessment of bentonite barrier performance, since it affects not only chemical but also hydrological and the mechanical properties of the engineered materials [47,48]. Several methods have been attempted to characterize porewater of bentonite. For examples, in situ extraction in borehole has been conducted to obtain porewater sample for characterization [49,50]. In laboratory, extraction of porewater from core sample was carried out by squeezing with a very high compaction pressure [51]. Liquid displacement with a solution of known composition was also studied [52]. However, alteration of porewater chemistry occurs during porewater extraction, resulting in a difficulty to obtain a representative solution. Geochemical modelling is another approach used in the characterization of the porewater [52–54].

It should be note that the porewater content in bentonite cannot be directly measured. It is thus calculated by subtracting the total water with the estimated interlayer water content [45]:

$$f_{pw} = 1 - \frac{A_{internal}\, d_{interlayer}\, \rho_w}{2m_w} \qquad (1\text{-}5)$$

where $A_{internal}$ is the specific surface area of the internal surface ($m^2\ kg^{-1}$) , m_w is the weight of water in 1 kg bentonite, ρ_w is the density of the porewater ($kg\ m^{-3}$) and $d_{interlayer}$ is the interlayer spacing (m) which can be determined by XRD measurement. The interlayer spacing is affected by dry density of bentonite [55] and salinity of the porewater [56]. These factors in turn affect the fraction of the porewater in bentonite.

The porewater itself contain electrical double layer (EDL) due to contact with the negatively charged external bentonite surfaces [46,57,58]. In general, the activity of water under the influence of surface potential can be calculated using Kelvin equation [59]:

$$a_w = exp\left(\frac{\psi V_w}{RT}\right) \qquad (1\text{-}6)$$

where ψ is the potential of the bentonite-water, and V_w is the molar volume of water. The activity of the porewater was reported to be different from that of bulk water because of this coulombic interactions [60–62]. This water-bentonite interaction may also affect the activity coefficients of dissolved ions in the porewater. If this is the case, it will affect various parameters, such as solubility, speciation, and reactivity of radionuclides in bentonite, which are used in the safety assessment of geological disposal.

1.3.4. Hydraulic conductivity of water and diffusivities of radionuclides in bentonite

One of the most important properties of bentonite as the engineered barrier is its very low hydraulic conductivity. The requirement for hydraulic conductivity of backfill materials in geological disposal is smaller than 4.5×10^{-13} m/s [63]. At such low hydraulic conductivity, mass transport by advection can be negligibly small and diffusion becomes the dominant process for migration of radionuclides [34,64,65]. Therefore, understanding diffusion processes in bentonite is essential to evaluate bentonite performance in isolating the radioactive waste from geosphere.

The mass flux of solutes in one-dimensional diffusion can be described by Fick's first law which is expressed as follows:

$$J = -D_0 \frac{\partial C}{\partial x} \qquad (1\text{-}7)$$

where J is the mass flux of diffusion, D_0 is the diffusion coefficient in free water, C is the concentration, and x is the distance of diffusion. The negative sign is required because diffusion occurs in the direction from higher to lower concentration.

Mass conservation at any location in bentonite sample can be express as:

$$\frac{\partial C}{\partial t} = -\frac{\partial}{\partial x} J \qquad (1\text{-}8)$$

Fick's first law and mass conservation can be combined, leading to Fick's second law which describes the temporal concentration distribution:

$$\frac{\partial C}{\partial t} = -D_0 \frac{\partial^2 C}{\partial x^2} \qquad (1\text{-}9)$$

A lot of experimental data of diffusion coefficients of water, cations, and anions in different types of bentonite have been reported. The data suggests that anions are considered as key radionuclides in the safety assessment of geological disposal [48,66]., since diffusivities of anions are higher than that of cations [67]. Experimental data on anions diffusion in bentonite, such as Cl^- [45,68–70], I^- [71–74], SO_4^{2-} [75,76], and SeO_3^{2-} ions [77], show that their diffusion coefficients decreased as the dry density of bentonite increased. On the other hand, their diffusion coefficients increased as a function of salinity which was attributed to the increase of porosity that is accessible for anions [70,78], but the total porosity stayed constant [78,79].

Due to the microstructure of compacted bentonite, three diffusion pathways in bentonite may be available for radionuclides: the porewater, the external surface of bentonite or the EDL, and the interlayer. Cations and neutral chemical species can diffuse through all of those pathways [80–82], whereas anions can only diffuse through the former two pathways because they are completely restricted in the interlayer spaces by the negatively charge of bentonite layers [83,84]. However, the diffusion mechanisms are still not clearly understood because they are influenced by physical and chemical states of bentonite, such as the existence of electrical double layer (EDL) from the negatively charged bentonite surface, the type of exchangeable cations, microstructure, and the porewater chemistry [26,56,85,86].

1.4. Long-term durability of bentonite in geological disposal

1.4.1. Alteration due to waste form and cementitious materials

Prediction of the long-term durability of bentonite is important for the safety assessment of geological disposal [48,52]. In a geological disposal facility, alteration of bentonite due to contacts with surrounding environment is inevitable. In addition, bentonite may be altered by gamma radiation and thermal loading from HLW, and corrosion products of waste canisters. Radiation from HLW is expected to have minor effect because of adequate radiation shielding provided by waste canisters. Although heat transferred from the waste form may affect density, water content and mineral composition of bentonite, this thermal loading was reported to have no negative effects on favorable bentonite properties [87]. Anaerobic corrosion of iron-based canisters will generate Fe^{2+} ions and H_2 gas, which can be accelerated in the presence of sulfate reducing bacteria. The Fe^{2+} ions will be deposited into bentonite which eventually can convert bentonite to non-swelling silicates [88,89]. The alteration of bentonite by Fe^{2+} ions may also increase the hydraulic conductivity [37,90]. The breakthrough of H_2 gas generated from corrosion can make pathways for migration, resulting in enhancement of radionuclide transport in bentonite.

Another potential alteration is induced by the interaction between bentonite and cementitious materials. Degradation of cement generates alkali leachate rich in K^+, Na^+, and Ca^{2+} ions [91]. Chemical reaction between this leachate and bentonite will occur, resulting in the mineralogical changes of bentonite over time. Alteration of bentonite begins with ion exchange processes which means conversion of Na-bentonite to Ca- and

K-bentonite. The alteration process eventually end up with complete transformation of bentonite to secondary mineral like zeolite and calcium silicate hydrate [92,93].

The cement leachate may also induce $CaCO_3$ precipitation which can change the performance of bentonite buffer [94,95]. The $CaCO_3$ precipitates may be generated by the reaction of Ca^{2+} ions from the cement leachate and CO_3^{2-} ions originated from the groundwater, described by the following reaction:

$$Ca^{2+} + CO_3^{2-} \leftrightarrow CaCO_{3\,(s)}$$

Table 1-3 indicates the reference composition of groundwater in geological disposal in Japan. The concentration of the total HCO_3^-/CO_3^{2-} ions is approximately 3.5 mM [20, 96]. The cement leachate can also promote the decomposition of dolomite ($CaMg(CO_3)_2$), resulting in a release of CO_3^{2-} ions to solution, according to the following reaction [97]:

$$MgCa(CO_3)_2 + 2OH^- \rightarrow Mg(OH)_2 + (CaCO_3)_2 + CO_3^{2-}$$

This reaction will increase the concentration of HCO_3^-/CO_3^{2-} ions in the groundwater and the porewater of bentonite, which eventually may promote the $CaCO_3$ precipitation in bentonite.

Table 1-3 The reference composition of groundwater and estimated porewater of bentonite for geological disposal in Japan [20].

Parameter		Groundwater	Bentonite porewater
pH		8.5	8.4
Eh (mV)		-281	-276
Concentration (M)	Na	3.6×10^{-3}	2.8×10^{-2}
	Ca	1.1×10^{-4}	5.3×10^{-5}
	K	6.2×10^{-5}	1.2×10^{-4}
	Mg	5.0×10^{-5}	4.2×10^{-6}
	C	3.5×10^{-3}	1.6×10^{-2}
	S	1.1×10^{-4}	1.1×10^{-4}
	B	2.9×10^{-4}	2.9×10^{-4}
	P	2.9×10^{-6}	2.9×10^{-6}
	F	5.4×10^{-5}	5.4×10^{-5}
	N	2.3×10^{-5}	2.3×10^{-5}
	Cl	1.5×10^{-5}	1.5×10^{-5}
	Si	3.4×10^{-4}	3.4×10^{-4}

1.4.2. Effect of $CaCO_3$ precipitation in geological disposal

The condition where $CaCO_3$ precipitation occurs in bentonite can be described by the product of the activity coefficients of dissolved Ca^{2+} and HCO_3/CO_3^{2-} ions in the porewater. For some important radionuclides in geological disposal, the chemical form of radionuclides may be affected by the presence of dissolved Ca^{2+} and HCO_3/CO_3^{2-} ions [98]. For example, the speciation of uranium in the presence of dissolved SiO_2, and Ca^{2+} and HCO_3/CO_3^{2-} ions is shown in Figure 1-6. At the pH of 8.5, which is the value for reference groundwater for geological disposal in Japan [20], the U(VI) species is dominated by ternary uranyl-calcium-carbonato complexes $Ca_2UO_2(CO_3)_3^0$ and $Ca_2UO_2(CO_3)_3^{2-}$ ions. The formation of these complexes was reported to decrease the adsorption of U(VI) on iron oxides and sediments [99]. It is also reported that the uranylcarbonato complexes sorb preferentially to the edge sites of montmorillonite,

whereas UO_2^{2+} ions to interlayer through cation exchange reaction [100]. Considering this adsorption mechanism, the assessment of uranium transport in geological disposal should consider the presence of Ca^{2+} and HCO_3/CO_3^{2-} ions in the porewater.

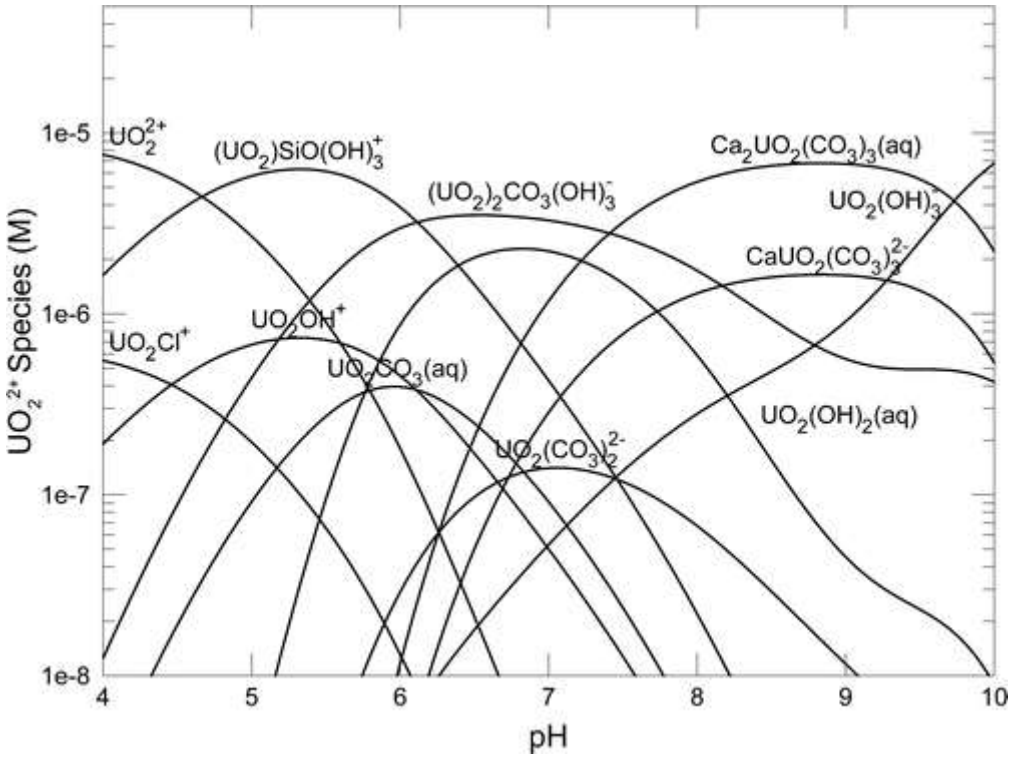

Figure 1-6. Speciation of U(VI) in the presence of Ca^{2+}, HCO_3/CO_3^{2-}, and SiO_2. The figure is for the total concentration of dissolved U(VI), Ca, and SiO_2 are10^{-5}, 10^{-2}, and $10^{-2.5}$ M, respectively, and CO_2 partial pressure $10^{-2.5}$ atm [98].

The precipitation of $CaCO_3$ may also affect the transport of radionuclides by coprecipitation [101–103]. For examples, strong partitioning of actinides in $CaCO_3$ precipitates has been reported [104]. The partitioning of radionuclides may also be affected by the type of $CaCO_3$ polymorph [101].The $CaCO_3$ precipitates may affect the mechanical properties of bentonite. Molecular dynamics study suggests that the mechanical strength of bentonite decreases in the bentonite-$CaCO_3$ system [105]. The

formation of $CaCO_3$ precipitates in bentonite may also affect the transport of radionuclides by porosity clogging. Study on the precipitation of $CaCO_3$ in quartz sand revealed that only 5% amount of precipitates was enough to create impermeable layer [106]. Considering large amount of $CaCO_3$ precipitates are predicted to form in compacted bentonite and their importance in affecting the transport of radionuclides, understanding the $CaCO_3$ precipitation phenomena in bentonite is an important issue to be studied for the long-term performance assessment of geological disposal of HLW.

1.5. Calcium carbonate precipitation

1.5.1. Dissolved carbonate equilibria

It is important to note that dissolved carbonate exists as four different chemical species: CO_2, H_2CO_3, HCO_3^-, and CO_3^{2-}, the distribution of which depends on pH. The equilibrium of dissolved carbonate can be written as:

$$H_2CO_3 \overset{K_{a1}}{\leftrightarrow} H^+ + HCO_3^- \overset{K_{a2}}{\leftrightarrow} 2\,H^+ + CO_3^{2-}$$

The equilibrium shows that two protons are stepwisely released from dissociation of H_2CO_3, of which the dissociation constants are given by $K_{a1} = 2.5 \times 10^{-4}$ and $K_{a2} = 4.6 \times 10^{-7}$ [107–109]. The activity of each carbonate species can be calculated by solving the equilibrium equation:

$$[H_2CO_3] = \frac{[H^+]^2}{[H^+]^2 + [H^+]K_{a1} + K_{a1}K_{a2}} \qquad (1\text{-}10)$$

$$[HCO_3^-] = \frac{[H^+]K_{a1}}{[H^+]^2 + [H^+]K_{a1} + K_{a1}K_{a2}} \qquad (1\text{-}11)$$

$$[CO_3{}^{2-}] = \frac{K_{a1}K_{a2}}{[H^+]^2 + [H^+]K_{a1} + K_{a1}K_{a2}} \qquad (1\text{-}12)$$

The distributions of dissolved carbonate calculated for closed and open systems are shown in Figure 1-7. In the closed system, the solution is considered to be closed with respect to atmosphere, thus the total dissolved carbonate in the solution is constant. In the open system, dissolved carbonate in the solution is considered to be in equilibrium with the atmospheric CO_2 gas. The concentration of dissolved CO_2 is constant which is determined by its partial pressure according Henry's Law.

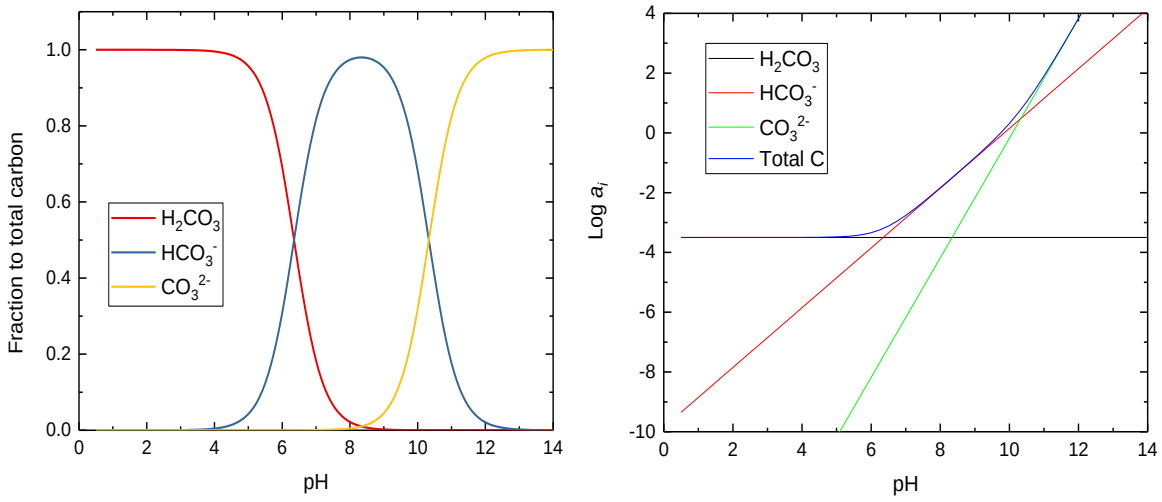

Figure 1-7. Distribution of dissolved carbonate species as a function of pH in (a) a closed system and (b) an open system at a constant CO_2 partial pressure of 10^{-2} atm.

1.5.2. $CaCO_3$ precipitation in bulk solution

The models of $CaCO_3$ precipitation has been studied extensively. In the classical concept of precipitation, nucleation occurs in a solution when ions have become saturated and the size of earliest crystal is considered to be a critical cluster. Recent studies,

however, suggests that $CaCO_3$ precipitation is non-classical; stable prenucleation clusters of $CaCO_3$ are formed and act as precursors for precipitation [110,111]. Furthermore, in situ TEM study revealed that the formation of $CaCO_3$ precipitates occurs through multiple pathways, starting from amorphous then transforming into crystalline phase [112].

There are six types of polymorphs for $CaCO_3$ in nature; three are anhydrous and the other three are hydrous states. The anhydrous polymorphs are calcite, aragonite, and vaterite, while the hydrous polymorphs are monohydrocalcite ($CaCO_3 \cdot H_2O$), ikaite ($CaCO_3 \cdot 6H_2O$) and amorphous $CaCO_3$. Of these $CaCO_3$ polymorphs, calcite (hexagonal crystal) and aragonite (orthorhombic) are dominant in nature, whereas others are less stable and easily transform into calcite or aragonite in a solution at ambient conditions. This is because the radius of Ca^{2+} ion is 0.98 Å which is close to the limiting value of rhombohedral (<0.99 Å) and orthorhombic (>0.99 Å). Vaterite is the least stable unhydrated polymorph which occur under a specific condition and subsequently transform to calcite or aragonite. All the hydrated $CaCO_3$ polymorphs are unstable towards the conversion to calcite or aragonite.

The solubility of $CaCO_3$ is represented by its solubility product constant values (K_{sp}), which is the equilibrium constant between dissolved ions and the solid phase in an aqueous solution. The K_{sp} of $CaCO_3$ precipitates can be written as:

$$K_{sp\ CaCO_3} = a_{Ca^{2+}}\ a_{CO_3^{2-}} \qquad (1\text{-}13)$$

Saturation index (log Ω) is often used to express whether the solution is undersaturated, at equilibrium, or supersaturated with respect to $CaCO_3$ precipitates.

$$\Omega_{CaCO_3} = \frac{a_{Ca^{2+}}\ a_{CO_3^{2-}}}{K_{sp\ CaCO_3}} \qquad (1\text{-}14)$$

The value of $K_{sp\ CaCO_3}$ varies depending on the types of $CaCO_3$ polymorphs and on the temperature. The compilation data of $K_{sp\ CaCO_3}$ for all the polymorphs as a function of temperature are shown in Figure 1-8.

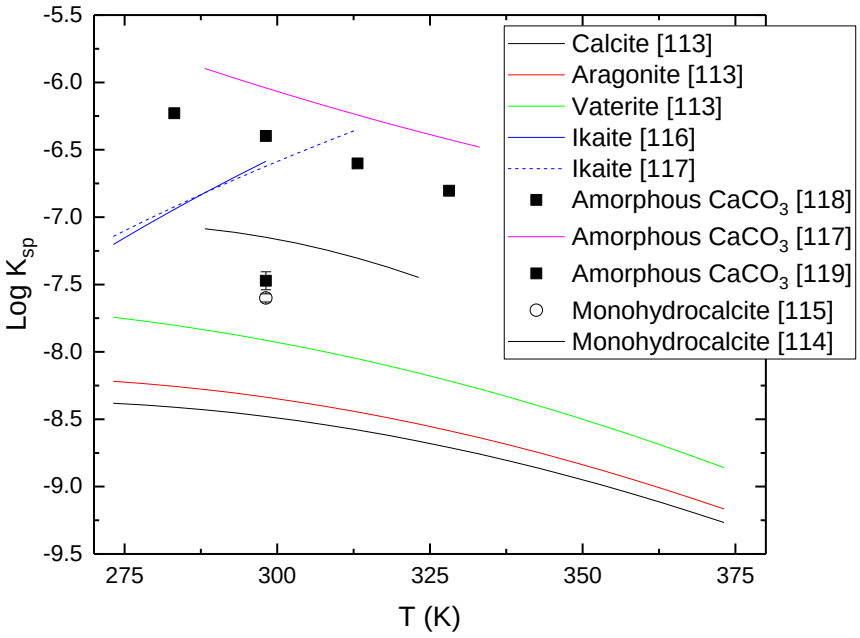

Figure 1-8. Solubility products of $CaCO_3$ polymorphs: calcite, aragonite, vaterite [113], monohydrocalcite [114,115], ikaite [116,117], and amorphous $CaCO_3$ [117–119].

At constant temperature and partial pressure of CO_2, the model for the rate of dissolution/ precipitation of $CaCO_3$ can be expressed as [113]:

$$R = k_1\, a_{H^+} + k_2\, a_{H_2CO_3} + k_3\, a_{H_2O} - k_4\, a_{Ca^{2+}}\, a_{HCO_3^-} \qquad (1\text{-}15)$$

where R is the rate of dissolution/ precipitation of $CaCO_3$ (mmol cm^{-2} s^{-1}), k_1, k_2, and k_3 are temperature dependent, first order rate constants for dissolution, and k_4 is the

precipitation rate constant as the solution approaches saturation with respect to calcite. The expression of k_1, k_2, k_3, and k_4 are as follows:

$$log\, k_1 = 0.198 - 444/T \quad (1\text{-}16)$$

$$log\, k_2 = 2.84 - 2177/T \quad (1\text{-}17)$$

$$log\, k_3 = -5.86 - 317/T \;\; (T < 298.15\, K) \quad (1\text{-}18)$$

$$log\, k_3 = 1.10 - 1737/T \; (T > 298.15\, K) \quad (1\text{-}19)$$

$$log\, k_4 = -7.5 + 0.016\, T - \;\; 0.64\, log\, P_{CO_2} \; (P_{CO_2} < \; 10^{-1.5}\, bars) \quad (1\text{-}20)$$

1.5.3. $CaCO_3$ precipitation in bentonite

Precipitation of minerals in porous media is important for the safety assessment of geological disposal of HLW because it may affect the porosity, permeability and particle size distributions [120–122]. The pore-scale $CaCO_3$ precipitation is a major interest because of its importance in the context of geological disposal as well as geologic carbon sequestration, permeable reactive barriers and contaminant host phase in environmental remediation. The processes are regarded very complex because it is affected by multiple factors, such as mineral reactivity, pore size, surface charges, and transport [123,124]. In natural systems, the heterogeneous nucleation for $CaCO_3$ precipitation is likely to be more favorable than homogenous nucleation. This is because the critical radius and the interfacial energy governing heterogeneous nucleation are significantly lower than those of homogenous nucleation [125,126]. This nucleation processes may also influence the transport of aqueous chemical species [127].

Precipitation of $CaCO_3$ in porous media has been studied for well mixed, homogenous and non-reactive systems. Even in the idealized systems, there are many factors affecting the $CaCO_3$ precipitation processes. For examples, the small pore effect can make the solubility of minerals higher than that in bulk solution [128,129]. Similarly, study on $CaCO_3$ precipitation in glass beads revealed that it preferentially occurs in larger pores [130]. The study on $CaCO_3$ precipitation in gelatin gel suggested that porosity can change the characteristics of $CaCO_3$ precipitates. Smaller porosity leads to the formation of smaller $CaCO_3$ crystal sizes with more complex morphology, which tend to develop as aggregates rather than a single crystal [131]. The study on $CaCO_3$ precipitation in polyacrylamide gel by diffusion mixing suggested that slower rate of $CaCO_3$ precipitation is needed to match the simulation of precipitation width with the experimental result [132].

Surface charge affects the composition of solution near the surface. The concentration profile of cations (C_+) and anions (C_-) as a function of distance from charged surface can be described with the following expressions:

$$C_+ = C_\infty \, exp\left(\frac{-zF\psi}{RT}\right) \qquad (1\text{-}21)$$

$$C_- = C_\infty \, exp\left(\frac{zF\psi}{RT}\right) \qquad (1\text{-}22)$$

where C_∞ is the concentration in bulk solution, z is charge of the ion, F is the Faraday constant (96,485 C/mol), R is the ideal gas constant (8.314 J/mol/K). It has been reported that the $CaCO_3$ precipitation is affected by the ratio of Ca^{2+} and CO_3^{2-} ions in the solution [133]; high ratio of Ca^{2+} to CO_3^{2-} ions may suppress the $CaCO_3$ precipitation [134]. This

seems to agree with a finding that precipitation of $CaCO_3$ is inhibited in the small pore of glass beads [123].

There can be similar pore size effect on $CaCO_3$ precipitation in compacted bentonite. The reaction rate of $CaCO_3$ precipitation may be different than those in bulk water because the transport in bentonite is very slow. It has been reported that the reaction rate in diffusion-limited conditions may be different from the rate in bulk solution [132,135]. Furthermore, complete mixing in porous media may not occur, resulting in the overestimation of precipitation product in the reactive transport model [136]. The heterogeneous composition of ions in the porewater due to the negative charge of bentonite surface may also influence the $CaCO_3$ precipitation. Another factor which may affect the $CaCO_3$ precipitation in compacted bentonite is the competition between solid formation and cation exchange reaction [137]. The observation of $CaCO_3$ precipitates in bentonite is more difficult than the above mentioned simple systems, such as column filled with glass beads. Therefore, no data has been reported about the study of $CaCO_3$ precipitation in compacted bentonite. Considering its importance in long-term assessment of geological disposal, the study on $CaCO_3$ precipitation in bentonite is essential.

1.6. Objective and experimental approach

1.6.1. Objective

The objective of this thesis is to improve the understanding of the fate and transport of radionuclides in compacted bentonite. This thesis can contribute to the safety assessment of the geological disposal of HLW. This thesis is composed of three aspects regarding to the fate and transport of radionuclides in bentonite; the porewater chemistry,

the precipitation processes, and the diffusion mechanism of ions in bentonite. This study was carried out by the following approaches:

1. Develop a sequential extraction method as a practical method to distinguish dissolved ions and precipitates species in compacted bentonite.
2. Determine the activity coefficients of dissolved ions in the porewater of compacted bentonite during $CaCO_3$ precipitation processes. The values of activity coefficients of reacting ions were compared with those of ions in bulk solution.
3. Observe the transport of ions in compacted bentonite during the precipitation of $CaCO_3$. Effects of precipitation on the transport of ions in bentonite are discussed.
4. Determine the D_a and E_a values for diffusion of $^{35}SO_4^{2-}$ ions in compacted bentonite as a function of dry density and NaCl concentration. Diffusion mechanism for anions in compacted bentonite is discussed from the viewpoints of dry density and salinity.

1.6.2. $CaCO_3$ precipitation enhanced by electrokinetic method

Electrokinetic method is the process of applying electrical potential gradient across the sample of interest. In this method, mass transport is enhanced by electrokinetic processes which include electromigration and electroosmosis phenomena as shown in Figure 1-9. Electromigration is the movement of ions under electrical field. Anions move towards the anode side (positive electrode) while cations move towards the cathode side (negative electrodes). When the ions migrate due to electromigration process, they transfer momentum to the surrounding water molecules. The flow of water molecules caused by this process is called electroosmosis [138–140].

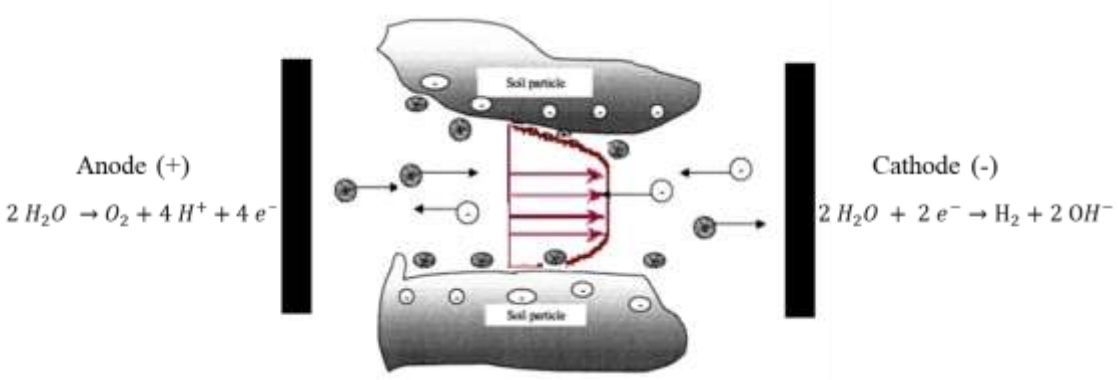

Figure 1-9 Schematic of the main phenomena during electrokinetic process [141,142].

Under electrical gradient, the mobility of neutral ions is influenced only by electroosmosis. On the other hand, the mobility of charged ions is affected by both of electromigration and electroosmosis. The apparent mobility of individual ions (μ_a^i) can thus be expressed as the sum of their electromigration mobility (μ_{em}^i) and electroosmosis flow (μ_{EOF}^i):

$$\mu_a^i = \mu_{em}^i + \mu_{EOF}^i \qquad (1\text{-}23)$$

The equation implies that the anions can move from anode to cathode regardless of their negative charge when the electroosmotic flow is higher than electromigration.

The electromigration may cause reduction-oxidation reaction as well. When electrical field is applied, electrolysis of water occurs at the electrodes. The reaction generates oxygen gas and hydrogen ions due to oxidation at the anode, and hydrogen gas and hydroxyl ions due to reduction at the cathode, according to the following reactions:

$$2\,H_2O \rightarrow O_2 + 4\,H^+ + 4\,e^- \quad E_0 = -1.229\,(Anode)$$

$$2\,H_2O + 2\,e^- \rightarrow H_2 + 2\,OH^- \quad E_0 = -0.828\,V\,(Cathode)$$

In the experimental setup, the effect of H^+ and OH^- generated by water electrolysis in the electrodes can be avoided by are continuously circulating the electrolyte solutions in the anode and the cathode side to neutralize the H^+ and OH^- [143]. Another method to avoid the effect of the generation of H^+ and OH^- is by separating electrodes with the anode and cathode reservoirs using salt bridge [143,144].

The electrical potential gradient can enhance mass transport as given by Nernst-Planck equation:

$$J_i = -D_i \frac{\partial c_i}{\partial x} - D_i z_i c_i \frac{F}{RT} \frac{\partial V}{\partial x} \qquad (1\text{-}24)$$

where J_i is the flux of ion *i*, D_i is the diffusion coefficient, *c* is the concentration (mol/m^3), *x* is the distance (m), *z* is the charge number, *F* is the Faraday constant (96485.3 C/eq), *R* is the gas constant (8.3145 VC/eq/K), *T* is the temperature (K), and *V* is the potential (V). The electrokinetic method enables enhanced transport resulting in the decrease of the time scale of the experiments [145]. The method has been applied in soil remediation [138,141,146], cement decontamination [147], determination of sorption in rock samples [148], and investigating pore connectivity [149]. In the context of bentonite, this method has been used as an alternative method to obtain diffusion coefficients of ions and radionuclides. The diffusion coefficients obtained by using this method were in agreement with those obtained by conventional in-diffusion method [143].

The migration of water and ions under electrical potential gradient was well produced to follow an advection-dispersion which described as [144,150–152]:

$$\frac{\partial c_i}{\partial x} = D_i \frac{\partial c_i}{\partial x^2} - V_c \frac{\partial C}{\partial x} \qquad (1\text{-}25)$$

Therefore, this method can also be used to study the chemical speciation in compacted bentonite, since different chemical species will have different migration behavior, which in turn can be distinguished from the concentration profile after the electromigration experiment [153]. The application of electrokinetic method has also been used to study precipitation generated by diffusion-reaction in porous media [154,155]. A study on gypsum precipitation in compacted bentonite using this method showed that the selectivity coefficient of two order magnitude higher than that previously reported is needed to explain the precipitation condition [156].

In this study, the electrokinetic method was used to enhance $CaCO_3$ precipitation in compacted bentonite, of which the hydraulic conductivity is very low. Under the electrical potential gradient, Ca^{2+} ions migrate towards the cathode side while HCO_3^- /CO_3^{2-} ions migrate towards the anode side in the opposite direction. As the process continues, $CaCO_3$ precipitates may occur by a chemical reaction between Ca^{2+} and HCO_3^- /CO_3^{2-} ions when the solution is oversaturated with respect to $CaCO_3$ precipitates.

1.6.3. Determination of diffusion coefficient by back-to-back diffusion

Three types of diffusion coefficients, pore diffusion coefficient (D_p), effective diffusion coefficient (D_e) and apparent diffusion coefficient (D_a), are often defined for porous media. The relationships among three different diffusion coefficients can be expressed as:

$$D_a = \frac{D_e}{\varepsilon+\rho K_d} = \frac{\varepsilon D_p}{\varepsilon+\rho K_d} \qquad (1\text{-}26)$$

where ε is the porosity, ρ is the dry density, and K_d is the distribution coefficient (dm^3/g). The common experimental methodologies to obtain the D_e and D_a values are back-to-back diffusion, through-diffusion, and reservoir-depletion method [157,158].

This study determined D_a values in compacted bentonite using the back-to-back method. In this method, a small amount of radiotracer solution is introduced at a mid-plane of compacted bentonite enclosed in a diffusion cell as illustrated in Figure 1-10. At a prescribed time for diffusion, the D_a value is calculated from the new spatial distribution of the species of interest using the following solution, which is derived from Fick's second with the condition of thin-layer diffusion in infinite sample [159]:

$$C\ (x,t) = \frac{M}{2\sqrt{\pi D_a t}}\ exp\left(-\frac{x^2}{4D_a t}\right) \qquad (1\text{-}27)$$

where c is the concentration of species of interest per sectioned bentonite sample, M is the total amount of diffusing source per unit area, x is the distance from the surface on which the species interest is placed. The activation energy for apparent diffusion (E_a) can be determined from the temperature dependence of D_a values using Arrhenius equation. The E_a values can be used as a parameter to elucidate diffusion processes. Generally, the E_a value in porewater can be considered to be equal to that in free water [55,160].

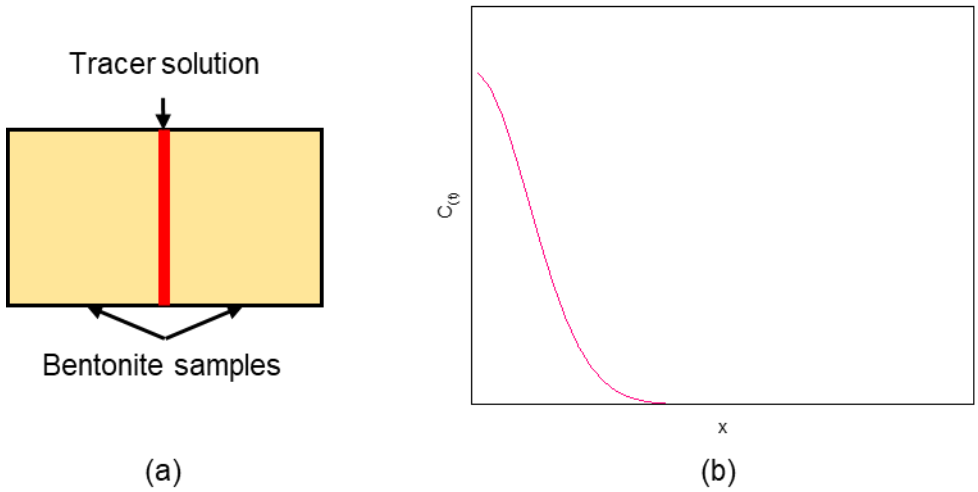

Figure 1-10. Schematic of back-to-back diffusion method (a) and typical concentration profile in each of bentonite (b).

1.7. Outline of this thesis

Chapter 2 is entitled "Precipitation of $CaCO_3$ enhanced by electrokinetic method and its application to determine the activity coefficient of dissolved ions in the porewater of compacted bentonite". It describes the estimation of the activity coefficients of dissolved ions in the porewater of compacted bentonite from the conditions at which $CaCO_3$ precipitation occurred. The formation of $CaCO_3$ precipitates was carried out in compacted Na-bentonite enhanced by electrokinetic method. The resulting $CaCO_3$ precipitates were analyzed by SEM/EDS images and X-ray diffraction. A sequential extraction has been developed to provide a practical method to determine the concentration of dissolved ions in the porewater and solid phase ions in the form of exchangeable cations and precipitates. The mean activity coefficients of Ca^{2+} and CO_3^{2-} ions was calculated using the concentrations of dissolved Ca^{2+} and HCO_3^-/CO_3^{2-} ions and assuming the porewater is in equilibrium with the $CaCO_3$ precipitates. The resulting values were compared to the theoretical approximation in bulk solution.

Chapter 3 is entitled “Travelling reaction front of $CaCO_3$ precipitation in compacted bentonite under electrical potential gradient”. In this chapter, the electromigration parameters of Ca^{2+} and HCO_3^-/CO_3^{2-} ions in compacted Na-bentonite were determined. The time dependence of $CaCO_3$ precipitation in compacted bentonite under electrical potential gradient was studied using the same method as in Chapter 2. The electromigration parameters values and the temporal spatial distributions of Ca^{2+} and HCO_3^-/CO_3^{2-} ions were then used to discuss $CaCO_3$ precipitation in bentonite under the experimental conditions. Finally, the transport mechanism of Ca^{2+} and HCO_3^-/CO_3^{2-} ions during the $CaCO_3$ precipitation reaction in bentonite is discussed.

Chapter 4 is entitled “Diffusion behavior of sulphate ions in compacted Na-montmorillonite at different dry density and salinity”. It provides the determination of D_a values of $^{35}SO_4^{2-}$ ions in compacted bentonite using back-to-back diffusion method. The D_a values were obtained as a function of different dry density and NaCl concentrations. The E_a values of $^{35}SO_4^{2-}$ ions were determined from the temperature dependence on the D_a values. The diffusion behavior of $^{35}SO_4^{2-}$ ions in was then discussed from the D_a and E_a data.

Chapter 5 provides summary for main results and conclusions for the overall study, and their importance for safety assessment of geological disposal of HLW.

1.8. References

[1] International Atomic Energy Agency. The Power Reactor Information System (PRIS). [accessed 2019 Jun 23]; <https://pris.iaea.org/PRIS/home.aspx>

[2] Ewing RC. The nuclear fuel cycle: A role for mineralogy and geochemistry. Elements. 2006;2(6):331–334.

[3] International Atomic Energy Agency. Fundamental Safety Principles: Safety Fundamentals. Safety Standards for protecting people and the environment. Fundamental Safety Principles. Vienna: IAEA; 2006. (IAEA Safety Standards Series No.SF-1).

[4] Lowenthal MD. Waste-acceptance criteria and risk-based thinking for radioactive-waste classification. Waste Manag. 1998;18:249–256.

[5] International Atomic Energy Agency. Classification of Radioactive Waste: General Safety Guide. Vienna: IAEA; 2009. (IAEA Safety Standards Series No. GSG-1).

[6] Nakayama S. Radioactive Waste Management. In: Nagasaki S, Nakayama S, editors. Radioactive Waste Engineering and Management, An Advance Course in Nuclear Engineering. Tokyo: Springer; 2015.p.1–16.

[7] Satoyama T, Kishimoto K, Hoshi A, et al. Clearance of Concrete Generated from Modification Activities of JRR-3 - Method for Measuring and Evaluating of Radioactivity Concentration -. Tokai: Japan Atomic Energy Agency; 2010. (JAEA-Technology 2011-003).

[8] International Atomic Energy Agency. Status and Trends in Spent Fuel and

Radioactive Waste Management. Vienna: IAEA; 2018. (IAEA Nuclear Energy Series No. NW-T-1.14).

[9] Nuclear Waste Management Organization. Frequently Asked Questions. [accessed 2019 Jul 4]; <www.numo.or.jp/q_and_a/>

[10] Niibori Y. Radioactive Waste Disposal. In: Nagasaki S, Nakayama S, editors. Radioactive Waste Engineering and Management, An Advance Course in Nuclear Engineering. Tokyo: Springer; 2015.p.153–174.

[11] Japan Atomic Energy Agency, The Federation of Electric Power Companies of Japan. Second progress report on research and development for TRU waste disposal in japan − repository design, safety assessment and means of implementation in the generic phase. Tokai: JAEA; 2007. (JAEA-Review 2007-010).

[12] Ewing RC, Whittleston RA, Yardley BWD. Geological disposal of nuclear waste: A primer. Elements. 2016;12(4):233–237.

[13] Hedin A. Spent nuclear fuel - how dangerous is it? A report from the project “Description of risk.” SKB Technical Report TR 97-13. Stockholm: Swedish Nuclear Fuel and Waste Management; 1997. (SKB Technical Report 97-13).

[14] Bruno J, Ewing RC. Spent Nuclear Fuel. Elements. 2006;2(6):343–349.

[15] Ewing RC. Long-term storage of spent nuclear fuel. Nat. Mater. 2015;14(3):252–257.

[16] Ewing RC, Hippel FN von. Nuclear Waste Management in the United States — Starting Over. Science (80-.). 2009;325:151–152.

[17] Grambow B. Nuclear Waste Glasses - how durable. Elements. 2006;2(6):357–364.

[18] Donald IW. Waste immobilization in glass and ceramic based hosts: radioactive, toxic and hazardous waste. Chichester: John Wiley & Sons; 2010.

[19] Gin S, Abdelouas A, Criscenti LJ, et al. An international initiative on long-term behavior of high-level nuclear waste glass. Mater. Today. 2013;16(6):243–248.

[20] Japan Nuclear Cycle Development Institute. H12: Project to establish the scientific and technical basis for HLW disposal in Japan, Supporting Report 3 Safety Assessment of the Geological Disposal System. JNC TN1410 2000-004. Tokai: JNC; 2000. (JNC TN1410 2000-004).

[21] Poinssot C, Bourg S, Ouvrier N, et al. Assessment of the environmental footprint of nuclear energy systems . Comparison between closed and open fuel cycles. 2014;69.

[22] Chapman N, Hooper A. The disposal of radioactive wastes underground. Proc. Geol. Assoc. 2012;123(1):46–63.

[23] International Atomic Energy Agency. Disposal of radioactive waste: Specific safety requirements. Vienna: IAEA; 2011. (IAEA Safety Standards Series No. SSR-5).

[24] Apted MJ, Ahn J. Multiple-barrier geological repository design and operation strategies for safe disposal of radioactive materials. In: Apted MJ, Ahn J, editors. Geological Repository Systems for Safe Disposal of Spent Nuclear Fuels and Radioactive Waste (Second Edition). Cambridge: Woodhead Publishing; 2017.p.3–26.

[25] Hedin A, Olsson O. Crystalline rock as a repository for Swedish spent nuclear fuel. Elements. 2016;12(4):247–252.

[26] Grambow B. Geological disposal of radioactive waste in clay. Elements. 2016;12(4):239–245.

[27] Von Berlepsch T, Haverkamp B. Salt as a host rock for the geological repository for nuclear waste. Elements. 2016;12(4):257–262.

[28] Japan Nuclear Cycle Development Institute. H12: Project to Establish Technical Basis for HLW Disposal in Japan, Project Overview Report. JNC TN1410 2000-001. Tokai: JNC; 2000. (JNC TN1410 2000-001).

[29] Nuclear Waste Management Organization. Preliminary Assessment for Siting a Deep Geological Repository for Canada 's Used Nuclear Fuel: The corporation of the town of Blind River, Ontario. NWMO; 2013. (APM-REP-06144-0001).

[30] Madsen FT. Clay Mineralogical Investigations Related to Nuclear Waste Disposal. Clay Miner. 1998;33(1):109–129.

[31] Higgo JJW. Clay as a barrier to radionuclide migration. Prog. Nucl. Energy. 1987;19(2):173–207.

[32] Pusch R. Use of bentonite for isolation of radioactive waste products. Clay Miner. 1992;27(3):353–361.

[33] Pusch R. Chapter 11.4 Clays and nuclear waste management. In: Bergaya F, Theng BKG, Lagaly G, editors. Handbook of clay science. Amsterdam: Elsevier; 2006.p.703–716.

[34] Altmann S, Tournassat C, Goutelard F, et al. Diffusion-driven transport in clayrock

formations. Appl. Geochemistry. 2012;27(2):463–478.

[35] Sellin P, Leupin OX. The use of clay as an engineered barrier in radioactive-waste management - A review. Clays Clay Miner. 2014;61(6):477–498.

[36] Xia X, Idemitsu K, Arima T, et al. Corrosion of carbon steel in compacted bentonite and its effect on neptunium diffusion under reducing condition. Appl. Clay Sci. 2005;28:89–100.

[37] Carlson L, Karnland O, Oversby VM, et al. Experimental studies of the interactions between anaerobically corroding iron and bentonite. Phys. Chem. Earth. 2007;32(1–7):334–345.

[38] Motamedi M, Karland O, Pedersen K. Survival of sulfate reducing bacteria at different water activities in compacted bentonite. FEMS Microbiol. Lett. 1996;141(1):83–87.

[39] Ahn J. Integrated Radionuclide Transport Model for a High-Level Waste Repository in Water-Saturated Geologic Formations. Nucl. Technol. 1998;121(1):24–39.

[40] Murray HH. Applied Clay Mineralogy: Occurrences, Processing and Applications of Kaolins, Bentonites, Palygorskitesepiolite, and Common Clays. Amsterdam (Netherlands): Elsevier; 2007.

[41] Grim RE, Guven N. Bentonites: Geology, mineralogy, properties and uses. Amsterdam (Netherlands): Elsevier; 1978.

[42] Brigatti MF, Galan E, Theng BKG. Chapter 2 Structures and Mineralogy of Clay Minerals. In: Bergaya F, Theng BKG, Lagaly G, editors. Handbook of Clay

Science. Amsterdam: Elsevier; 2006.p.19–86.

[43] Sato H, Ashida T, Kohara Y, et al. Effect of dry density on diffusion of some radionuclides in compacted sodium bentonite. J. Nucl. Sci. Technol. 1992;29(9):873–882.

[44] Kozaki T, Sato Y, Nakajima M, et al. Effect of particle size on the diffusion behavior of some radionuclides in compacted bentonite. Nucl. Mater. 1999;270:265–272.

[45] Kozaki T, Inada K, Sato S, et al. Diffusion mechanism of chloride ions in sodium montmorillonite. J. Contam. Hydrol. 2001;47(2–4):159–170.

[46] Tournassat C, Bourg IC, Steefel CI, et al. Chapter 1 - Surface Properties of Clay Minerals. In: Tournassat C, Steefel CI, Bourg IC, et al., editors. Natural and Engineered Clay Barriers. Elsevier; 2015.p.5–31.

[47] Ochs M, Lothenbach B, Shibata M, et al. Thermodynamic modeling and sensitivity analysis of porewater chemistry in compacted bentonite. Phys. Chem. Earth. 2004;29(1):129–136.

[48] Altmann S. 'Geo'chemical research: A key building block for nuclear waste disposal safety cases. J. Contam. Hydrol. 2008;102(3–4):174–179.

[49] Delay J, Vinsot A, Krieguer JM, et al. Making of the underground scientific experimental programme at the Meuse/Haute-Marne underground research laboratory, North Eastern France. Phys. Chem. Earth. 2007;32(1–7):2–18.

[50] Tournassat C, Vinsot A, Gaucher EC, et al. Chapter 3 - Chemical conditions in clay-rocks. In: Tournassat C, Steefel CI, Bourg IC, et al., editors. Natural and

Engineered Clay Barriers. Amsterdam (Netherlands): Elsevier; 2015.p.71–100.

[51] Fernández AM, Sánchez-Ledesma DM, Tournassat C, et al. Applying the squeezing technique to highly consolidated clayrocks for pore water characterisation: Lessons learned from experiments at the Mont Terri Rock Laboratory. Appl. Geochemistry. 2014;49:2–21.

[52] Grambow B, Landesman C, Ribet S. Nuclear waste disposal: I. Laboratory simulation of repository properties. Appl. Geochemistry. 2014;49:237–246.

[53] Appelo CAJ, Vinsot A, Mettler S, et al. Obtaining the porewater composition of a clay rock by modeling the in- and out-diffusion of anions and cations from an in-situ experiment. J. Contam. Hydrol. 2008;101(1–4):67–76.

[54] Fernández AM, Baeyens B, Bradbury MH, et al. Analysis of the porewater chemical composition of a Spanish compacted bentonite used in an engineered barrier. Phys. Chem. Earth, Parts A/B/C. 2004;29(1):105–118.

[55] Kozaki T, Sato H, Fujishima A, et al. Effect of dry density on activation energy for diffusion of strontium in compacted sodium montmorillonite. Material Resources Symposium Proceeding Volume 465 (Symposium II – Scienfific Basis for Nuclear Waste Management XX). 1997.p.893–900.

[56] Kozaki T, Liu J, Sato S. Diffusion mechanism of sodium ions in compacted montmorillonite under different NaCl concentration. Phys. Chem. Earth, Parts A/B/C. 2008;33(14–16):957–961.

[57] Bradbury MH, Baeyens B. Porewater chemistry in compacted re-saturated MX-80 bentonite. J. Contam. Hydrol. 2003;61(1–4):329–338.

[58] Bergaya F, Lagaly G. Chapter 1 General introduction: Clays, clay minerals, and clay science. In: Bergaya F, Theng BKG, Lagaly G, editors. Handbook of clay science. Elsevier; 2006.p.1–18.

[59] Scanlon BR, Andraski BJ, Bilskie J. Chapter 3.2.4 Miscellaneous methods for measuring matric or water potential. Methods of Soil Analysis: Part 4 Physical Methods. Soil Science Society of America; 2002.p.643–670.

[60] Serafeimidis K, Anagnostou G. The solubilities and thermodynamic equilibrium of anhydrite and gypsum. Rock Mech. Rock Eng. 2014;48(1):15–31.

[61] Torikai Y, Sato S, Ohashi H. Thermodynamic properties of water in compacted sodium montmorillonite. Nucl. Technol. 1996;115(1):73–80.

[62] Sato H. Thermodynamic model on swelling of bentonite buffer and backfill materials. Phys. Chem. Earth. 2008;33:538–543.

[63] Japan Nuclear Cycle Development Institute. H12: Project to establish the scientific and technical basis for HLW disposal in Japan, Supporting Report 2 Repository design and Engineering Technology. JNC TN1410 2000-003. Tokai: JNC; 2000. (JNC TN1410 2000-003).

[64] Shackelford CD. Diffusion as a transport process in fine-grained barrier materials. Geotech. News. 1998;6(2):24–27.

[65] Mazurek M, Alt-Epping P, Bath A, et al. Natural tracer profiles across argillaceous formations. Appl. Geochemistry. 2011;26(7):1035–1064.

[66] Grambow B. Mobile fission and activation products in nuclear waste disposal. J. Contam. Hydrol. 2008;102(3–4):180–186.

[67] Gimmi T, Leupin OX, Eikenberg J, et al. Anisotropic diffusion at the field scale in a 4-year multi-tracer diffusion and retention experiment – I: Insights from the experimental data. Geochim. Cosmochim. Acta. 2014;125:373–393.

[68] Kozaki T, Saito N, Fujishima A, et al. Activation energy for diffusion of chloride ions in compacted sodium montmorillonite. J. Contam. Hydrol. 1998;35(1–3):67–75.

[69] Molera M, Eriksen T, Jansson M. Anion diffusion pathways in bentonite clay compacted to different dry densities. Appl. Clay Sci. 2003;23(1–4):69–76.

[70] Van Loon LR, Glaus MA, Müller W. Anion exclusion effects in compacted bentonites: Towards a better understanding of anion diffusion. Appl. Geochemistry. 2007;22(11):2536–2552.

[71] Oscarson DW, Hume HB, Sawatsky NG, et al. Diffusion of iodide in compacted bentonite. Soil Sci. Soc. Am. J. 1992;56(5):1400–1406.

[72] Yukio Tachi, Kenji Yotsuji, Yoshimi Seida MY. Diffusion of cesium and iodine in compacted sodium montmorillonite under different saline conditions. Scientific Basis for Nuclear Waste Management XXXIII. Materials Research Society Proceeding. 2009.p.542–552.

[73] Tian W, Li C, Liu X, et al. The effect of ionic strength on the diffusion of ^{125}I in Gaomiaozi bentonite. J. Radioanal. Nucl. Chem. 2013;295(2):1423–1430.

[74] Ishidera T, Miyamotoy S, Sato H. Effect of sodium nitrate on the diffusion of Cl- and I- in compacted bentonite. J. Nucl. Sci. Technol. 2008;45(7):610–616.

[75] Aldaba D, Glaus MA, Van Loon LR, et al. Diffusion of radiosulphate and

radiocaesium in kaolinite clay (KGa-2): Testing the applicability of the pore water diffusion model. Appl. Geochemistry. 2017;86:84–91.

[76] Van Loon LR, Leupin OX, Cloet V. The diffusion of SO_4^{2-} in Opalinus Clay : Measurements of effective diffusion coefficients and evaluation of their importance in view of microbial mediated reactions in the near field of radioactive waste repositories. Appl. Geochemistry. 2018;95:19–24.

[77] Idemitsu K, Kozaki H, Yuhara M, et al. Diffusion behavior of selenite in purified bentonite. Prog. Nucl. Energy. 2016;92:279–285.

[78] Wigger C, Van Loon LR. Effect of the pore water composition on the diffusive anion transport in argillaceous, low permeability sedimentary rocks. J. Contam. Hydrol. 2018;213(September 2017):40–48.

[79] Wigger C, Kennell-Morrison L, Jensen M, et al. A comparative anion diffusion study on different argillaceous, low permeability sedimentary rocks with various pore waters. Appl. Geochemistry. 2018;92(September 2017):157–165.

[80] Appelo CAJ, Wersin P. Multicomponent diffusion modeling in clay systems with application to the diffusion of tritium, iodide, and sodium in Opalinus Clay. Environ. Sci. Technol. 2007;41(14):5002–5007.

[81] Appelo CAJ, Van Loon LR, Wersin P. Multicomponent diffusion of a suite of tracers (HTO, Cl, Br, I, Na, Sr, Cs) in a single sample of Opalinus Clay. Geochim. Cosmochim. Acta. 2010;74(4):1201–1219.

[82] Van Loon LR, Mibus J. A modified version of Archie's law to estimate effective diffusion coefficients of radionuclides in argillaceous rocks and its application in

safety analysis studies. Appl. Geochemistry. 2015;59:85–94.

[83] Chagneau A, Tournassat C, Steefel CI, et al. Complete restriction of $^{36}Cl^-$ diffusion by celestite precipitation in densely compacted illite. Environ. Sci. Technol. Lett. 2015;2(5):139–143.

[84] Wigger C, Van Loon LR. Importance of interlayer equivalent pores for anion diffusion in clay-rich sedimentary rocks. Environ. Sci. Technol. 2017;51(4):1998–2006.

[85] Leroy P, Revil A, Coelho D. Diffusion of ionic species in bentonite. J. Colloid Interface Sci. 2006;296(1):248–255.

[86] Shackelford CD, Moore SM. Fickian diffusion of radionuclides for engineered containment barriers: Diffusion coefficients, Porosities, And complicating issues. Eng. Geol. 2013;152(1):133–147.

[87] Zhang CL, Conil N, Armand G. Thermal effects on clay rocks for deep disposal of high-level radioactive waste. J. Rock Mech. Geotech. Eng. 2017;9(3):463–478.

[88] Bildstein O, Trotignon L, Perronnet M, et al. Modelling iron-clay interactions in deep geological disposal conditions. Phys. Chem. Earth. 2006;31(10–14):618–625.

[89] Savage D, Watson C, Benbow S, et al. Modelling iron-bentonite interactions. Appl. Clay Sci. 2010;47(1–2):91–98.

[90] Ito H, Miyasaka N, Kozaki T, et al. A study on hydraulic properties of compacted Fe(III)-montmorillonite. J. Nucl. Sci. Technol. 2010;47(11):1005–1010.

[91] Atkinson A, Everitt NM, Guppy RM. Time Dependence of pH in a Cementitious

Repository. Materials Research Society Symposium Proceedings. Cambridge University Press; 1988.p.439–446.

[92] Gaucher EC, Blanc P. Cement/clay interactions - A review: Experiments, natural analogues, and modeling. Waste Manag. 2006;26(7):776–788.

[93] Gaucher EC, Robelin C, Matray JM, et al. ANDRA underground research laboratory: Interpretation of the mineralogical and geochemical data acquired in the Callovian-Oxfordian formation by investigative drilling. Phys. Chem. Earth. 2004;29(1):55–77.

[94] Jenni A, Mäder U, Lerouge C, et al. In situ interaction between different concretes and Opalinus Clay. Phys. Chem. Earth. 2014;70–71:71–83.

[95] Gaboreau S, Prêt D, Tinseau E, et al. 15 years of in situ cement-argillite interaction from Tournemire URL: Characterisation of the multi-scale spatial heterogeneities of pore space evolution. Appl. Geochemistry. 2011;26(12):2159–2171.

[96] Sasamoto H, Yui M, Arthur RC. Status of geochemical modeling of groundwater evolution at the Tono in-situ tests site, Japan. Tokai: Japan Nuclear Cycle Development Institute; 1999. (JNC TN8400 99-074).

[97] Moyce EBA, Rochelle C, Morris K, et al. Rock alteration in alkaline cement waters over 15 years and its relevance to the geological disposal of nuclear waste. Appl. Geochemistry. 2014;50:91–105.

[98] Maher K, Bargar JR, Brown GE. Environmental speciation of actinides. Inorg. Chem. 2013;52(7):3510–3532.

[99] Stewart BD, Mayes MA, Scott Fendorf. Impact of Complexes on Uranium (VI)

Adsorption to Synthetic and Natural Sediments. Environ. Sci. Technol. 2010;44:928–934.

[100] Catalano JG, Brown GE. Uranyl adsorption onto montmorillonite: Evaluation of binding sites and carbonate complexation. Geochim. Cosmochim. Acta. 2005;69(12):2995–3005.

[101] Kitano Y, Oomori T. The coprecipitation of uranium with calcium carbonate. J. Oceanogr. Soc. Japan. 1971;27(1):34–42.

[102] Meece DE, Benninger LK. The coprecipitation of Pu and other radionuclides with $CaCO_3$. Geochim. Cosmochim. Acta. 1993;57(7):1447–1458.

[103] Hellebrandt SE, Hofmann S, Jordan N, et al. Incorporation of Eu(III) into calcite under recrystallization conditions. Sci. Rep. 2016;6:1–10.

[104] Curti E. Coprecipitation of radionuclides with calcite: estimation of partition coecients based on a review of laboratory investigations and geochemical data. Appl. Geochemistry. 1999;14:433–445.

[105] Zaoui A, Sekkal W. Can clays ensure nuclear waste repositories? Sci. Rep. 2015;5:1–5.

[106] Tartakovsky AM, Redden G, Lichtner PC, et al. Mixing-induced precipitation : Experimental study and multiscale numerical analysis. Water Resour. Res. 2008;44:1–19.

[107] Benjamin MM. Water Chemistry. Waveland Press; 2010.

[108] Gebauer D, Völkel A, Cölfen H. Supporting Materials: Stable prenucleation calcium carbonate clusters. Science. 2008;322(5909):1819–1822.

[109] Appelo CAJ, Postma D. Geochemistry, Groundwater and Pollution. 2nd Editio. London: A.A. Balkema Publishers; 2004.

[110] Gebauer D. Stable Prenucleation Calcium Carbonate Clusters. 2008;120(December):1819–1822.

[111] Gebauer D, Cölfen H. Prenucleation clusters and non-classical nucleation. Nano Today. 2011;6(6):564–584.

[112] Nielsen MH, Aloni S, De Yoreo JJ. In situ TEM imaging of CaCO<inf>3</inf> nucleation reveals coexistence of direct and indirect pathways. Science (80-.). 2014;345(6201):1158–1162.

[113] Plummer LN, Busenberg E. The solubilities of calcite, aragonite and vaterite in CO_2-H_2O solutions between 0 and 90°C, and an evaluation of the aqueous model for the system $CaCO_3$-CO_2-H_2O. Geochim. Cosmochim. Acta. 1982;46(6):1011–1040.

[114] Hull H, Turnbull AG. A thermochemical study of monohydrocalcite. Geochim. Cosmochim. Acta. 1973;37(3):685–694.

[115] Kralj D, Brečević L. Dissolution kinetics and solubility of calcium carbonate monohydrate. Colloids Surfaces A Physicochem. Eng. Asp. 1995;96(3):287–293.

[116] Bischoff JL, Fitzpatrick JA, Rosenbauer RJ. The Solubility and Stabilization of Ikaite ($CaCO_3.6H_2O$) from 0° to 25°C: Environmental and Paleoclimatic Implications for Thinolite Tufa. J. Geol. 1993;101(1):21–33.

[117] Clarkson JR, Price TJ, Adams CJ. Role of metastable phases in the spontaneous precipitation of calcium carbonate. J. Chem. Soc. Faraday Trans. 1992;88(2):243–

249.

[118] Brečević L, Nielsen AE. Solubility of amorphous calcium carbonate. J. Cryst. Growth. 1989;98(3):504–510.

[119] Kellermeier M, Picker A, Kempter A, et al. A straightforward treatment of activity in aqueous $CaCO_3$ solutions and the consequences for nucleation theory. Adv. Mater. 2014;26(5):752–757.

[120] Saripalli KP, Meyer PD, Bacon DH, et al. Changes in Hydrologic Properties of Aquifer Media Due to Chemical Reactions : A Review. Crit. Rev. Environ. Sci. Technol. 2001;31(4):311–349.

[121] Chagneau A, Claret F, Enzmann F, et al. Mineral precipitation-induced porosity reduction and its effect on transport parameters in diffusion-controlled porous media. Geochem. Trans. 2015;16(1):1–16.

[122] Mackenzie PD, Horney DP, Sivavec TM. Mineral precipitation and porosity losses in granular iron columns. J. Hazard. Mater. 1999;68(1–2):1–17.

[123] Stack AG. Precipitation in Pores : A Geochemical Frontier. Rev. Mineral. Geochemistry. 2015;80(1):165–190.

[124] Noiriel C, Daval D. Pore-Scale Geochemical Reactivity Associated with CO_2 Storage: New Frontiers at the Fluid-Solid Interface. Acc. Chem. Res. 2017;50(4):759–768.

[125] Jun YS, Kim D, Neil CW. Heterogeneous Nucleation and Growth of Nanoparticles at Environmental Interfaces. Acc. Chem. Res. 2016;49(9):1681–1690.

[126] De Yoreo JJ, Vekilov PG. Principles of crystal nucleation and growth. Rev.

Mineral. Geochemistry. 2003;54(1):57–93.

[127] Waychunas GA. In Situ Observations of Nanoparticle Early Development Kinetics at Mineral - Water Interfaces. 2010;44(21):8182–8189.

[128] Rijniers LA, Huinink HP, Pel L, et al. Experimental evidence of crystallization pressure inside porous media. Phys. Rev. Lett. 2005;94(7):23–26.

[129] Prieto M. Nucleation and supersaturation in porous media (revisited). Mineral. Mag. 2014;78(6):1437–1447.

[130] Stack AG, Fernandez-Martinez A, Allard LF, et al. Pore-size-dependent calcium carbonate precipitation controlled by surface chemistry. Environ. Sci. Technol. 2014;48(11):6177–6183.

[131] Nindiyasari F, Fernández-Díaz L, Griesshaber E, et al. Influence of gelatin hydrogel porosity on the crystallization of CaCO 3. Cryst. Growth Des. 2014;14(4):1531–1542.

[132] Gebrehiwet TA, Guo L, Fox D, et al. Precipitation of calcium carbonate and calcium phosphate under diffusion controlled mixing. Appl. Geochemistry. 2014;46:43–56.

[133] Gebrehiwet TA, Redden GD, Fujita Y, et al. The Effect of the CO_3^{2-} to Ca^{2+} Ion activity ratio on calcite precipitation kinetics and Sr^{2+} partitioning. Geochem. Trans. 2012;13(1):1.

[134] Stack AG. Next generation models of carbonate mineral growth and dissolution. 2014;288:278–288.

[135] Giammar DE, Wang F, Guo B, et al. Impacts of diffusive transport on carbonate

mineral formation from magnesium silicate-CO_2-water reactions. Environ. Sci. Technol. 2014;48(24):14344–14351.

[136] Gramling CM, Harvey CF, Meigs LC. Reactive transport in porous media: A comparison of model prediction with laboratory visualization. Environ. Sci. Technol. 2002;36(11):2508–2514.

[137] Shao H, Kulik DA, Berner U, et al. Modeling the competition between solid solution formation and cation exchange on the retardation of aqueous radium in an idealized bentonite column. Geochem. J. 2009;43(6):37–42.

[138] Acar YB, Alshawabkeh AN. Principles of Electrokinetic Remediation. Environ. Sci. Technol. 1993;27(13):2638–2647.

[139] Kim BK, Baek K, Ko SH, et al. Research and field experiences on electrokinetic remediation in South Korea. Sep. Purif. Technol. 2011;79(2):116–123.

[140] Dziubakiewicz EBB. Principles of Electromigration Techniques. In: Buszewski B, Dziubakiewicz E, Szumski M, editors. Electromigration Techniques : Theory and Practice. Heidelberg: Springer; 2013.p.5–26.

[141] Virkutyte J, Sillanpää M, Latostenmaa P. Electrokinetic soil remediation - Critical overview. Sci. Total Environ. 2002;289(1–3):97–121.

[142] Gingine V, Shah R, Venkata Koteswara RP, et al. A review on study of Electrokinetic stabilization of expansive soil. Int. J. Earth Sci. Eng. 2013;6(2):176–181.

[143] Maes N, Moors H, Dierckx A, et al. The assessment of electromigration as a new technique to study diffusion of radionuclides in clayey soils. J. Contam. Hydrol.

1999;36(3–4):231–247.

[144] Higashihara T, Kinoshita K, Sato S, et al. Electromigration of sodium ions and electro-osmotic flow in water-saturated, compacted Na-montmorillonite. Appl. Clay Sci. 2004;26(1–4):91–98.

[145] Gomes HI, Dias-Ferreira C, Ribeiro AB, et al. Enhanced transport and transformation of zerovalent nanoiron in clay using direct electric current. Water. Air. Soil Pollut. 2013;224(12):1–12.

[146] Yang J-S, Kwon MJ, Choi J, et al. The transport behavior of As, Cu, Pb, and Zn during electrokinetic remediation of a contaminated soil using electrolyte conditioning. Chemosphere. 2014;117C:79–86.

[147] Kim C, Choi S, Shin M. Review—Electro-Kinetic Decontamination of Radioactive Concrete Waste from Nuclear Power Plants. J. Electrochem. Soc. 2018;165(9):E330–E344.

[148] André M, Malmström ME, Neretnieks I. Determination of sorption properties of intact rock samples: new methods based on electromigration. J. Contam. Hydrol. 2009;103(3–4):71–81.

[149] Löfgren M, Neretnieks I. Through-electromigration: a new method of investigating pore connectivity and obtaining formation factors. J. Contam. Hydrol. 2006;87(3–4):237–252.

[150] Tanaka S, Noda N, Higashihara T, et al. Kinetic behavior of water as migration media in compacted montmorillonite using $H_2{}^{18}O$ and applying electric potential gradient. Phys. Chem. Earth, Parts A/B/C. 2008;33:S163–S168.

[151] Tanaka S, Noda N, Sato S, et al. Electrokinetic study of migration of anions, cations, and water in water-saturated compacted sodium montmorillonite. J. Nucl. Sci. Technol. 2011;48(3):454–462.

[152] Higashihara T, Kinoshita K, Akagi Y, et al. Transport number of sodium ions in water-saturated, compacted Na-montmorillonite. Phys. Chem. Earth, Parts A/B/C. 2008;33:S142–S148.

[153] Beauwens T, De Cannière P, Moors H, et al. Studying the migration behaviour of selenate in Boom Clay by electromigration. Eng. Geol. 2005;77(3–4):285–293.

[154] Deman J. Precipitation during Electromigration of Ions. 1970;42(3):321–324.

[155] Cao C-X, Fan L, Zhang W. Review on the theory of moving reaction boundary, electromigration reaction methods and applications in isoelectric focusing and sample pre-concentration. Analyst. 2008;133:1139–1157.

[156] Tanaka S. Gypsum precipitation enhanced by electrokinetic method and porewater chemistry in compacted montmorillonite. Appl. Clay Sci. 2018;161:482–493.

[157] Shackelford CD. Laboratory diffusion testing for waste disposal - A review. J. Contam. Hydrol. 1990;7:177–217.

[158] Bourg IC, Tournassat C. Chapter 6 - Self-Diffusion of Water and Ions in Clay Barriers. In: Tournassat C, Steefel CI, Bourg IC, et al., editors. Natural and Engineered Clay Barriers. Elsevier; 2015.p.189–226.

[159] Crank J. The mathematics of diffusion. 2nd ed. Oxford: Clarendon Press; 1975.

[160] Kozaki T, Sato H, Sato S, et al. Diffusion mechanism of cesium ions in compacted montmorillonite. Eng. Geol. 1999;54:223–230.

2. Calcium carbonate precipitation in compacted bentonite using electromigration reaction method and its application to estimate the ion activity coefficient in the porewater

2.1. Introduction

Geological disposal is recognized as safe and secure means to dispose of high-level radioactive waste [1]. It requires multiple safety functions to isolate radionuclides in the waste forms from the biosphere [2]. A multi-barrier approach consisting of a series of engineered and natural barriers is adopted to contain the waste for a long period of time. Compacted bentonite is one part of the engineered barrier system, which is expected to provide the protection for the waste forms from the physical and chemical processes and to limit the rate of transport of radionuclides that may be released from the waste forms.

In the actual radioactive waste disposal facilities, perturbation of bentonite buffer may occur over time due to interactions with the surrounding materials. One of the potential perturbations is $CaCO_3$ precipitation [3,4]. Cementitious materials are used in the structure of radioactive waste repository, and the leachate from them is rich with Ca^{2+} ions [3,5]. This leachate may also raise the pH of the surrounding environment and promote rock alteration that results in the release of CO_3^{2-} ions [6]. The reaction of these two ions can generate $CaCO_3$ precipitates, which may affect the transport of radionuclides by porosity clogging [5,7,8] and/or incorporation of radionuclides in the precipitates [9,10]. Although $CaCO_3$ precipitation has been studied extensively in bulk solution [11,12] and in porous media [13–16], little is known about its behavior in compacted bentonite.

Montmorillonite, which is the major component of bentonite clays, has two types of pore spaces: interlayer space which is filled with interlayer water containing cations to compensate the excess negative charge of montmorillonite layers, and interparticle space which is filled with free porewater [17–20]. Due to the negative charge of montmorillonite layers, anions, including HCO_3^-/CO_3^{2-} ions, are excluded from the interlayer space, thus the precipitation of $CaCO_3$ is expected to occur only in the interparticle space where both Ca^{2+} and CO_3^{2-} ions can be present in the porewater. Moreover, concentrations of ions in the interparticle porewater are also heterogeneous due to electric double layer effect. The ion activity product of Ca^{2+} and CO_3^{2-} may not be high enough to form $CaCO_3$ precipitates near the surface of the clay, and as a result, precipitation preferentially occurs in larger pores [15,21]. Micro-scale porewater chemistry controls the precipitation of $CaCO_3$ in compacted bentonite, or reversely, analysis of the conditions under which precipitation takes place in compacted bentonite may provide insight into micro-scale porewater chemistry.

Studying the porewater chemistry in compacted bentonite is challenging because it is difficult to directly analyze it in-situ, and to sample it without potential alteration [22]. Experimental data of porewater composition have been obtained by water sampling with borehole instrumentation [23], extraction using squeezing techniques [24], liquid displacement with a solution of known composition [25]. These data are often complemented with geochemical modelling assuming that the dissolved ions in porewater have the same activity coefficients as in bulk water [25–29]. However, it has been reported that the porewater behaves like solutions with high ionic strength due to interactions between the ions in porewater and montmorillonite surfaces [30]. This contradicts with the basic assumption that the ionic strength in compacted bentonite

system is the same as in bulk water, and the lack of quantitative understanding on the activities of the ions in porewater in compacted bentonite system is limiting the advance of the discussion on migration behaviors and chemical reactions of ions.

The objective of this study is to determine the activity coefficients of dissolved ions in the porewater of compacted montmorillonite using $CaCO_3$ precipitation processes as an indicator of activities of reacting ions. Electrokinetic method was used to enhance the migration of reacting ions because the hydraulic conductivity in compacted bentonite is very low (less than 10^{-11} m/s). This method has been used to study radionuclides migration [31–34] and gypsum ($CaSO_4$) precipitation in compacted bentonite [35]. Under the electrical potential gradient, Ca^{2+} ions migrate towards the cathode side while HCO_3^- /CO_3^{2-} ions migrate towards the anode side in the opposite direction. As the process continues, $CaCO_3$ precipitates are produced by a chemical reaction between Ca^{2+} and HCO_3^-/CO_3^{2-} ions when the solution is oversaturated with respect to $CaCO_3$ precipitates. A sequential extraction method was developed to separately quantify cations in the porewater in ionic forms from the precipitates in the solid phase. Activity coefficients were estimated assuming that after precipitation, the ionic activity product (IAP) is equal to the solubility product (K_{sp}).

2.2. Method

2.2.1. Materials

Kunipia F (Kunimine Industries Co., Tokyo, Japan), which contains more than 95% montmorillonite, was used as a starting bentonite material. All chemicals used in this study were of analytical grade (Junsei Chemical Co., Tokyo, Japan). Deionized water

was prepared using EYELA Still Ace SA-2100E1 (Tokyo Rikakikai Co., Tokyo, Japan). The radioisotopes $^{45}CaCl_2$ and $NaH^{14}CO_3$ (PerkinElmer, Boston, USA) were obtained from Japan Radioisotope Association.

2.2.2. Preparation of Saturated Compacted Na-Bentonite

Kunipia F was purified to obtain a homoionized Na-montmorillonite with particle size between 75 and 150 μm using the method described in detail elsewhere [36]. Compacted Na-montmorillonite was prepared to have the dry density of 1.0 kg/dm^3 in acrylic resin cells with both inner diameter and length of 20 mm. The one end of the inner cylindrical cell was closed with stainless steel sintered filter having a pore size of 2 μm. Dry homoionized Na-bentonite was weighed to have a predetermined density and was placed into the cell from the other open end. A pressure was applied to pack the bentonite powder in the inner cylinder of the acrylic cell, then the open end was closed with the stainless-steel filter. The cells containing compacted bentonite sample were immersed in 0.7 M $NaHCO_3$ solution in a closed container for 30 days at room temperature and atmospheric pressure.

2.2.3. Electromigration Experiment

The saturated sample was subjected to electromigration to enhance the migration of Ca^{2+} and HCO_3^-/CO_3^{2-} ions in compacted montmorillonite so that they form precipitate $CaCO_3$. The experimental setup is shown in Figure 2-1. The sample was set in a sample holder between the anode and the cathode reservoir containing 1 M $CaCl_2$ and 0.7 M $NaHCO_3$, respectively. Saturated $ZnSO_4$ solution and salt bridges were used so that the

electrolysis cell is separated from the bentonite sample in order to avoid the water electrolysis effect.

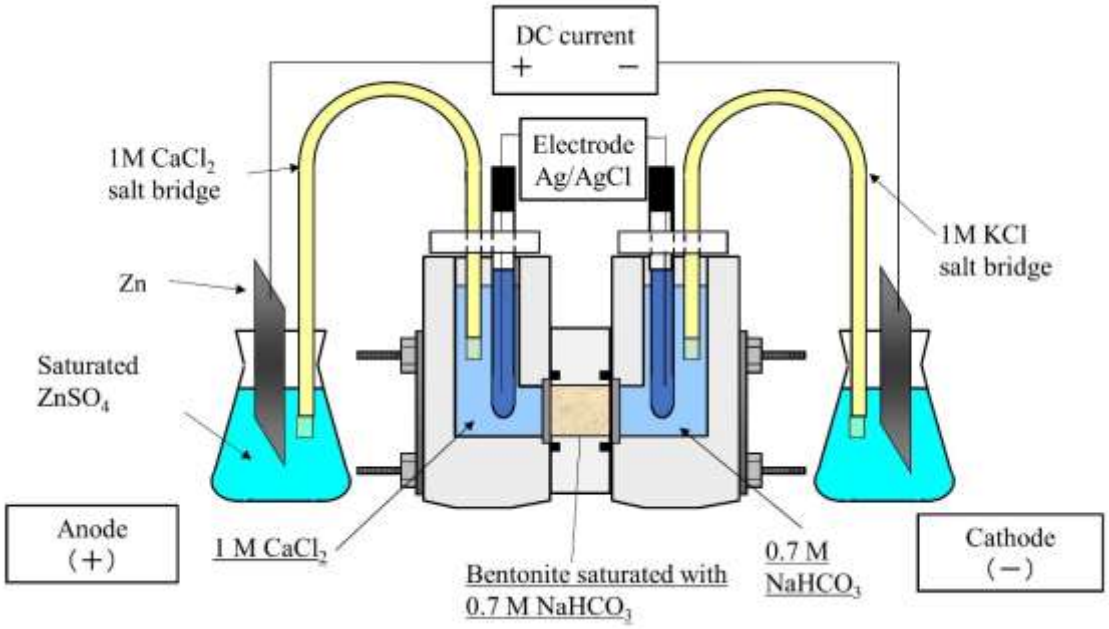

Figure 2-1. Schematic electromigration experiment set up.

Three kinds of electromigration experiments were carried out, using ^{45}Ca, ^{14}C, and without tracers, respectively, to obtain the concentration profiles of Ca and C (HCO_3^- /CO_3^{2-}) in the sample after migration and precipitation reaction. The solution used in the electromigration experiment for each tracer is summarized in Table 2-1. Prior to electromigration, the initial specific radioactivities (cpm/mmol) in the reservoir solutions were measured by radiation measurement. Then, an electric potential gradient was applied at a constant current of 5 mA at 298 K for 16 hours. The experiment was performed three times under the same experimental conditions. After the electromigration

experiment, the acrylic cell was disassembled, and the bentonite sample was sliced to 0.5 mm thickness. The sliced montmorillonite samples were analyzed by sequential extraction, X-ray diffraction (XRD), and Scanning Electron Microscope equipped with Energy Dispersive X-ray Spectroscope (SEM/EDS).

Table 2-1. Tracers and Solutions used in the electromigration experiment.

Experiment Number	Tracer	Solution		
		Solution used to saturate the compacted Na-bentonite	Anolyte	Catholyte
Experiment 1	^{45}Ca	0.7 M $NaHCO_3$	1 M $^{45}CaCl_2$	0.7 M $NaHCO_3$
Experiment 2	^{14}C	0.7 M $NaH^{14}CO_3$	1 M $CaCl_2$	0.7 M $NaH^{14}CO_3$
Experiment 3	-	0.7 M $NaHCO_3$	1 M $CaCl_2$	0.7 M $NaHCO_3$

2.2.4. Sequential extraction of Ca

A sequential extraction procedure was developed to determine the concentrations of Ca in solution and in solid phase separately: Ca^{2+} ions dissolved as free ions in porewater, and Ca in the solid phase either as exchangeable cations in the interlayer of bentonite or as $CaCO_3$ precipitates. The first extraction used saturated $CaCO_3$ solution to only extract the free Ca^{2+} ions without dissolving $CaCO_3$ precipitates. The second extraction used 1 M HCl to target the remaining Ca fractions in the solid phase in the interlayer of montmorillonite and in $CaCO_3$ precipitates.

Prior to using this method with the samples after the electromigration experiment, recoveries of the Ca^{2+} ions in porewater and in the interlayer of montmorillonite were tested. Saturated $CaCO_3$ solution was prepared by stirring $CaCO_3$ powder in deionized water for 1 day at room temperature and atmospheric pressure. The resulting solution was filtered with a 0.45 μm membrane (Advantec, Tokyo, Japan) prior to use. Suspensions of 0.25 g dry Ca-bentonite and 1 ml $CaCl_2$ solution was prepared with a known radioactivity distribution of $^{45}Ca^{2+}$ as free and as exchangeable ions. They were mixed with 10 ml saturated $CaCO_3$ solution and shaked for 1 hour, then the supernatant was collected after centrifuging at 10,000 rpm (12,000 g) for 10 minutes. Extraction with 10 ml saturated $CaCO_3$ solution was repeated one more time, similarly the supernatant was collected. After saturated $CaCO_3$ solution was removed, 10 ml of 1 M HCl were added to the sample and mixed in a shaker for 24 hours. The supernatant was then collected by centrifuging the sample at 10,000 rpm (12,000 g) for 10 minutes. The extraction with 1 M HCl was repeated one more time as well. Each of the supernatants was then ultra-filtered (USY-1 MWCO 10,000, Advantec, Tokyo, Japan) to remove colloidal particles of bentonite prior to radiation measurement of the $^{45}Ca^{2+}$ radioactivities with Aloka AccuFlex LSC-8000 (Hitachi, Tokyo, Japan). The recovery tests were conducted in duplicate.

This sequential extraction was applied to each of the sliced bentonite samples from experiment 1 which used ^{45}Ca as a tracer. The concentration of Ca^{2+} ions were calculated using the ratio of the $^{45}Ca^{2+}$ radioactivities in the filtrates to the initial specific radioactivities previously determined by radiation measurement.

2.2.5. Concentration profiles of other ions

The same supernatant from sequential extraction in experiment 1 was subjected to ICP-AES measurement (ICPE-9000, Shimadzu, Kyoto, Japan) to determine the concentration of Na^+ ions. Each of the sliced bentonite samples was mixed with 10 ml deionized water for 30 minutes in a closed bottle at room temperature and atmospheric pressure. The pH of the slurry was measured using a glass electrode (Laqua F-72, Horiba, Kyoto, Japan).

Free and total $H^{14}CO_3^-/^{14}CO_3^{2-}$ concentrations were determined by extraction with saturated $CaCO_3$ solution and 0.5 M $NaHCO_3$, respectively. The total $H^{14}CO_3^-/^{14}CO_3^{2-}$ concentrations were checked with direct measurement of the ^{14}C radioactivities. The sliced bentonite sample from experiment 2 with ^{14}C was divided into two. A portion of each was added with 5 ml saturated $CaCO_3$ solution and 0.5 M $NaHCO_3$, then they are mixed in a shaker for 1 and 24 hour, respectively. Centrifugation, filtration, and measurement of the concentration of $H^{14}CO_3^-/^{14}CO_3^{2-}$ was carried out with the same procedure for $^{45}Ca^{2+}$.

2.2.6. XRD and SEM/EDS Analysis

XRD analysis was carried out to get the information about the polymorph of $CaCO_3$ precipitates. Sliced bentonite samples from experiment 3 without tracers were vacuum dried at 378K and then ground into powder with mortar and pestle. The XRD analyses of the powdered samples were conducted using Rigaku RU-300 X-ray diffractometer with Cu Kα radiation (Rigaku, Tokyo, Japan). The scanning range was 2θ = 5 to 80 degrees with a step scan 0.05 and scanning speed of 1 s per scan.

The deposit of $CaCO_3$ precipitates was analyzed with a SEM/EDS. A portion of sliced bentonite sample from experiment 3 without tracers was placed onto a piece of double-sided carbon tape on a SEM stub. The morphology and elemental mapping for Si, Ca, Al, Mg and Na on sliced bentonite samples were observed in perpendicular to the electromigration direction using JSM-7001FA (JEOL, Tokyo, Japan) with beam energy of 15 kV.

2.3. Results

2.3.1. Sequential extraction test

Table 2-2 summarizes the result of the tested sequential extraction. The recoveries of the free $^{45}Ca^{2+}$ ions in the solution phase from the first and second extraction were 92.9 and 1.3% in average, respectively. Majority of $^{45}Ca^{2+}$ ions were extracted in the first extraction with saturated $CaCO_3$ solution. The amount of $^{45}Ca^{2+}$ extracted in the first extraction can be approximated as the free ions in the porewater. The recoveries of extraction of exchangeable $^{45}Ca^{2+}$ ions by HCl was 97.1% in average. This result shows that only free Ca^{2+} ions were extracted in the first extraction with saturated $CaCO_3$ solution, while exchangeable $^{45}Ca^{2+}$ ions remained in the interlayer of montmorillonite. Therefore, the proposed sequential extraction can be applied to distinctly determine the amount of $^{45}Ca^{2+}$ ions in the liquid and in the solid phase.

Table 2-2. Recoveries of free and exchangeable $^{45}Ca^{2+}$ ions in sequential extraction.

Sample	$^{45}Ca^{2+}$ radioactivities (cpm)		Recovery (%)		
	1st batch	2nd batch	1st batch	2nd batch	Average
$^{45}Ca^{2+}$ aqueous	35864	35820			
$^{45}Ca^{2+}$ solid	48096	48540			
Extraction by saturated $CaCO_3$ solution					
1st	33037	33532	92.1	93.6	92.9
2nd	457	484	1.3	1.4	1.3
Total	33493	34016	93.4	95.0	94.2
Extraction by 1 M HCl					
1st	45570	45780	94.7	94.3	94.5
2nd	1383	1070	2.9	2.2	2.5
Total	46953	46850	97.6	96.5	97.1

2.3.2. Spatial distribution of ions in bentonite after the electromigration

Temporal spatial distribution of dissolved and solid phase of Ca^{2+} and Na^{+} ions in compacted bentonite was determined by the sequential extraction method after 16 hours electromigration experiment and is depicted in Figure 2-2**.** Initially before the electromigration experiment, only Na^{+} ions existed as both free and exchangeable cations all through the sample. Once the electromigration starts, these Na^{+} ions were attracted by the negatively charged electrode in the cathode side and started to migrate towards the cathode side. On the other hand, Ca^{2+} ions entered the compacted bentonite from the reservoir $^{45}CaCl_2$ solution on the anode side. Consequently, through these transport processes, the initially existed Na^{+} ions in the bentonite sample were progressively replaced from the anode side towards the cathode side by the incoming Ca^{2+} ions.

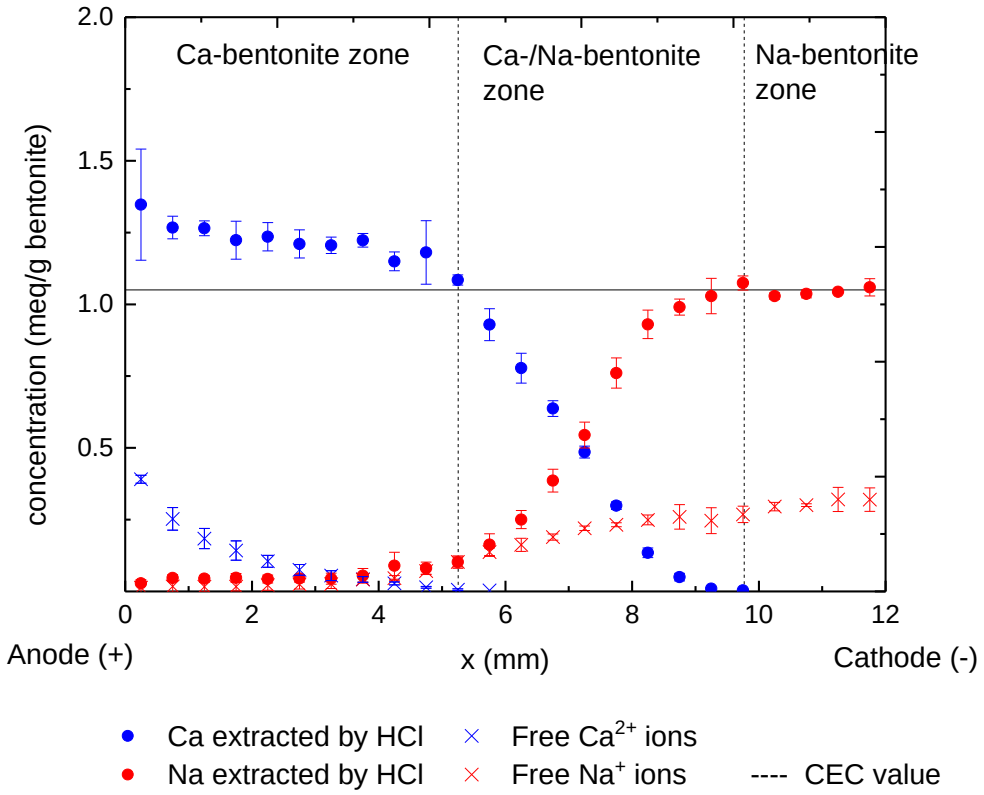

Figure 2-2. Spatial distribution of Ca^{2+} and Na^{+} ions in compacted montmorillonite after 16 hours of electromigration experiment. The free Ca^{2+} and Na^{+} ions are their respective concentration from extraction with saturated $CaCO_3$ solution. The figure has the plotting concentrations (meq/g-dry bentonite) per sliced bentonite sample versus the position of the distance of the center of each slice from the anode side. The acid extractable Ca^{2+} and Na^{+} from sequential extraction are the concentration of Ca^{2+} and Na^{+} ions as exchangeable cations and solid phases. The horizontal straight line is the CEC value of bentonite sample which equals 1.05 meq/g-dry bentonite. The error bars are calculated from the standard deviation of average value in triplicate experiments.

Acid extractable cations, which represent the sum of the ions in the interlayer and in precipitates, show that the compacted bentonite sample can be divided into three zones based on their exchangeable cation composition. The left part of Figure 2-2, from 0 to 5.25 mm distance from the anode side, is the zone where almost all of the exchangeable Na^+ ions initially existed in the interlayer of bentonite were replaced by Ca^{2+} ions (hereafter Ca-bentonite zone). The zone in the center of the compacted bentonite from 5.25 to 9.75 mm distance from the anode side has the mixture of Ca-bentonite and Na-bentonite (hereafter Ca-/Na-bentonite zone). Finally, the right part of Figure 2-2, from 9.75 mm towards the cathode side, is where the interlayer of bentonite contains only Na^+ ions (hereafter Na-bentonite zone). This zone remained as a Na-bentonite type unchanged from initial state. The maximum amount of Ca^{2+} ions which can occupy the interlayer of bentonite is equal to the CEC value (1.05 meq/g-dry bentonite [35]). Therefore, the concentration of acid extractable Ca^{2+} ions which exceed the CEC value by approximately 0.25 meq/g-dry bentonite in the Ca-bentonite zone is the evidence of the presence of $CaCO_3$ precipitates.

The spatial distribution of HCO_3^-/CO_3^{2-} in aqueous and solid phase is shown in Figure 2-3. The solid phase HCO_3^-/CO_3^{2-}, which is likely $CaCO_3$ precipitates, was present in the Ca-bentonite zone and in the mixture of Ca-/Na- bentonite zone. The concentration of precipitates in the Ca-bentonite zone was approximately 0.12 mmol/g-dry bentonite, which is consistent with the excess of acid extractable Ca^{2+} ions shown previously in Figure 2-2. A sharp decrease of $CaCO_3$ precipitates profile can be seen in the Ca/Na-bentonite zone, suggesting this zone exhibits the precipitation reaction front, where $CaCO_3$ is first formed. The concentration of free HCO_3^-/CO_3^{2-} in the Ca-bentonite zone decreased to almost zero because it was consumed by the incoming Ca^{2+} to produce

$CaCO_3$ precipitates. However, the profile in Na-bentonite zone shows that it also has been depleted although no precipitation occurred in this zone because Ca ions had not arrived yet. The plausible explanation is that the electromigration velocity of HCO_3^-/CO_3^{2-} is lower than the electroosmotic flow which made them migrate to the cathode side even with their negative charge. Another possibility is that a part of HCO_3^-/CO_3^{2-} ions migrated to the cathode side as neutral $NaHCO_3$ ions. However, discussion for this dynamic process requires additional experimental data and it is beyond the scope of the discussion in this paper.

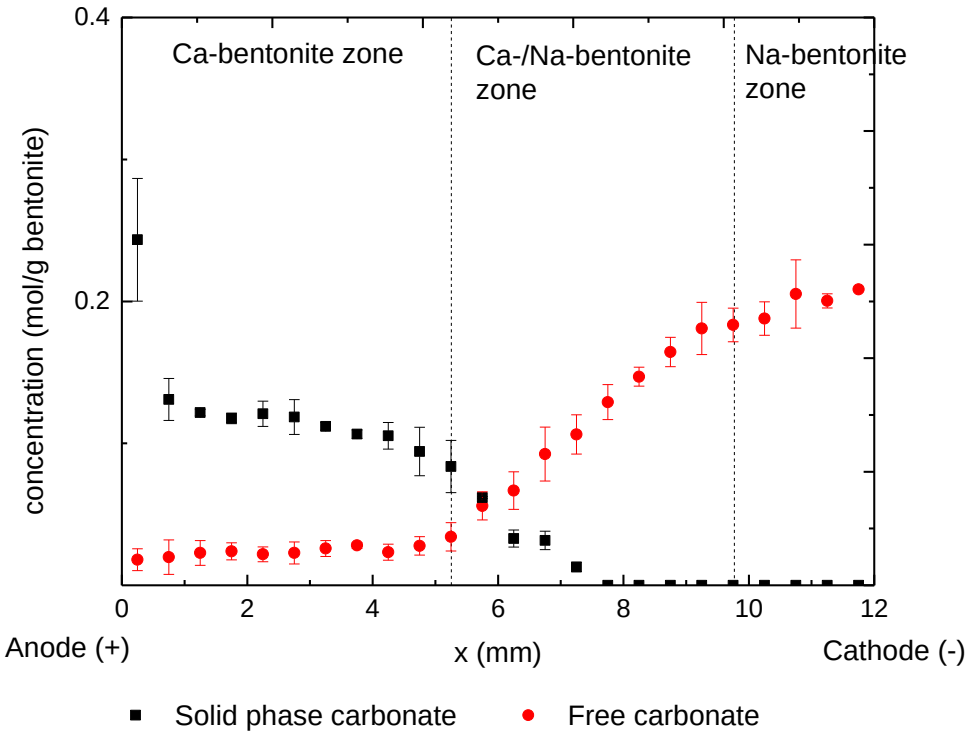

Figure 2-3. Spatial distribution of carbonate as free ions and solid phase in compacted bentonite after 16 hours of electromigration.

2.3.3. pH profile

Figure 2-4 shows the spatial pH profile of dispersed sliced bentonite in deionized water. A peak in the Ca-/Na-bentonite zone could be attributed to the dissolution of amorphous $CaCO_3$ precipitates when the sliced bentonite is dispersed in water. Indeed, the $CaCO_3$ precipitates in this zone should be in more disordered phase than in the Na-bentonite zone because it is closer to the reaction front. From x = 7.75 mm distance towards the cathode side, the pH gradually increases which in line with the profile of free HCO_3^-/CO_3^{2-} ions shown previously in Figure 2-3.

.

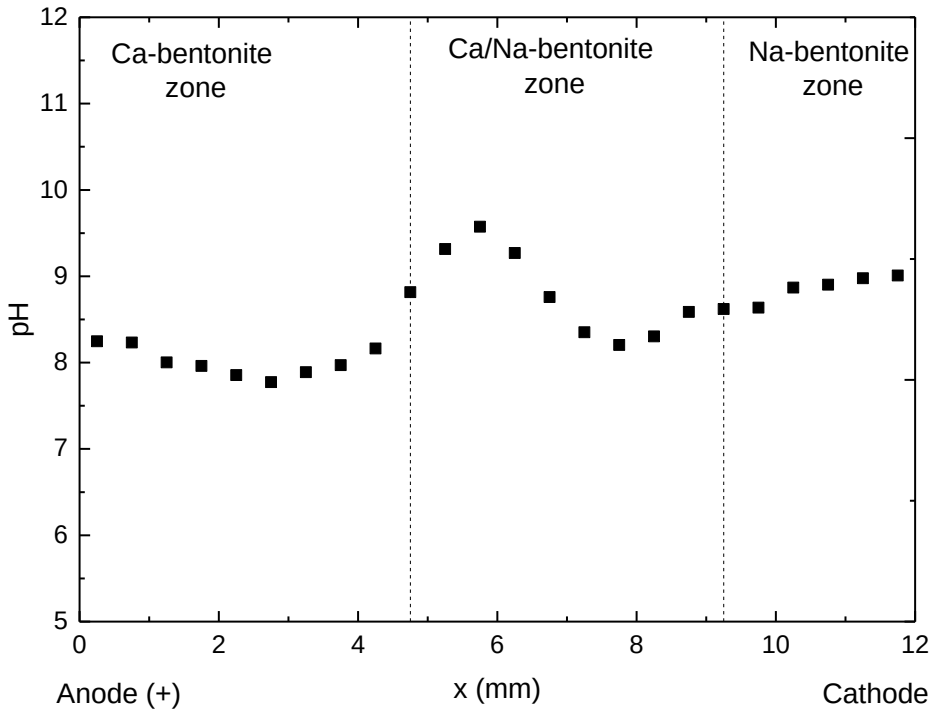

Figure 2-4. Spatial distribution of pH of sliced bentonite sample dispersed in 10 ml deionized water.

2.4.1. XRD and SEM-EDS analysis

Figure 2-5 shows SEM/EDS images of bentonite sample from the initial condition. Figure 2-6 and Figure 2-7 show SEM/EDS images sliced bentonite sample after the experiment at x = 3.25 and x = 7.75 mm, respectively, as a representative of Ca-bentonite and Ca-/Na-bentonite zone. Ca-rich areas, shown by the bright spots in Ca-map image, were not observed in the Ca-map image of initial bentonite sample (Figure 2-5). In contrast, Ca-rich areas sparsely distributed in bentonite were observed after the experiment (Figure 2-6 and Figure 2-7). These results clearly confirm that the electromigration experiment generates the $CaCO_3$ precipitates. The diameter of the Ca-rich area from the Ca-map image was approximately 2 μm. The Si, Al, and Mg-map images show that these elements were also detected in the Ca-rich areas, suggesting that the Ca-rich areas contained a mixture of $CaCO_3$ precipitates and bentonite.

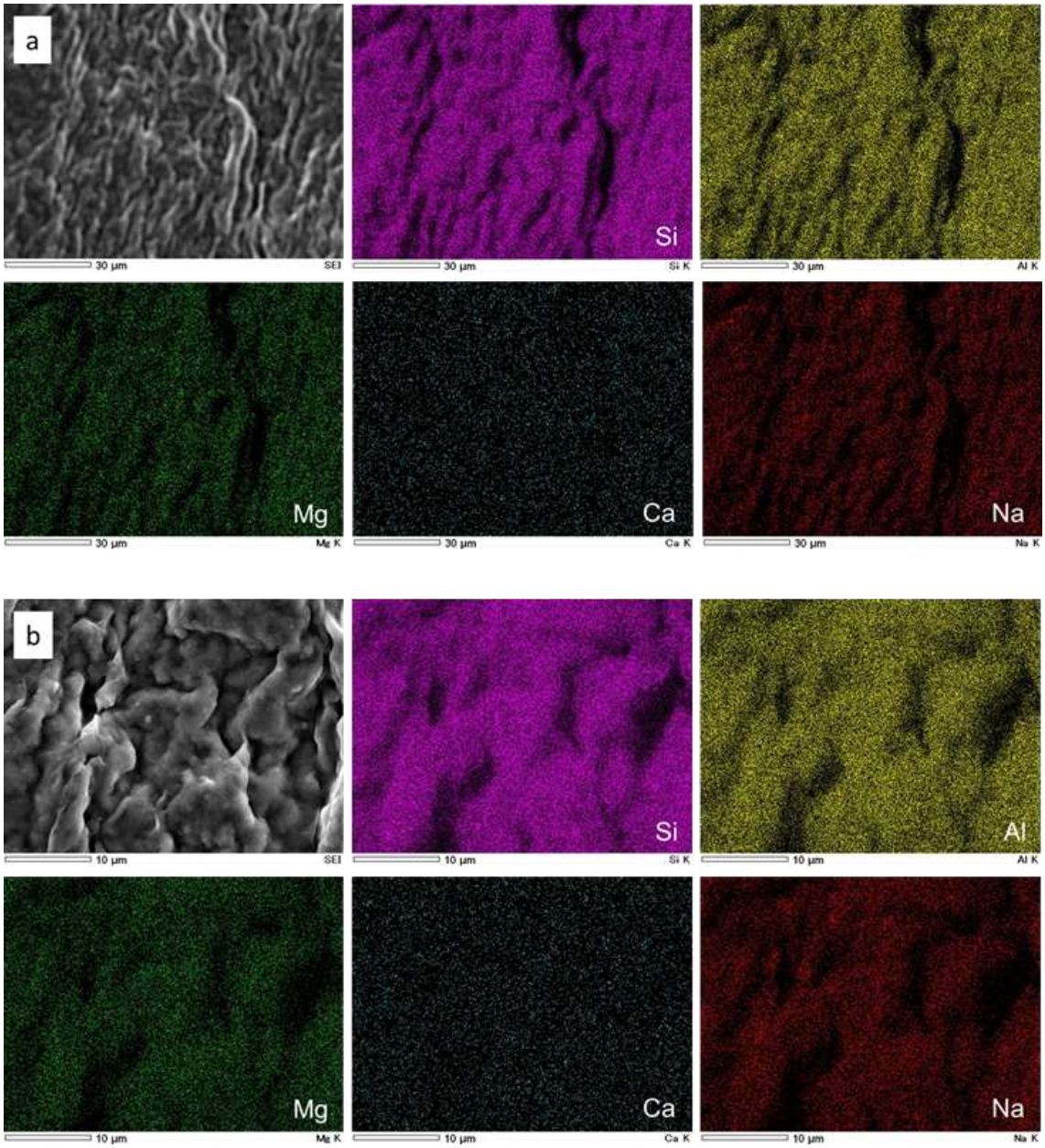

Figure 2-5. SEM/EDS images of initial bentonite sample in different closed-view positions.

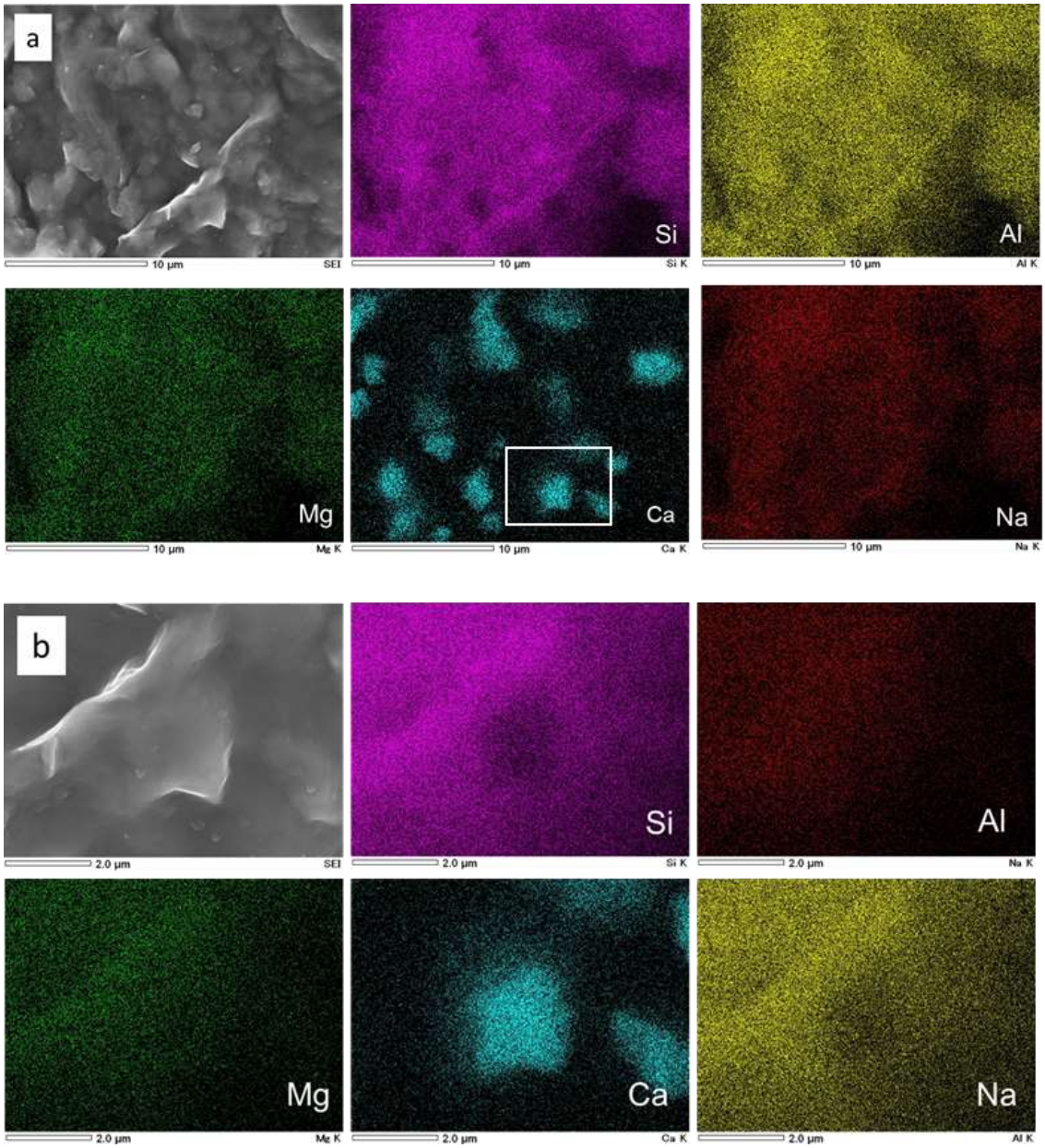

Figure 2-6. SEM/EDS images of sliced bentonite sample at x = 3.25 mm with magnification of 5000 (a) and 15000 times (b). The (b) image is magnification of an area of white square in the image (a). The bright spots in Ca-map in the images show rich areas with relatively higher concentration of Ca.

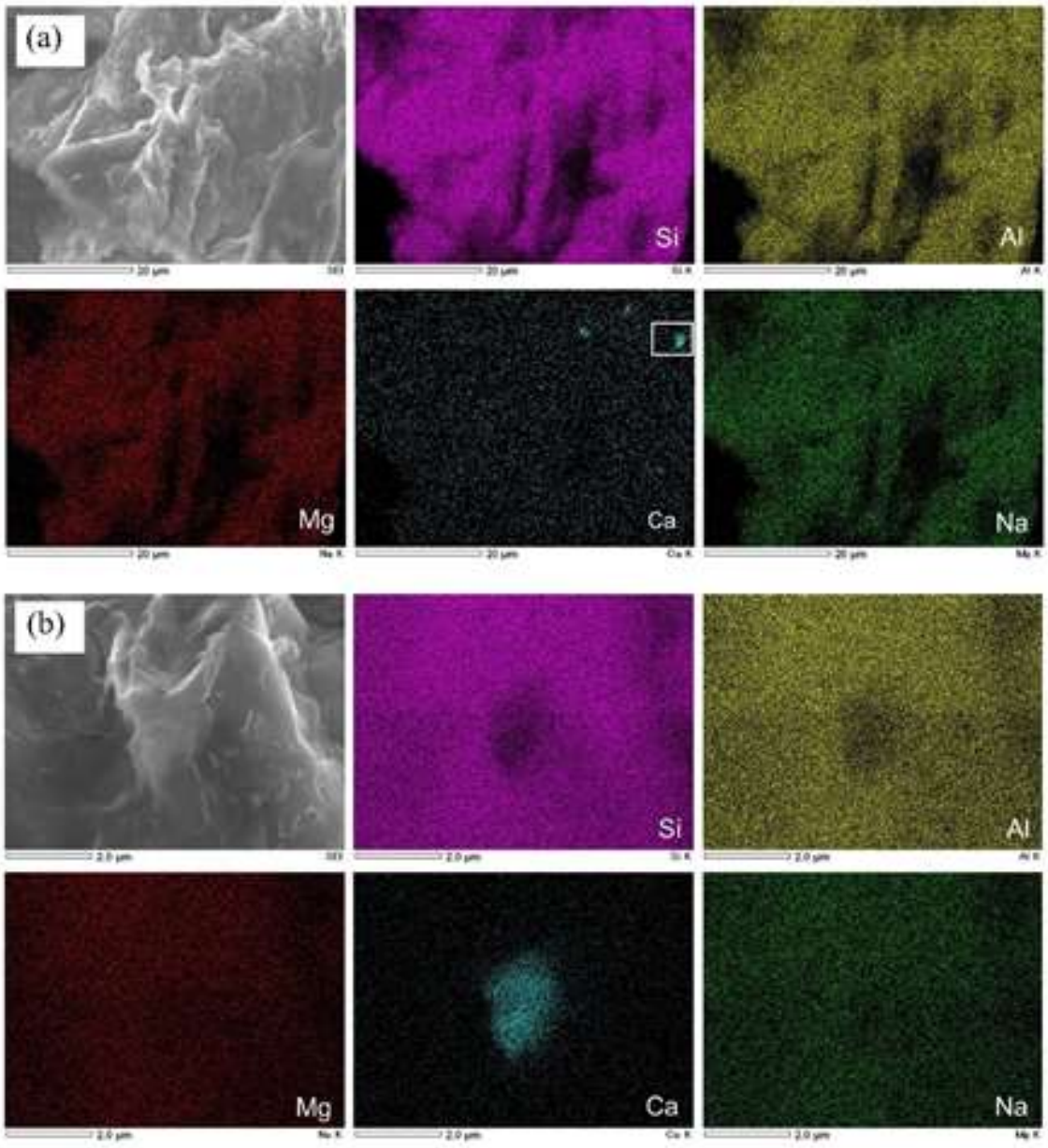

Figure 2-7. SEM/EDS images of sliced bentonite sample at x = 7.75 mm with magnification of 2200 (a) and 15000 times (b). The (b) image is magnification of an area of white square in the image (a). The bright spots in Ca-map in the images show rich areas with relatively higher concentration of Ca.

Figure 2-8 shows the diffraction pattern of powder sample of sliced bentonite at x = 0.5 mm after the experiment. The occurrence of the $CaCO_3$ precipitates at this point has been confirmed in the above explained spatial distribution of Ca^{2+} and HCO_3^-/CO_3^{2-}. However, the diffraction pattern of the sliced bentonite sample agreed well with the reference Ca-bentonite peaks, and the peaks of calcite, the most stable crystalline $CaCO_3$, cannot be distinctly observed. This result suggests that the $CaCO_3$ precipitates formed after the electromigration experiment are amorphous, thus did not exhibit sharp diffraction peaks, while the crystalline phase of $CaCO_3$ might not have been attained in the experiment.

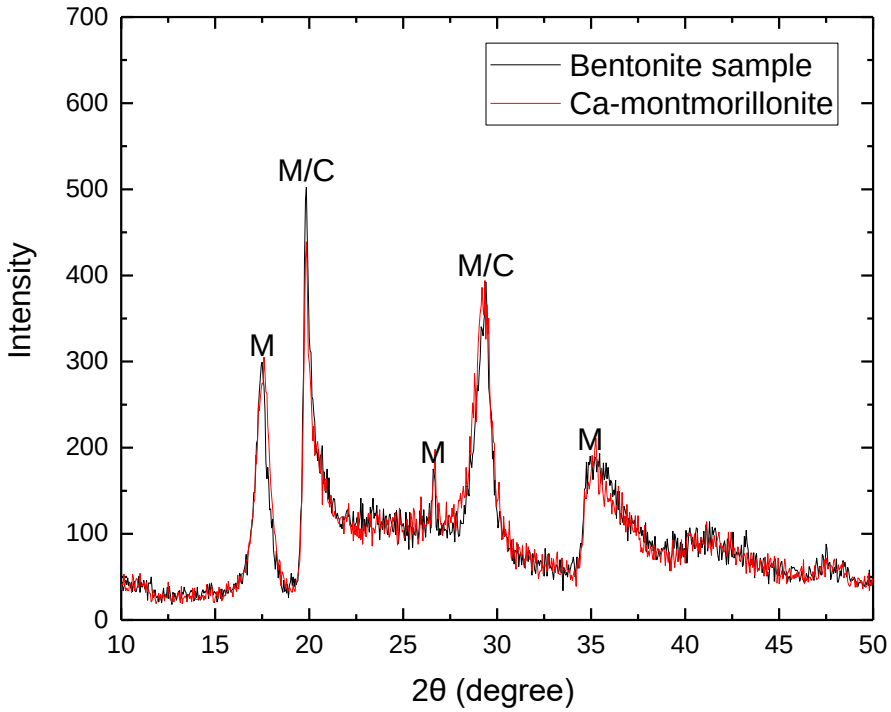

Figure 2-8. X-ray diffraction patterns of bentonite sample at x = 0.5 mm distance from the anode side after the electromigration experiment compared with Ca-bentonite (M: Ca-montmorillonite, C: calcite).

2.4. Discussion

2.4.1. Estimation of mean activity coefficient from electromigration experiment

After $CaCO_3$ precipitated, the porewater should be in equillibrium with respect to $CaCO_3$ precipitates. It implies that the IAP of Ca^{2+} and CO_3^{2-} is equal to the K_{sp} of $CaCO_3$ precipitates when assuming the activity of solid phase $CaCO_3$ is unity, expressed by:

$$IAP = [Ca^{2+}]\gamma_{Ca^{2+}} \left[CO_3{}^{2-}\right] \gamma_{CO_3{}^{2-}} = K_{sp\ CaCO_3} \quad (2\text{-}1)$$

where $[Ca^{2+}]$ and $[CO_3^{2-}]$ are the concentration of Ca^{2+} and CO_3^{2-} ions, respectively, $\gamma_{Ca^{2+}}$ and $\gamma_{CO_3{}^{2-}}$ are their respective activity coefficients.

According to Equation (2-1), the mean activity coefficients ($\gamma_{\pm}$) of Ca^{2+} and CO_3^{2-} ions can be directly obtained once the concentrations of Ca^{2+} and CO_3^{2-} ions, and the value of $K_{sp\ CaCO_3}$ are known. For this purpose, recalculation of the concentrations of Ca^{2+} and CO_3^{2-} ions expressed in units per dry weight of bentonite to molarity in porewater is necessary. An important issue for this calculation is the distribution of water types for estimation of the fraction of porewater in water-compacted bentonite system. The porewater fraction for compacted bentonite with dry density of 1.0 kg/dm^3 was reported to be 0.36 ml/g dry bentonite [18]. The recalculation of the concentration of CO_3^{2-} ions is, however, not as straightforward as Ca^{2+} ions since the speciation of HCO_3^- /CO_3^{2-} depend on the pH value. For this consideration, the concentration of CO_3^{2-} ions is calculated in a range of pH value for dispersed bentonite in water measured in this study.

The value for K_{sp} depends on the mineral type and the temperature. There are six $CaCO_3$ polymorphs: calcite, aragonite, vaterite, monohydrocalcite ($CaCO_3 \cdot H_2O$), ikaite

($CaCO_3 \cdot 6H_2O$) and amorphous $CaCO_3$ with the solubility decreasing from the former to the latter [37–41]. Of these $CaCO_3$ polymorphs, the SEM/EDS images and diffraction patterns results strongly suggest that the amorphous $CaCO_3$ is the most likely candidate polymorph. Recent study also reported that precipitation of $CaCO_3$ occurred via amorphous $CaCO_3$ as a pre-nucleation [12]. Moreover, confinement effect could stabilize amorphous $CaCO_3$ [42]. The amorphous phase was also often used as solubility-limiting solid phase in the calculation of radionuclides solubilities and speciation for a conservative estimation [43,44]. The commonly employed K_{sp} value of amorphous $CaCO_3$ is $10^{-6.4}$ [40]. However, recent study reported that the value is $10^{-7.54}$ which is about an order of magnitude lower than the previously reported. The author reasoned that the previously higher K_{sp} value might be due to the polyamorphism of $CaCO_3$ [45]. Therefore, those two K_{sp} values are used in the mean activity coefficient calculation.

The small pore effect could make the value of the K_{sp} value higher than in bulk solution [46,47]. The pore size effect to the value of K_{sp} can be estimated as [15,48]:

$$\frac{K_{sp_{pore}}}{K_{sp_{bulk}}} = exp\left(\frac{2\,V_m\,\gamma_{sl}}{RTr}\right) \qquad (2\text{-}2)$$

where V_m is the molar volume of the precipitates (m^3/mol), γ_{sl} is the interfacial free energy (J/m^2), R is the ideal gas constant (J/mol·K), T is the absolute temperature (K), and r is the radius of the pore (m). Using $V_m = 3.69 \times 10^{-5}$ m^3/mol which calculated from calcite density = 2.645 g/cm^3 , γ_{sl} = 0.094 J/m^2 [49], and r = 15.9 nm from the average pore spacing of compacted bentonite at dry density of 1.0 kg/dm^3 [18], the solubility of $CaCO_3$ in the porewater should be increased by a factor of 1.2. This value corresponds to a

saturation index of 0.08 which means that the small pore effect to the value of $K_{sp\ CaCO_3}$ in the porewater under the experimental conditions can be neglected.

Based thereon, the $\gamma_{\pm}$ values in the porewater are estimated and the resulting values are shown in Figure 2-9. The values are estimated for the porewater composition in the precipitation zone at x = 5.25 and 5.75 mm. Beyond x = 5.75 mm the concentration of free Ca^{2+} ions were below detection limit, thus the $\gamma_{\pm}$ values cannot be obtained. Figure 2-9 also shows the theoretical approximation of $\gamma_{\pm}$ values for a direct comparison with the experimental result. The theoretical $\gamma_{\pm}$ values are obtained from the average of individual activity coefficients of Ca^{2+} and CO_3^{2-} ions which calculated using PHREEQC code [50]. The equilibrium constants used for speciation calculation are listed in Table 2-3. Note that the concentration of free ions corresponding to the ionic strength of the porewater after the electromigration experiment are different than that of the initial condition. The theoretical $\gamma_{\pm}$ values are different depending on the location because the ionic strength of the porewater after the experiment is not spatially uniform. Nonetheless, it is evident that the experimentally determined $\gamma_{\pm}$ values within the range of pH under the experimental conditions are smaller than the theoretical values approximately by a factor of three and eight, using K_{sp} value of $10^{-6.4}$ and $10^{-7.54}$, respectively.

Table 2-3. Equilibrium constant for speciation calculation at a temperature of 298 K [50].

Reaction	Log K
$Ca^{2+} + H_2O \leftrightarrow Ca(OH)^+ + H^+$	-12.78
$Ca^{2+} + CO_3^{2-} \leftrightarrow CaCO_3^0$	3.224
$Ca^{2+} + CO_3^{2-} + H^+ \leftrightarrow CaHCO_3^+$	11.435
$CO_2 + H_2O \leftrightarrow HCO_3^- + H^+$	-6.352
$HCO_3^- \leftrightarrow CO_3^{2-} + H^+$	-10.329
$Na^+ + CO_3^{2-} \leftrightarrow NaCO_3^-$	1.27
$Na^+ + HCO_3^- \leftrightarrow NaHCO_3$	-0.25
$Na^+ + H_2O \leftrightarrow NaOH + H^+$	-14.18

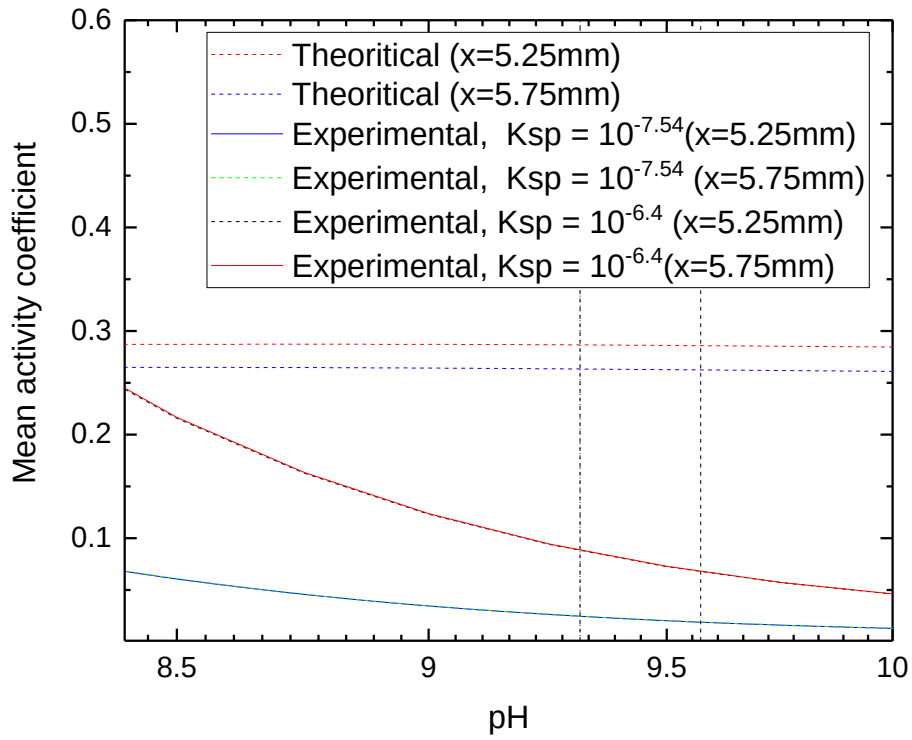

Figure 2-9. Experimentally determined and theoretical mean activity coefficients calculated using PHREEQC code in the porewater at x = 5.25 and 5.75 mm. The vertical dash lines are the pH of dispersed bentonite in deionized water which were obtained from the experiment.

2.4.2. Porewater chemistry in bentonite

In line with previous studies [30,51], the lower activity coefficient than the theoretical approximation could be attributed to the interaction of the bentonite surface with the porewater. Therefore, the ions in the porewater experience stronger coulombic interactions than in the bulk water. For example, previous study reported that the activity of the porewater becomes less than unity when the total water content is less than 0.40 [52]. On the other hand, the results of this study show that such deviation was found for dissolved Ca^{2+} and CO_3^{2-} ions in bentonite with total water content of 0.65, which corresponds to the dry density of 1.0 kg/dm^3 used in this study. This difference is possibly because of the charged ions experiencing stronger effects of the bentonite surface than water molecules and/or the difference in ionic strength of the porewater. Nevertheless, this result confirms that the activity coefficient in the porewater is significantly lower than that in free water.

The fact that the experimental value of activity coefficient in the porewater is lower than the theoretical approximation has important implications in the safety assessment for radioactive waste geological disposal. For example, lower activity coefficient directly related to higher solubilities of radionuclides in the porewater. The solubilities of radionuclides are the source term for modelling fate and transport of radionuclides through engineered barriers. Knowing the solubilities of key radionuclides is one of the most important issues for performance assessment [53]. The activity coefficient also has deeper impact in transport, chemical speciation and reaction in bentonite. Therefore, further reexamination of activity coefficient approximation in the

porewater is critical for safety assessment in engineered barrier of radioactive waste disposal.

2.5. Conclusions

The precipitation of $CaCO_3$ in compacted Na-bentonite with dry density of 1.0 kg/dm^3 from counter diffusion of Ca^{2+} and HCO_3^-/CO_3^{2-} ions enhanced by electrokinetic method were successfully achieved. The sequential extraction developed in this study provide a practical method to distinguish the free Ca^{2+}ions from the exchangeable and precipitates species. After the experiment, the Na-bentonite sample changed to three different types: Ca-, Ca-/Na-, and Na-bentonite. The occurrence of $CaCO_3$ precipitates was observed in the Ca- and Ca-/Na-bentonite zone. SEM/EDS images and X-ray diffraction patterns suggested that the $CaCO_3$ precipitates was likely amorphous phase. The experimentally determined mean activity coefficients of Ca^{2+} and CO_3^{2-} were at least smaller by a factor of three than the theoretical approximation. This result raised the importance of reexamination of the activity coefficient in the porewater, because it is a critical parameter in safety assessment of geological disposal.

2.6. References

[1] Japan Atomic Energy Agency, The Federation of Electric Power Companies of Japan. Second progress report on research and development for TRU waste disposal in japan − repository design, safety assessment and means of implementation in the generic phase. Tokai: JAEA; 2007. (JAEA-Review 2007-010).

[2] International Atomic Energy Agency. Disposal of radioactive waste: Specific safety requirements. Vienna: IAEA; 2011. (IAEA Safety Standards Series No. SSR-5).

[3] Tinseau E, Bartier D, Hassouta L, et al. Mineralogical characterization of the Tournemire argillite after in situ interaction with concretes. Waste Manag. 2006;26(7):789–800.

[4] Gaucher EC, Blanc P. Cement/clay interactions - A review: Experiments, natural analogues, and modeling. Waste Manag. 2006;26(7):776–788.

[5] Jenni A, Mäder U, Lerouge C, et al. In situ interaction between different concretes and Opalinus Clay. Phys. Chem. Earth. 2014;70–71:71–83.

[6] Moyce EBA, Rochelle C, Morris K, et al. Rock alteration in alkaline cement waters over 15 years and its relevance to the geological disposal of nuclear waste. Appl. Geochemistry. 2014;50:91–105.

[7] Steefel CI, Lichtner PC. Diffusion and reaction in rock matrix bordering a hyperalkaline fluid-filled fracture. Geochim. Cosmochim. Acta. 1994;58(17):3595–3612.

[8] Gaboreau S, Prêt D, Tinseau E, et al. 15 years of in situ cement-argillite interaction from Tournemire URL: Characterisation of the multi-scale spatial heterogeneities of pore space evolution. Appl. Geochemistry. 2011;26(12):2159–2171.

[9] Smith KF, Bryan ND, Swinburne AN, et al. U(VI) behaviour in hyperalkaline calcite systems. Geochim. Cosmochim. Acta. 2015;148:343–359.

[10] Hellebrandt SE, Hofmann S, Jordan N, et al. Incorporation of Eu(III) into calcite under recrystallization conditions. Sci. Rep. 2016;6:1–10.

[11] Morse JW, Arvidson RS, Lüttge A. Calcium carbonate formation and dissolution. Chem. Rev. 2007;107(2):342–381.

[12] Gebauer D, Völkel A, Cölfen H. Supporting Materials: Stable prenucleation calcium carbonate clusters. Science. 2008;322(5909):1819–1822.

[13] Tartakovsky AM, Redden G, Lichtner PC, et al. Mixing-induced precipitation : Experimental study and multiscale numerical analysis. Water Resour. Res. 2008;44:1–19.

[14] Redden G, Fox D, Zhang C, et al. $CaCO_3$ precipitation, transport and sensing in porous media with in situ generation of reactants. Environ. Sci. Technol. 2014;48(1):542–549.

[15] Stack AG, Fernandez-Martinez A, Allard LF, et al. Pore-size-dependent calcium carbonate precipitation controlled by surface chemistry. Environ. Sci. Technol. 2014;48(11):6177–6183.

[16] Genovese D, Montalti M, Otálora F, et al. Role of $CaCO_3$° neutral pair in calcium carbonate crystallization. Cryst. Growth Des. 2016;16(8):4173–4177.

[17] Bourg IC, Bourg ACM, Sposito G. Modeling diffusion and adsorption in compacted bentonite: A critical review. J. Contam. Hydrol. 2003;61(1–4):293–302.

[18] Kozaki T, Inada K, Sato S, et al. Diffusion mechanism of chloride ions in sodium montmorillonite. J. Contam. Hydrol. 2001;47(2–4):159–170.

[19] Van Loon LR, Glaus MA, Müller W. Anion exclusion effects in compacted bentonites: Towards a better understanding of anion diffusion. Appl. Geochemistry. 2007;22(11):2536–2552.

[20] Glaus MA, Frick S, Rossé R, et al. Comparative study of tracer diffusion of HTO, $^{22}Na^{+}$ and $^{36}Cl^{-}$ in compacted kaolinite, illite and montmorillonite. Geochim. Cosmochim. Acta. 2010;74(7):1999–2010.

[21] Stack AG. Precipitation in Pores : A Geochemical Frontier. Rev. Mineral. Geochemistry. 2015;80(1):165–190.

[22] Tournassat C, Vinsot A, Gaucher EC, et al. Chapter 3 - Chemical conditions in clay-rocks. In: Tournassat C, Steefel CI, Bourg IC, et al., editors. Natural and Engineered Clay Barriers. Amsterdam (Netherlands): Elsevier; 2015.p.71–100.

[23] Vinsot A, Mettler S, Wechner S. In situ characterization of the Callovo-Oxfordian pore water composition. Phys. Chem. Earth. 2008;33:S75–S86.

[24] Muurinen A. Development and testing of analysis methods for bentonite porewater. Helsinki: Posiva Oy; 2001. (Working Report 2001-07).

[25] Grambow B, Landesman C, Ribet S. Nuclear waste disposal: I. Laboratory simulation of repository properties. Appl. Geochemistry. 2014;49:237–246.

[26] Fernández AM, Baeyens B, Bradbury MH, et al. Analysis of the porewater chemical composition of a Spanish compacted bentonite used in an engineered barrier. Phys. Chem. Earth, Parts A/B/C. 2004;29(1):105–118.

[27] Appelo CAJ, Vinsot A, Mettler S, et al. Obtaining the porewater composition of a clay rock by modeling the in- and out-diffusion of anions and cations from an in-situ experiment. J. Contam. Hydrol. 2008;101(1–4):67–76.

[28] Fernández AM, Sánchez-Ledesma DM, Tournassat C, et al. Applying the squeezing technique to highly consolidated clayrocks for pore water characterisation: Lessons learned from experiments at the Mont Terri Rock Laboratory. Appl. Geochemistry. 2014;49:2–21.

[29] Tachi Y, Ochs M, Suyama T. Integrated sorption and diffusion model for bentonite. Part 1: clay–water interaction and sorption modeling in dispersed systems. J. Nucl. Sci. Technol. 2014;51(10):1177–1190.

[30] Torikai Y, Sato S, Ohashi H. Thermodynamic properties of water in compacted sodium montmorillonite. Nucl. Technol. 1996;115(1):73–80.

[31] Maes N, Moors H, Dierckx A, et al. The assessment of electromigration as a new technique to study diffusion of radionuclides in clayey soils. J. Contam. Hydrol. 1999;36(3–4):231–247.

[32] Higashihara T, Kinoshita K, Sato S, et al. Electromigration of sodium ions and electro-osmotic flow in water-saturated, compacted Na-montmorillonite. Appl. Clay Sci. 2004;26(1–4):91–98.

[33] Beauwens T, De Cannière P, Moors H, et al. Studying the migration behaviour of

selenate in Boom Clay by electromigration. Eng. Geol. 2005;77(3–4):285–293.

[34] Tanaka S, Noda N, Sato S, et al. Electrokinetic study of migration of anions, cations, and water in water-saturated compacted sodium montmorillonite. J. Nucl. Sci. Technol. 2011;48(3):454–462.

[35] Tanaka S. Gypsum precipitation enhanced by electrokinetic method and porewater chemistry in compacted montmorillonite. Appl. Clay Sci. 2018;161:482–493.

[36] Kozaki T, Fujishima A, Sato S, et al. Self-diffusion of sodium ions in compacted sodium montmorillonite. Nucl. Technol. 1998;121(1):63–69.

[37] Plummer LN, Busenberg E. The solubilities of calcite, aragonite and vaterite in CO_2-H_2O solutions between 0 and 90°C, and an evaluation of the aqueous model for the system $CaCO_3$-CO_2-H_2O. Geochim. Cosmochim. Acta. 1982;46(6):1011–1040.

[38] Hull H, Turnbull AG. A thermochemical study of monohydrocalcite. Geochim. Cosmochim. Acta. 1973;37(3):685–694.

[39] Kralj D, Brečević L. Dissolution kinetics and solubility of calcium carbonate monohydrate. Colloids Surfaces A Physicochem. Eng. Asp. 1995;96(3):287–293.

[40] Brečević L, Nielsen AE. Solubility of amorphous calcium carbonate. J. Cryst. Growth. 1989;98(3):504–510.

[41] Clarkson JR, Price TJ, Adams CJ. Role of metastable phases in the spontaneous precipitation of calcium carbonate. J. Chem. Soc. Faraday Trans. 1992;88(2):243–249.

[42] Wang Y, Zeng M, Meldrum FC, et al. Using confinement to study the

crystallisation pathway of calcium carbonate. Cryst. Growth Des. 2017;17(12):6787–6792.

[43] Takeda S, Shima S, Kimura H, et al. The aqueous solubility and speciation analysis for uranium, neptunium and selenium by the geochemical code (EQ3/6). Tokai: JAERI; 1995. (JAERI Research 95-069).

[44] Kim SS, Baik MH, Kang KC, et al. Solubilities of actinides in a domestic groundwater and a bentonite porewater calculated by using PHREEQC. J. Ind. Eng. Chem. 2008;14(6):739–746.

[45] Kellermeier M, Picker A, Kempter A, et al. A straightforward treatment of activity in aqueous $CaCO_3$ solutions and the consequences for nucleation theory. Adv. Mater. 2014;26(5):752–757.

[46] Rijniers LA, Huinink HP, Pel L, et al. Experimental evidence of crystallization pressure inside porous media. Phys. Rev. Lett. 2005;94(7):23–26.

[47] Prieto M. Nucleation and supersaturation in porous media (revisited). Mineral. Mag. 2014;78(6):1437–1447.

[48] De Yoreo JJ, Vekilov PG. Principles of crystal nucleation and growth. Rev. Mineral. Geochemistry. 2003;54(1):57–93.

[49] Stumm W, Morgan JJ. Aquatic chemistry: Chemical equilibria and rates in natural waters. 3rd ed. New York (NY): Wiley; 1995.

[50] Parkhurst DL, Appelo CAJ. Description of input and examples for PHREEQC version 3--A computer program for speciation, batch-reaction, one-dimensional transport, and inverse geochemical calculations. Denver (CO): U.S. Geological

Survey; 2013.

[51] Serafeimidis K, Anagnostou G. The solubilities and thermodynamic equilibrium of anhydrite and gypsum. Rock Mech. Rock Eng. 2014;48(1):15–31.

[52] Sato H. Thermodynamic model on swelling of bentonite buffer and backfill materials. Phys. Chem. Earth. 2008;33:538–543.

[53] McKinley IG, Savage D. Comparison of solubility databases used for HLW performance assessment. J. Contam. Hydrol. 1996;21(1–4):335–350.

3. Migration behavior of Ca^{2+} and carbonate ions in compacted bentonite under electrical potential gradient

3.1. Introduction

Geological disposal is considered to be the safe and reasonable method to dispose of high-level radioactive waste since it has an ability to isolate the waste from geosphere for long-term [1,2]. The performance of the isolation of geological repository relies on the multi barrier systems, which are composed of engineered and natural barriers. Compacted bentonite is expected as buffer material in the engineered barriers due to its favorable properties, such as high sorption capacity for radionuclides, high swelling ability, and good durability [3–8]. However, the properties of bentonite may be altered over time due to interaction with surrounding materials in the repository, resulting in lower performance as a barrier [8,9].

Cementitious materials are considered as one of the important alteration sources which can interact with the compacted bentonite. Large quantities of cementitious materials which are used for tunnel construction in the repository will release alkali cations, such as K^+, Na^+, and Ca^{2+} ions, to groundwater [10,11]. Chemical reaction between bentonite and this leachate of alkali cations will lead to the mineralogical changes of bentonite over long-period of time [12]. The leachate is also able to promote considerable amount of $CaCO_3$ precipitates in compacted bentonite due to reaction with CO_3^{2-} ions which can be provided from the groundwater [13]. The $CaCO_3$ precipitation at the interface of cement and bentonite has been studied not only in laboratory experiment [14,15], but also in the field study [16,17].

The $CaCO_3$ precipitation may affect the fate and transport of radionuclides in bentonite. For examples, the precipitation limits the concentration of Ca^{2+} and HCO_3/CO_3^{2-} ions in the porewater of bentonite. For some important radionuclides, their chemical speciation, and so in turn their mobilities, are affected by the concentration of Ca^{2+} and HCO_3/CO_3^{2-} ions [18,19]. The formation of $CaCO_3$ precipitates in bentonite may also affect the transport of radionuclides by porosity clogging [20–22] and coprecipitation [23–26]. Furthermore, molecular dynamics study suggests that the mechanical strength of bentonite decrease in the bentonite-$CaCO_3$ system [27]. Despite this importance, however, no study on $CaCO_3$ precipitation in bentonite has been reported.

Precipitation of $CaCO_3$ in porous media has been studied in well mixed, homogenous and non-reactive systems, such as a column filling with glass beads. Even in the idealized systems, many factors are potentially affect the $CaCO_3$ precipitation processes, including pore size, precipitation kinetics and transport of ions [28]. For examples, the study on $CaCO_3$ precipitation in glass beads revealed that the precipitation preferentially occurs in larger pores [29], which may be caused by the high ratio of Ca^{2+} to CO_3^{2-} ions in the solution due to the effect of negatively surface charge [28,30,31]. On the other hand, the study on $CaCO_3$ precipitation in gelatin gel suggested that smaller pores lead to the formation of smaller size of $CaCO_3$ crystal with more complex morphology and tend to have aggregates rather than a single crystal [32]. The study on $CaCO_3$ precipitation in polyacrylamide gel formed by diffusion mixing suggested that slower rate of $CaCO_3$ precipitation is needed to explain the relatively wider precipitation zone in the experiment than that is predicted by simulation [33].

The objective of this study is to investigate the transport of ions in compacted bentonite during the precipitation of $CaCO_3$. Two kinds of electromigration experiments

were carried out. The first experiment was using thin-layer $^{45}Ca^{2+}$ and $H^{14}CO_3/^{14}CO_3^{2-}$ radiotracer sources to determine electromigration parameters of individual Ca^{2+} and HCO_3/CO_3^{2-} ions. The second experiment was carried out using the same method as in Chapter 2 to form $CaCO_3$ precipitation in compacted bentonite. The Ca^{2+} ions from the anode reservoir were introduced to compacted bentonite sample initially saturated with a solution containing HCO_3^-/CO_3^{2-} ions. The reaction occurred as the two ions come in contact in bentonite, forming $CaCO_3$ precipitates. The experiments were carried out at different duration times, after which the spatial distributions of ions in bentonite sample were determined. The dynamics of reaction front of the $CaCO_3$ precipitation in compacted bentonite under was investigated and the transport of Ca^{2+} and HCO_3/CO_3^{2-} as the reacting ions during the precipitation were discussed.

3.2. Method

3.2.1. Preparation of Saturated Compacted Na-Bentonite

Kunipia F (Kunimine Industries Co., Tokyo, Japan) was mixed with 1 M NaCl to obtain a homoionized Na-bentonite. The excess salt was removed by dialysis method in deionized water. The detailed procedure is described elsewhere [34]. Dry Na-bentonite with particle size 75-150 μm was packed in an acrylic resin cells with both inner diameter and length of 20 mm to have the dry density of 1.0 kg/dm^3. Each one end of the inner cylindrical cell was closed with stainless steel sintered filter having a pore size of 2 μm. The cells containing compacted bentonite sample were immersed in 0.7 M $NaHCO_3$ solution in a closed container for 30 days at room temperature and atmospheric pressure.

3.2.2. Determination of electromigration parameters of Ca^{2+} and HCO_3^-/CO_3^{2-} ions

Electromigration experiments were carried out to determine the electromigration parameters of $^{45}Ca^{2+}$ and $H^{14}CO_3^-/^{14}CO_3^{2-}$ ions. The experimental setup is similar to that described in Chapter 2 and in another study [35]. In this study, a small amount of each $^{45}Ca^{2+}$ and $H^{14}CO_3^-/^{14}CO_3^{2-}$ solution was spiked as radiotracers uniformly to each one end of the two samples of compacted bentonite. The four compacted bentonite samples were then assembled into arrangement as illustrated in Figure 3-1. These samples were placed between the anode and cathode reservoir containing 0.1 M KCl. An electric potential gradient was applied at a constant current of 15 mA at 298 K for 6 hours. After the electromigration experiment, the compacted bentonite sample was removed from the acrylic cell and was cut into 0.5 mm-thick slices oriented perpendicular to the electromigration direction. Each slice of the bentonite sample was then mixed with scintillation cocktail solution (PerkinElmer). The concentrations of $^{45}Ca^{2+}$ and $H^{14}CO_3^-/^{14}CO_3^{2-}$ ions in each slice were determined by radioactivity measurement for the ^{45}Ca and ^{14}C radioactivities with Aloka AccuFlex LSC-8000 (Hitachi, Tokyo, Japan).

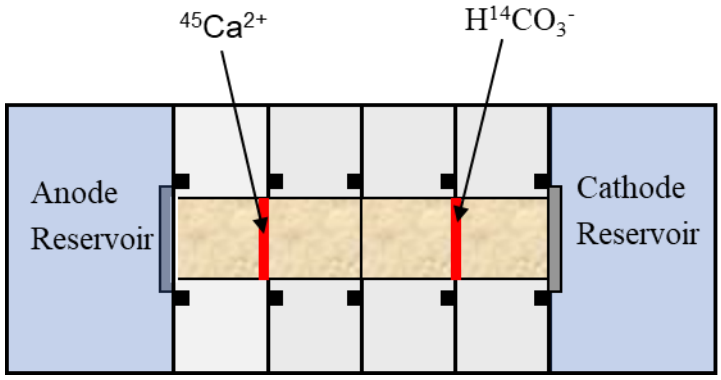

Figure 3-1. Schematic tracer arrangement

The spatial distribution of Ca^{2+} and HCO^{3-}/CO_3^{2-} ions at a certain time in electromigration experiment can be expressed by the one-dimensional advection dispersion equation as follows [35,36]:

$$C_r = \frac{1}{2\sqrt{\pi D_h t}} exp\left\{-\frac{(x-V_a t)^2}{4D_h t}\right\} \quad (3\text{-}1)$$

where C_r is the relative concentration, D_h is the hydrodynamic dispersion (m^2/s), and V_a is the apparent migration velocity (m/s). The D_h and V_a values were obtained from least square fits of Equation (3-1).

3.2.3. Electromigration of Ca^{2+} with HCO_3^-/CO_3^{2-} ions during precipitation of $CaCO_3$

Electromigration reaction experiments of Ca^{2+} with HCO_3^-/CO_3^{2-} ions, as illustrated in Figure 3-2, were carried out to form $CaCO_3$ precipitates in compacted montmorillonite. The Na-bentonite which saturated with 0.7 M $NaHCO_3$ was placed between two reservoirs containing 1 M $CaCl_2$ and 0.7 M $NaHCO_3$ solutions, respectively. A constant current of 5 mA was applied from $CaCl_2$ reservoir (anode side) to $NaHCO_3$ reservoir (cathode side) at a temperature of 298 K. Two kinds of electromigration experiments were carried out, using ^{45}Ca and ^{14}C radio-tracers. After the prescribed time, the bentonite sample was sliced into 5 mm thickness perpendicular to electromigration direction. The detail procedure of the electromigration reaction has been described previously in Chapter 2.

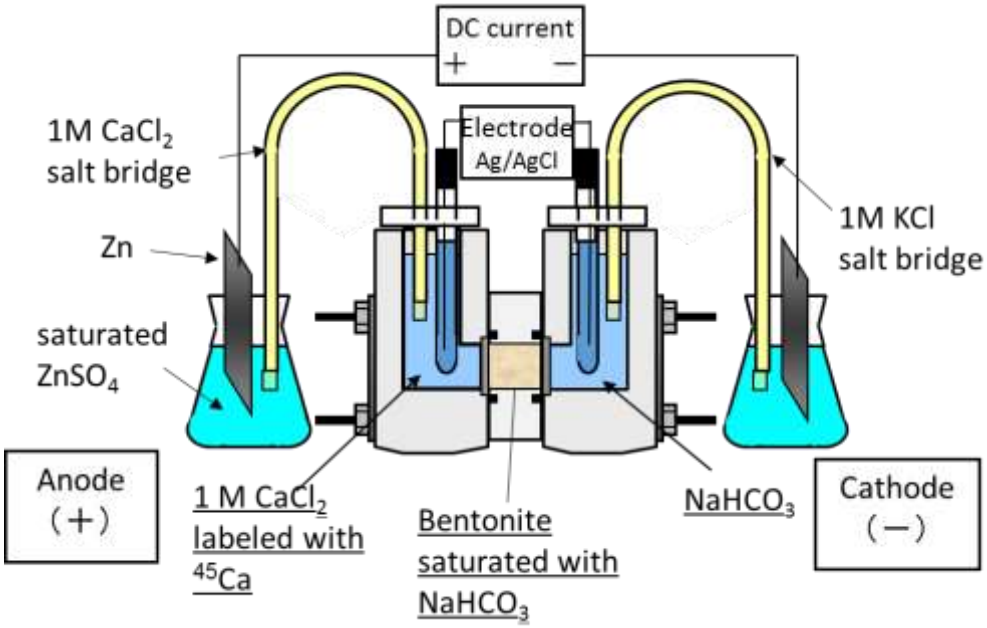

Figure 3-2. Schematic electromigration experiment set up.

The composition of solid phase and dissolved ion in each sliced sample were distinctly determined by sequential extraction to obtain the spatial distribution of chemical species in the bentonite sample. The detailed procedures and the applicability of this sequential extraction method has been described and explained in Chapter 2. The first extraction used saturated $CaCO_3$ solution to only extract the free $^{45}Ca^{2+}$ or $H^{14}CO_3^-$ /$^{14}CO_3^{2-}$ ions without dissolving $CaCO_3$ precipitates. The second extraction used 1 M HCl to dissolve the remaining ^{45}Ca fractions as exchangeable cations of bentonite and as $CaCO_3$ precipitates. After the extraction, supernatant was collected by centrifuging the sample at 10,000 rpm (12,000 g) for 10 minutes. The radioactivities of $^{45}Ca^{2+}$ or $H^{14}CO_3^-$ /$^{14}CO_3^{2-}$ were determined by radioactivity measurement of the ^{45}Ca or ^{14}C, respectively, with Aloka AccuFlex LSC-8000 (Hitachi, Tokyo, Japan). The concentration of Ca^{2+} and

HCO_3^-/CO_3^{2-} ions were calculated using their initial specific radioactivities, which was determined before uses.

The pH value in the porewater of compacted bentonite was estimated from the pH value measured for bentonite slurry. For this purpose, the same electromigration experiments without radiotracer was conducted under the same experimental conditions as the precipitation experiment. Each of the sliced bentonite samples was mixed with 10 ml deionized water for 30 minutes in a closed bottle at room temperature and atmospheric pressure. The pH of the slurry was measured using a glass electrode (Laqua F-72, Horiba, Kyoto, Japan).

3.3. Result

3.3.1. Electromigration parameters of Ca^{2+} and HCO_3^-/CO_3^{2-} ions

Spatial distribution of concentration of $^{45}Ca^{2+}$ and $H^{14}CO_3^-/^{14}CO_3^{2-}$ ions after electromigration is depicted in Figure 3-3. The figure shows that under the influence of electrical potential gradient, Ca^{2+} ions migrate towards the cathode side due to their positive charge. On the other hand, HCO_3^-/CO_3^{2-} ions relatively unmoved from their initial position despite their negative charge. It can be explained because migration of ions under the influence of electrical potential gradient is governed not only by electromigration, but also electroosmosis flow as described as follows:

$$v_a = v_{em} + v_{EOF} \qquad (3\text{-}2)$$

where v_a is the apparent migration velocity, v_{em} is the electromigration velocity and v_{EOF} is the electroosmosis flow. The equation implies that the $H^{14}CO_3^-/^{14}CO_3^{2-}$ ions can stay on the initial position or move from anode to cathode regardless of their negative charge if the electroosmotic flow is equal or higher than electromigration velocity.

Table 3-1 summarizes the electromigration parameters of $^{45}Ca^{2+}$ and $H^{14}CO_3^-$ /$^{14}CO_3^{2-}$ ions in compacted bentonite. The values were obtained from least-square fit of Equation (3-1) to the corresponding concentration profile in Figure 3-3. The apparent migration velocity (μ_a) of individual Ca^{2+} and HCO_3^-/CO_3^{2-} ions is calculated by the following expression:

$$v_a = \mu_a E \qquad (3\text{-}3)$$

where *E* is the electrical potential gradient (v/m). The apparent mobility of $^{45}Ca^{2+}$ ions under the experimental conditions is approximately one order of magnitude greater than that of HCO_3^-/CO_3^{2-} ions.

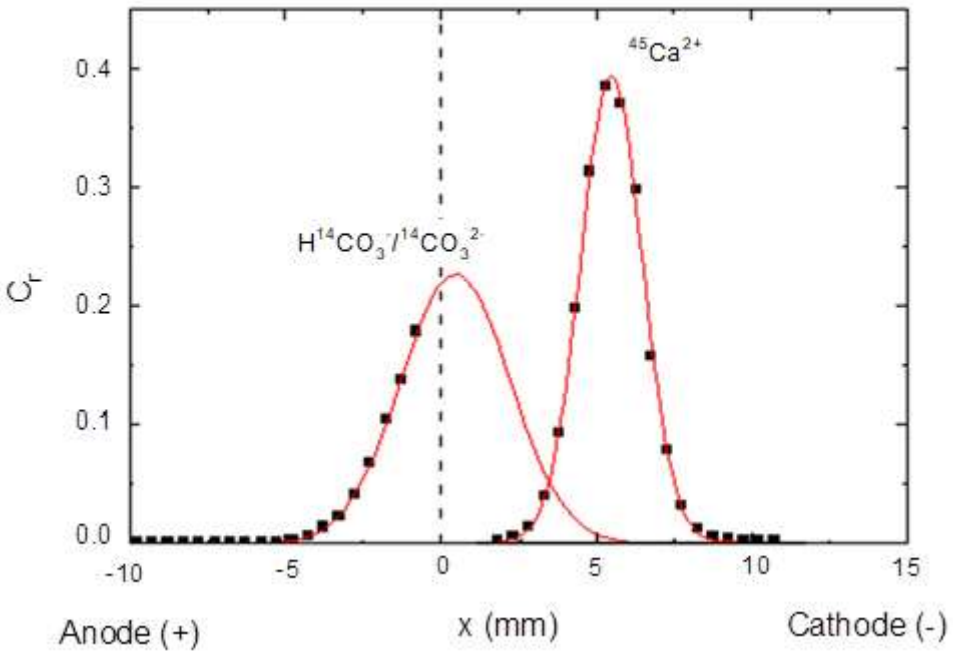

Figure 3-3. Spatial distribution of relative concentration of $^{45}Ca^{2+}$ and $H^{14}CO_3^-/^{14}CO_3^{2-}$ ions after 6 hours of electromigration experiment with constant electrical current of 15 mA. The initial positions of radiotracers are at $x = 0$. The solid lines are the least square fit of the concentration profile of each ion.

Table 3-1. Electromigration parameters of Ca^{2+} and HCO_3^- ions in compacted bentonite having dry density 1 kg/cm^3 at 298 K.

Parameter	Tracer	
	$^{45}Ca^{2+}$	$H^{14}CO_3^-$
Electrical potential gradient E (v/m)	128	128
Apparent migration velocity V_a (m/s)	2.52×10^{-7}	1.97×10^{-8}
Hydrodynamic dispersion coefficient D_h (m^2/s)	2.30×10^{-11}	6.90×10^{-11}
Apparent mobility μ_a (m^2/s·V)	1.97×10^{-9}	1.5×10^{-10}

3.3.2. Spatial distributions of ions after electromigration reaction

Figure 3-4 shows the spatial distribution of the solid HCO_3^-/CO_3^{2-} ions, which are likely $CaCO_3$ precipitates, after 6 and 16 hours electromigration time. At 6 hours profile, the concentration of $CaCO_3$ precipitates sharply decreased between 0 and 3.25 mm distance from the anode side. After 16 hours of experimental time, the $CaCO_3$ precipitates became distributed wider from 0 to 8.25 mm. The concentration profile of $CaCO_3$ precipitates at this time stayed at approximately 0.12 mmol/g and decreased to zero at the distance between 4.25 and 8.25 mm from the anode side. These profiles suggest that the formation of $CaCO_3$ precipitates was started at the surface of bentonite contacted with the anode reservoir and became wider across the bentonite sample towards the cathode side with the increasing experimental time.

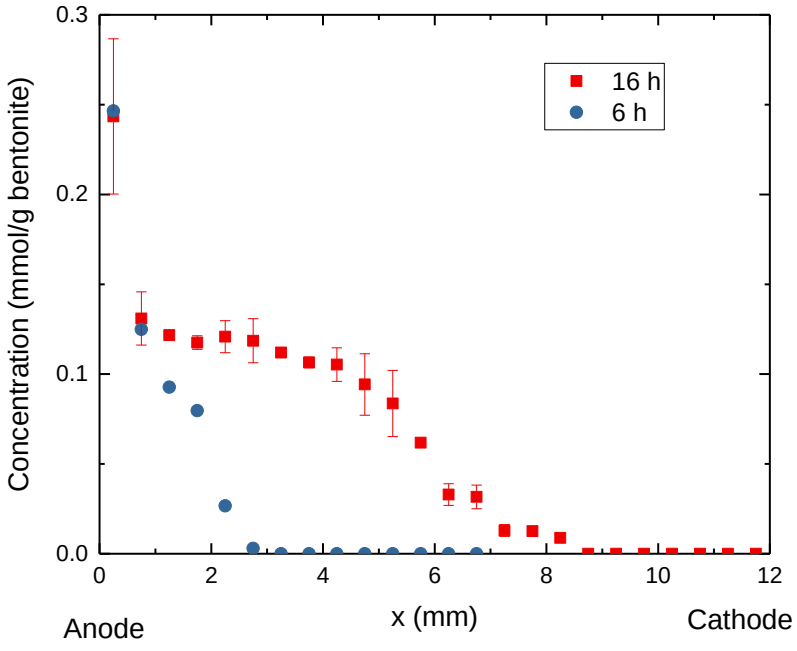

Figure 3-4. Spatial distribution of solid carbonate

Figure 3-5 shows the concentration distributions of dissolved HCO_3^-/CO_3^{2-} ions after 6 and 16 hours electromigration time. The concentration profiles of dissolved HCO_3^-/CO_3^{2-} ions at 6 and 16 hours were similar in shape, but advanced towards the cathode side in the 16 hours result. The bentonite sample can be divided into three zones based on these concentration profiles. The first zone is where the concentration of HCO_3^-/CO_3^{2-} ions is very low. This zone is located at $0 \leq x \leq 1.75$ and at $0 \leq x \leq 4.25$ mm for 6 and 16 hours electromigration time, respectively. The very low concentration of HCO_3^-/CO_3^{2-} ions suggesting that in this zone the HCO_3^-/CO_3^{2-} ions available for the $CaCO_3$ precipitation have been consumed by the precipitation reaction and no further reaction is occurring in this zone (hereafter reacted zone). The second zone is where the concentration profiles of HCO_3^-/CO_3^{2-} ions show steep gradient which located at$1.75 \leq x \leq 5.25$ mm and $4.25 \leq x \leq 8.75$ mm for 6 and 16 hours electromigration time, respectively. The profiles suggest that HCO_3^-/CO_3^{2-} ions in this zone is being consumed by the reaction of $CaCO_3$ precipitation (hereafter reaction zone). The third zone is where the concentration profiles of HCO_3^-/CO_3^{2-} ions approximately constant at high concentration. This zone is located from $x \geq 5.25$ and $x \geq 9.25$ mm for 6 and 16 hours experimental time, respectively. This zone is the unreacted bentonite zone where the reaction of $CaCO_3$ precipitation has not been started (hereafter unreacted zone).

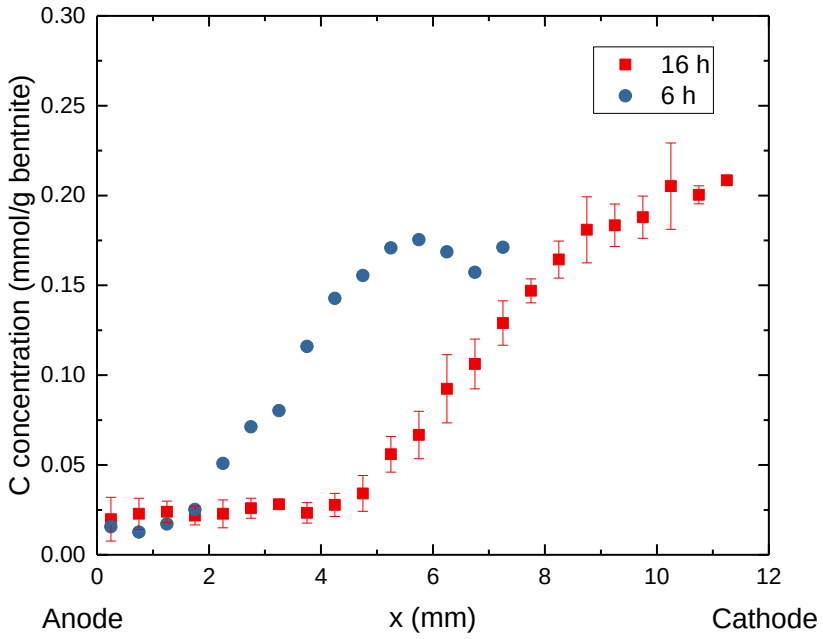

Figure 3-5. Spatial distribution dissolved carbonate at 6 and 16 hours electromigration reaction time.

Figure 3-6 shows distribution of Ca species in bentonite after 6 and 16 hour electromigration time. The zone where the concentration of Ca extracted by HCl exceeds CEC value indicates the formation of $CaCO_3$ precipitates. At 6 hours, this zone is located between 0 and 2.25 mm and become wider up to 4.75 mm after 16 hours. This result is consistent with the spatial distribution of the solid carbonate after 6 and 16 hour electromigration time shown previously in Figure 3-4.

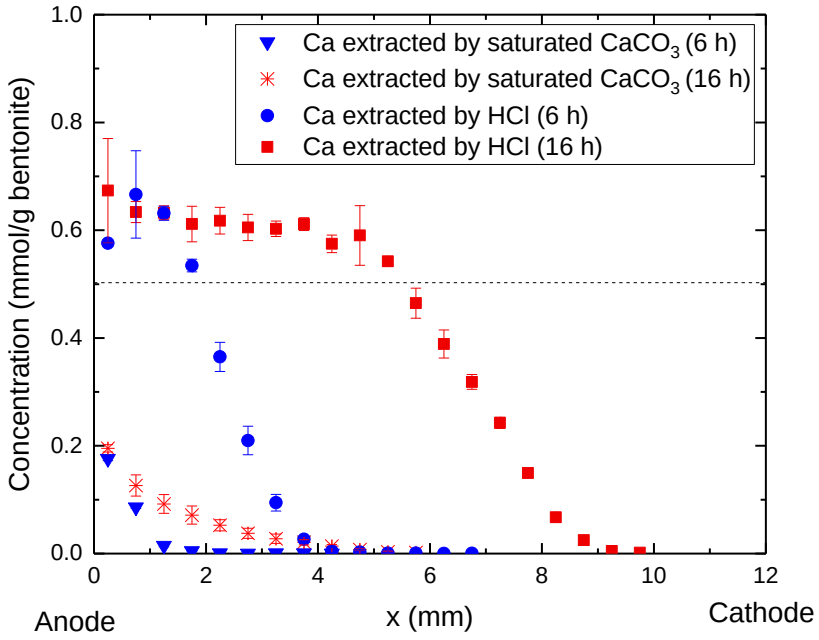

Figure 3-6. Spatial distribution of calcium extracted by saturated CaCO3 solution and HCl in sequential extraction at 6 and 16 hours electromigration time. Horizontal dash line is calculated from CEC value of bentonite (1.05 meq/g bentonite [37])

3.3.3. Spatial distribution of pH after electromigration reaction

Figure 3-7 shows the spatial pH profile of dispersed sliced bentonite in deionized water after 6 and 16 hours electromigration reaction time. A peak in the Ca-/Na-bentonite zone could be attributed to the dissolution of amorphous $CaCO_3$ precipitates when the sliced bentonite is dispersed in water as discussed in Chapter 2. As can be seen from the profile, the peak of pH moved towards the cathode side as a function of time which in line with the profile of HCO_3^-/CO_3^{2-} and Ca^{2+}ions shown previously. The highest pH value after 6 hours electromigration time was at x = 2.25 mm. The position of highest pH value was shifted to x = 5.75 mm after 16 hours electromigration time.

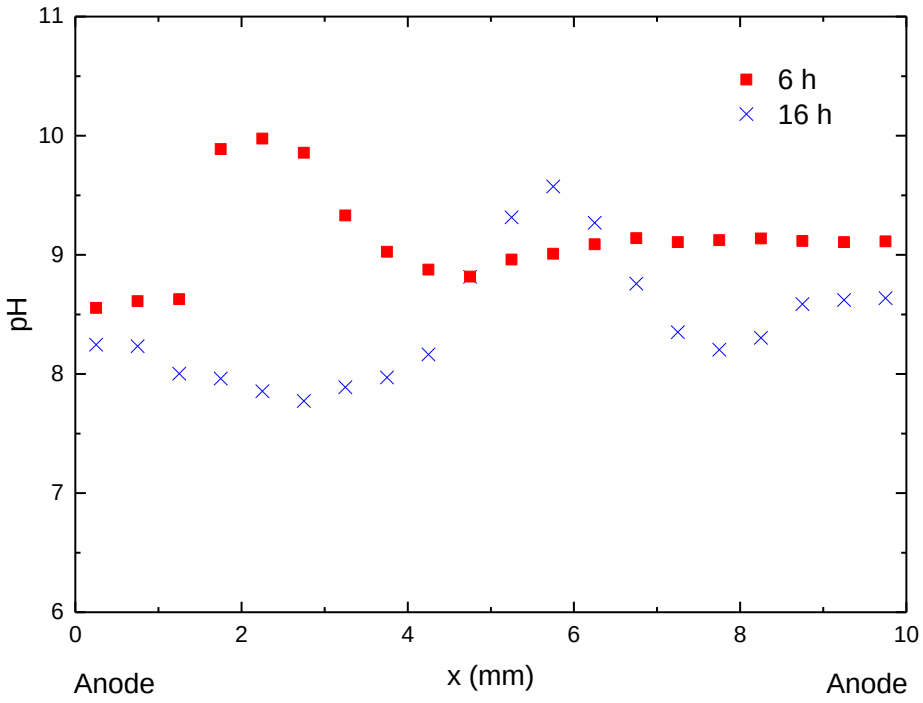

Figure 3-7. Spatial distribution of pH of sliced bentonite sample dispersed in 10 ml deionized water.

3.4. Discussion

3.4.1. Moving reaction front of $CaCO_3$ precipitation

$CaCO_3$ precipitates, as neutral chemical species, should not mobile under electrical potential gradient. Therefore, the broadening precipitation zones of $CaCO_3$ precipitates as was indicated in Figure 3-5 and Figure 3-6 suggests that the reaction front between Ca^{2+} and HCO_3^-/CO_3^{2-} ions moved from the anode side towards the cathode side. The advancing reaction front can be attributed to the difference in mobility between Ca^{2+} and HCO_3^-/CO_3^{2-} ions as the reacting ions. As shown in Table 3-1, the apparent mobility of Ca^{2+} is about one order magnitude greater than that of HCO_3^-/CO_3^{2-} ions. This significant difference implies that HCO_3^-/CO_3^{2-} ions should not migrate significantly before reacting with Ca^{2+} ions. The incoming Ca^{2+} ions convert HCO_3^-/CO_3^{2-} ions at their initial position into $CaCO_3$ precipitates. Once the available HCO_3^-/CO_3^{2-} ions is completely consumed, the reaction stops and the incoming Ca^{2+} ions passing through to create a new reaction front further towards the cathode side.

The relatively constant position of HCO_3^-/CO_3^{2-} ions compared to that of Ca^{2+} ions under the influence of electrical potential gradient as shown previously in Figure 3-3 also suggest that the initial concentration of HCO_3^-/CO_3^{2-} ions determines the amount of $CaCO_3$ precipitates which can be formed. Considering the range of experimental pH shown in Figure 3-7, the HCO_3^-/CO_3^{2-} ions in bentonite is dominated by HCO_3^- species. The reaction of $CaCO_3$ precipitation can be expressed with the following equilibrium:

$$Ca^{2+} + 2HCO_3^- \leftrightarrow CaCO_{3\,(s)} + H_2O + CO_2$$

The reaction shows that complete $CaCO_3$ precipitation from HCO_3^- species should generates $CaCO_3$ precipitates half of the initial concentration. The amount of $CaCO_3$ precipitates after complete reaction is approximately 0.12 mmol/g-dry bentonite. This value is close to half of the concentration of HCO_3^-/CO_3^{2-} ions in unreacted zone as shown previously in Figure 3-6 which agrees with the stoichiometry of the reaction.

Assuming the advancement of reaction front of $CaCO_3$ precipitation corresponds to the width of $CaCO_3$ precipitates zone, the velocity of moving reaction front (v_{MRF}) can be expressed as follows:

$$v_{MRF} = \frac{dx_{f(t)}}{dt} \qquad (3\text{-}4)$$

where $x_{f(t)}$ is the width of $CaCO_3$ precipitates zone which has been formed at time t. The width of $CaCO_3$ precipitates zone from Figure 3-4 and the v_{MRF} values obtained by using the equation (3-3) and are summarized in Table 3-2. The v_{MRF} values which were obtained for 6 and 16 hours are about the same, suggesting that the reaction front of $CaCO_3$ precipitation in compacted bentonite advanced with approximately constant velocity.

Table 3-2. Approximated value of moving reaction front of $CaCO_3$ precipitation in compacted bentonite at dry density of 1 kg/dm^3 under the influence of electrical current of 5 mA.

Experimental time (h)	Width $CaCO_3$ precipitation zone (m)	Velocity of moving reaction front V_{MRF} (m/s)
6	3.25×10^{-3}	1.50×10^{-7}
16	8.25×10^{-3}	1.43×10^{-7}

3.4.2. Transport process to the site of reaction front

Porosity clogging may occur due to precipitates formation in porous media. The amount of precipitates may have non-linear effect to the permeability. The study on $CaCO_3$ precipitation in quartz sand revealed that $CaCO_3$ precipitates occupying only 5% of porosity was sufficient enough to create impermeable layer [38]. In this study, the amount of $CaCO_3$ precipitates in compacted bentonite generated from the electromigration experiment was about 0.12 mmol/g-bentonite. Using molar volume of calcite (31.20 cm^3/mol) and interparticle porosity of compacted bentonite at dry density of 1 g/cm^3 (0.36) [39], $CaCO_3$ precipitates occupy approximately 10% of the interparticle porosity. However, the relatively constant v_{MRF} as listed in Table 3-2 suggests that the effect of $CaCO_3$ precipitates on the transport of Ca^{2+} and HCO_3^-/CO_3^{2-} ions under the experimental condition is negligible even at higher $CaCO_3$-occupied porosity.

Further evidence on the negligible porosity clogging in the experiment is shown by the approximately constant of $CaCO_3$ precipitates near the anode side. When the reaction front of $CaCO_3$ precipitation moved toward the cathode side, the Ca^{2+} ions from supplied from the anode reservoir need to pass through the $CaCO_3$ precipitate zone in order to reach the reaction front. If the $CaCO_3$ precipitates block the transport of Ca^{2+} ions, the solution surrounding the precipitates will become undersaturated and then dissolution of precipitates will occur. However, the profile of $CaCO_3$ precipitates near the anode side was constant, indicating no dissolution occurred between 6 and 16 hours electromigration time.

A plausible explanation for the discrepancy effect of $CaCO_3$ precipitates in compacted bentonite and in quartz sand is due to their microstructure difference. Unlike

quartz sand which exhibits single pore type, compacted bentonite is considered to exhibit two types of pores: interparticle and interlayer pores. Both pores are accessible for cations, including Ca^{2+} ions. Therefore, the negligible effect of $CaCO_3$ precipitates to the transport of Ca^{2+} ions suggests that Ca^{2+} ions can migrate through not only the interparticle but also the interlayer pores, resulting in the fact that are not affected by the presence of $CaCO_3$ precipitates. It is assumed that the interlayer Ca^{2+} ions can react with HCO_3^-/CO_3^{2-} ions in the interparticle spaces through cation exchange reaction with Na^+ ions. If this is the case, the transport of cations in compacted bentonite will not be affected by porosity clogging regardless the amount of precipitates in the interparticle spaces. This result also suggests the importance of $CaCO_3$ precipitates formation mechanism through cation exchange reaction in compacted bentonite.

3.5. Conclusion

The electromigration parameters for Ca^{2+} and HCO_3^-/CO_3^{2-} ions and the time dependence of $CaCO_3$ precipitation in compacted Na-bentonite with dry density of 1.0 kg/dm^3 from counter diffusion of Ca^{2+} and HCO_3^-/CO_3^{2-} ions enhanced by electrokinetic method have been studied. The reaction front of $CaCO_3$ precipitation under the experimental conditions was found to move from the anode side towards the cathode side. This advancing reaction front can be attributed to the faster mobility of Ca^{2+} compared to HCO_3^-/CO_3^{2-} ions. The velocity of the reaction front of $CaCO_3$ precipitation was obtained to be constant during the experiments, unaffected by $CaCO_3$ formation. The results suggest that major migration pathways of cations in compacted bentonite include the interlayers and the formation of precipitates may not affect migration of cationic radionuclides.

3.6. References

[1] Chapman N, Hooper A. The disposal of radioactive wastes underground. Proc. Geol. Assoc. 2012;123(1):46–63.

[2] Ewing RC, Whittleston RA, Yardley BWD. Geological disposal of nuclear waste: A primer. Elements. 2016;12(4):233–237.

[3] Higgo JJW. Clay as a barrier to radionuclide migration. Prog. Nucl. Energy. 1987;19(2):173–207.

[4] Pusch R. Use of bentonite for isolation of radioactive waste products. Clay Miner. 1992;27(3):353–361.

[5] Pusch R. Chapter 11.4 Clays and nuclear waste management. In: Bergaya F, Theng BKG, Lagaly G, editors. Handbook of clay science. Amsterdam: Elsevier; 2006.p.703–716.

[6] Altmann S, Tournassat C, Goutelard F, et al. Diffusion-driven transport in clayrock formations. Appl. Geochemistry. 2012;27(2):463–478.

[7] Sellin P, Leupin OX. The use of clay as an engineered barrier in radioactive-waste management - A review. Clays Clay Miner. 2014;61(6):477–498.

[8] Grambow B. Geological disposal of radioactive waste in clay. Elements. 2016;12(4):239–245.

[9] Japan Nuclear Cycle Development Institute. H12: Project to establish the scientific and technical basis for HLW disposal in Japan, Supporting Report 3 Safety Assessment of the Geological Disposal System. JNC TN1410 2000-004. Tokai: JNC; 2000. (JNC TN1410 2000-004).

[10] Atkinson A, Everitt NM, Guppy RM. Time Dependence of pH in a Cementitious Repository. Materials Research Society Symposium Proceedings. Cambridge University Press; 1988.p.439–446.

[11] Alonso MC, García Calvo JL, Cuevas J, et al. Interaction processes at the concrete-bentonite interface after 13 years of FEBEX-Plug operation. Part I: Concrete alteration. Phys. Chem. Earth. 2017;99:38–48.

[12] Gaucher EC, Blanc P. Cement/clay interactions - A review: Experiments, natural analogues, and modeling. Waste Manag. 2006;26(7):776–788.

[13] Arcos D, Grandia F, Domènech C. Geochemical evolution of the near field of a KBS-3 repository. SKB Technical Report. Stockholm; 2006. (SKB Tecknical Report TR-06016).

[14] Dauzères A, Le Bescop P, Cau-Dit-Coumes C, et al. On the physico-chemical evolution of low-pH and CEM i cement pastes interacting with Callovo-Oxfordian pore water under its in situ CO2 partial pressure. Cem. Concr. Res. 2014;58:76–88.

[15] Yamaguchi T, Sawaguchi T, Tsukada M, et al. Mineralogical changes and associated decrease in tritiated water diffusivity after alteration of cement–bentonite interfaces. Clay Miner. 2016;51(2):279–287.

[16] Techer I, Bartier D, Boulvais P, et al. Tracing interactions between natural argillites and hyper-alkaline fluids from engineered cement paste and concrete: Chemical and isotopic monitoring of a 15-years old deep-disposal analogue. Appl. Geochemistry. 2012;27(7):1384–1402.

[17] Fernández R, Torres E, Ruiz AI, et al. Interaction processes at the concrete-bentonite interface after 13 years of FEBEX-Plug operation. Part II: Bentonite contact. Phys. Chem. Earth. 2017;99:49–63.

[18] Maher K, Bargar JR, Brown GE. Environmental speciation of actinides. Inorg. Chem. 2013;52(7):3510–3532.

[19] Catalano JG, Brown GE. Uranyl adsorption onto montmorillonite: Evaluation of binding sites and carbonate complexation. Geochim. Cosmochim. Acta. 2005;69(12):2995–3005.

[20] Steefel CI, Lichtner PC. Diffusion and reaction in rock matrix bordering a hyperalkaline fluid-filled fracture. Geochim. Cosmochim. Acta. 1994;58(17):3595–3612.

[21] Gaboreau S, Prêt D, Tinseau E, et al. 15 years of in situ cement-argillite interaction from Tournemire URL: Characterisation of the multi-scale spatial heterogeneities

of pore space evolution. Appl. Geochemistry. 2011;26(12):2159–2171.

[22] Jenni A, Mäder U, Lerouge C, et al. In situ interaction between different concretes and Opalinus Clay. Phys. Chem. Earth. 2014;70–71:71–83.

[23] Kitano Y, Oomori T. The coprecipitation of uranium with calcium carbonate. J. Oceanogr. Soc. Japan. 1971;27(1):34–42.

[24] Meece DE, Benninger LK. The coprecipitation of Pu and other radionuclides with $CaCO_3$. Geochim. Cosmochim. Acta. 1993;57(7):1447–1458.

[25] Hellebrandt SE, Hofmann S, Jordan N, et al. Incorporation of Eu(III) into calcite under recrystallization conditions. Sci. Rep. 2016;6:1–10.

[26] Smith KF, Bryan ND, Swinburne AN, et al. U(VI) behaviour in hyperalkaline calcite systems. Geochim. Cosmochim. Acta. 2015;148:343–359.

[27] Zaoui A, Sekkal W. Can clays ensure nuclear waste repositories? Sci. Rep. 2015;5:1–5.

[28] Stack AG. Precipitation in Pores : A Geochemical Frontier. Rev. Mineral. Geochemistry. 2015;80(1):165–190.

[29] Stack AG, Fernandez-Martinez A, Allard LF, et al. Pore-size-dependent calcium carbonate precipitation controlled by surface chemistry. Environ. Sci. Technol. 2014;48(11):6177–6183.

[30] Gebrehiwet TA, Redden GD, Fujita Y, et al. The Effect of the CO_3^{2-} to Ca^{2+} Ion activity ratio on calcite precipitation kinetics and Sr^{2+} partitioning. Geochem. Trans. 2012;13(1):1.

[31] Stack AG. Next generation models of carbonate mineral growth and dissolution. 2014;288:278–288.

[32] Nindiyasari F, Fernández-Díaz L, Griesshaber E, et al. Influence of gelatin hydrogel porosity on the crystallization of CaCO 3. Cryst. Growth Des. 2014;14(4):1531–1542.

[33] Gebrehiwet TA, Guo L, Fox D, et al. Precipitation of calcium carbonate and calcium phosphate under diffusion controlled mixing. Appl. Geochemistry.

2014;46:43–56.

[34] Kozaki T, Fujishima A, Sato S, et al. Self-diffusion of sodium ions in compacted sodium montmorillonite. Nucl. Technol. 1998;121(1):63–69.

[35] Tanaka S, Noda N, Sato S, et al. Electrokinetic study of migration of anions, cations, and water in water-saturated compacted sodium montmorillonite. J. Nucl. Sci. Technol. 2011;48(3):454–462.

[36] Maes N, Moors H, Dierckx A, et al. The assessment of electromigration as a new technique to study diffusion of radionuclides in clayey soils. J. Contam. Hydrol. 1999;36(3–4):231–247.

[37] Tanaka S. Gypsum precipitation enhanced by electrokinetic method and porewater chemistry in compacted montmorillonite. Appl. Clay Sci. 2018;161:482–493.

[38] Tartakovsky AM, Redden G, Lichtner PC, et al. Mixing-induced precipitation : Experimental study and multiscale numerical analysis. Water Resour. Res. 2008;44:1–19.

[39] Kozaki T, Inada K, Sato S, et al. Diffusion mechanism of chloride ions in sodium montmorillonite. J. Contam. Hydrol. 2001;47(2–4):159–170.

4. Diffusion behavior of sulphate ions in compacted bentonite at different dry density and salinity

4.1. Introduction

Geological disposal is recognized as safe and secure means to dispose of high-level radioactive waste. Its concept is based on multi-barrier system consisting of a series of engineered and natural barriers which ensure to inhibit the release of radionuclides from waste form for long period of time [1–4]. Compacted bentonite is considered to be used as a one part of the multi-barrier systems because of its several advantageous properties, such as low hydraulic conductivity, high sorption capacity for radionuclides, high swelling ability, and good durability [5,6]. Low diffusivity of bentonite is considered to be advantageous, since it can retards the radionuclides transport [7]. Therefore, diffusion is one of important issue to be studied for the safety assessment of geological disposal. However, the diffusion processes are still not clearly understood because the diffusion is influenced by several phenomena, such as the existence of electrical double layer (EDL) from the negatively charged bentonite surface, the type of exchangeable cations, and the porewater chemistry [8–10].

Compacted bentonite is considered to have two types of pore spaces: the spaces between bentonite layer (interlayer spaces) and the spaces between external surfaces (interparticle spaces). The interlayer spaces contain interlayer water and exchangeable cations, while the interparticle spaces contain porewater which or part of which is affected by the EDL due to permanent negative charge of montmorillonite, which is the major clay mineral in bentonite [11–13]. Radionuclides in compacted bentonite thus can diffuse through three different pathways: the porewater, the external surface of bentonite or the

EDL, and the interlayer. Cations and neutral chemical species can diffuse through all of those pathways [14–16], whereas anions can only diffuse through the former two pathways due to the negative charge of montmorillonite layers [17,18]. The activation energy for diffusion (E_a) can be used as a parameter to distinguish diffusion processes among those pathways. Generally, diffusion in the porewater can be considered to have the same E_a values as that in free water, whereas the diffusion in other two ways may have different E_a values from that in free water [19,20].

Diffusion of anion in bentonite is an important issue to studied for the safety assessment of geological disposal [2,21]. It is reported that diffusion coefficients in bentonite decrease as the dry density of bentonite increase for Cl^- [22–25], I^- [26–29], SO_4^{2-} [30,31], and SeO_3^{2-} ions [32]. On the other hand, the diffusion coefficients of anions were reported to be increased by the increase of the salinity. In the previous work, this salinity effect was attributed to the increase of accessible porosity for anions [25,33], although the total porosity kept constant [33,34]. From the viewpoint of the E_a, almost the same E_a value as those in free water were reported for I^- [26] and SeO_3^{2-} ions [32], suggesting that these anions diffuse predominantly in the porewater. However, it was reported that diffusion of Cl^- ions has both lower and higher E_a values than that in free water, suggesting that their predominant diffusion mechanism is different from that in free water [22,23].

The purpose of this study is to investigate the diffusion mechanism of $^{35}SO_4^{2-}$ ions in compacted bentonite. This anion is relatively stable as compared with carbonate, which easily associate according to the chemical environment. It is considered that diffusion of SO_4^{2-} ions is closely related to the activities of sulphate-reducing bacteria, which can reduce SO_4^{2-} ions to S^{2-} ions and can enhance the corrosion of copper canister

[35,36]. The SO_4^{2-} ions also may contribute to the formation of pyrite (FeS_2) which have strong association with ^{79}Se [37]. In this study, back-to-back diffusion experiments were carried out to obtained apparent diffusion coefficient (D_a) of $^{35}SO_4^{2-}$ in compacted bentonite at various dry densities. The effect of NaCl concentration on the diffusion of $^{35}SO_4^{2-}$ ions was studied at dry density of 1 kg/dm^3, at which salinity dependence on diffusion coefficients of anions is reported to be relatively significant [9,38]. The E_a values were determined from the dependences of D_a on temperatures. Based on the experimental data of D_a and E_a, the diffusion mechanism of $^{35}SO_4^{2-}$ ions in compacted bentonite is discussed from the viewpoints of microstructure of compacted bentonite which can be changed by dry density and/or salinity.

4.2. Method

Homoionized Na-bentonite with particle size between 75 and 150 μm was prepared by mixing Kunipia F (Kunimine Industries Co., Tokyo, Japan) and 1 M NaCl solution with ratio of 1:100 g/ml. The mixing was carried out three times with fresh 1 M NaCl solution in each step. The excess salt was removed by dialysis method in demineralized water prepared using EYELA Still Ace SA-2100E1 (Tokyo Rikakikai Co., Tokyo, Japan). Detailed procedure of hominization is described in previous studies [39,40].

Dry Na-bentonite was packed in acrylic resin cells with inner diameter and length of 20 mm to dry density of 0.8, 1.0, 1.2, 1.4, and 1.6 kg/dm^3. Each pair of the cells containing bentonite sample was immersed in deionized water in a closed container for 30 days at room temperature and atmospheric pressure. For sample with dry density of 1.0 kg/dm^3, the cells were also immersed in 0.3 or 0.5 M NaCl.

The diffusion experiments were carried out using a small amount of radioactive tracer solution containing $Na_2{}^{35}SO_4$ (American Radiolabeled Chemicals obtained from Japan Radioisotope Association). The radiotracer solution was spiked uniformly to each one end of the two samples of compacted bentonite. The samples were then assembled into sandwich configuration and kept for the prescribed diffusion time to allow $^{35}SO_4{}^{2-}$ ions to diffuse into two compacted bentonite samples as illustrated in Figure 4-1. The experiments were carried out at constant temperatures of 288, 298, 313, or 323 K. After diffusion process, the compacted bentonite samples were removed from the cells and cut into 0.5 mm-thick slice which was oriented perpendicular to the diffusion direction. Each of sliced samples was suspended in a liquid scintillation cocktail (Insta-Gel, PerkinElmer). The concentration of $^{35}SO_4{}^{2-}$ ions in each sliced bentonite samples was determined by direct radiation measurement of the ^{35}S radioactivities with Aloka AccuFlex LSC-8000 (Hitachi, Tokyo, Japan).

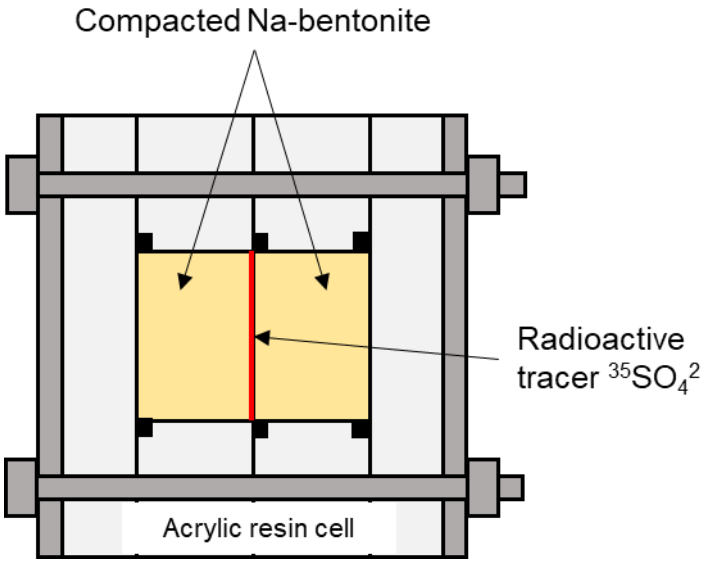

Figure 4-1. Schematic of diffusion experiment.

The D_a values of $^{35}SO_4^{2-}$ were calculated assuming the spiked radiotracer diffuse from thin diffusion source in infinite length of sample in both directions. The spatial distribution of $^{35}SO_4^{2-}$ ions after the prescribed period of time for diffusion can be described by the following equation, which is derived from Fick's second law with boundary conditions for diffusant occupying half-spaces are $-\infty < x < 0$ and $0 < x < \infty$ [41]:

$$c\,(x,t) = \frac{M}{2\sqrt{\pi D_a t}}\; exp\left(-\frac{x^2}{4D_a t}\right) \qquad (4\text{-}5)$$

where c is the radioactivities of $^{35}SO_4^{2-}$ ions per sliced compacted bentonite sample (Bq/m^3), M is the total amount of the spiked radiotracer per unit area (Bq/m^2), x is the distance between the center of the sliced bentonite sample and the surface on which the radiotracer was spiked (m), and t is the diffusion time (s). Two D_a values were obtained from each pair bentonite samples which were calculated from the slope of least-square fitting *ln C* against x^2.

The E_a values of $^{35}SO_4^{2-}$ ions were determined from the temperature dependence of D_a values by using the following Arrhenius law:

$$D_a = D_0\; exp\;\frac{-E_a}{RT} \qquad (4\text{-}6)$$

where D_0 is the constant for a given diffusion system (m^2/s), R is the gas constant (8.314×10^{-3} kJ/mol·K), and T is the absolute temperature in which the diffusion experiment was carried out (K). The E_a values (kJ/mol) were then calculated from the slope of least-square fitting of *ln* D_a against reciprocal T.

4.3. Result

4.3.1. Diffusivity of $^{35}SO_4^{2-}$ ions in compacted bentonite

Table 4-1 summarizes experimental results of the diffusion coefficients of $^{35}SO_4^{2-}$ ions in compacted bentonite under different dry densities, diffusion temperatures and NaCl concentrations. When the bentonite was saturated with deionized water (at NaCl concentration of zero), the D_a values at each diffusion temperature significantly decreased as the dry density of compacted bentonite increased from 0.8 to 1.6 kg/dm^3. Figure 4-2 shows the D_a values at 298 K as a function of dry density, together with those of Cl^- ions [22,23]. The D_a of SO_4^{2-} ions were smaller than those of Cl^- ions by approximately a factor of three in average.

Table 4-1. Summary of the D_a and E_a values of $^{35}SO_4^{2-}$ ions in compacted bentonite at various experimental conditions.

NaCl concentration (M)	Dry density (kg/dm^3)	D_a (m^2/s)			
		288 K	298 K	313 K	323 K
0	0.8	4.7×10^{-11}	5.8×10^{-11}	8.8×10^{-11}	1.3×10^{-10}
		4.5×10^{-11}	5.7×10^{-11}	8.2×10^{-11}	1.1×10^{-10}
	1.0	3.2×10^{-11}	3.8×10^{-11}	5.0×10^{-11}	6.6×10^{-11}
		3.4×10^{-11}	3.8×10^{-11}	5.2×10^{-11}	6.5×10^{-11}
	1.2	2.4×10^{-11}	3.0×10^{-11}	3.1×10^{-11}	4.7×10^{-11}
		2.5×10^{-11}	2.9×10^{-11}	3.6×10^{-11}	4.4×10^{-11}
	1.4	1.4×10^{-11}	1.7×10^{-11}	2.6×10^{-11}	3.0×10^{-11}
		1.4×10^{-11}	1.8×10^{-11}	2.5×10^{-11}	3.2×10^{-11}
	1.6	8.1×10^{-12}	1.2×10^{-11}	1.8×10^{-11}	1.5×10^{-11}
		7.4×10^{-12}	1.3×10^{-11}	1.9×10^{-11}	1.7×10^{-11}
0.3	1.0	5.9×10^{-11}	7.1×10^{-11}	9.7×10^{-11}	1.0×10^{-10}
		5.4×10^{-11}	6.8×10^{-11}	7.5×10^{-11}	1.2×10^{-10}
0.5	1.0	5.8×10^{-11}	7.6×10^{-11}	1.1×10^{-10}	1.5×10^{-10}
		6.1×10^{-11}	8.0×10^{-11}	1.2×10^{-10}	1.5×10^{-10}

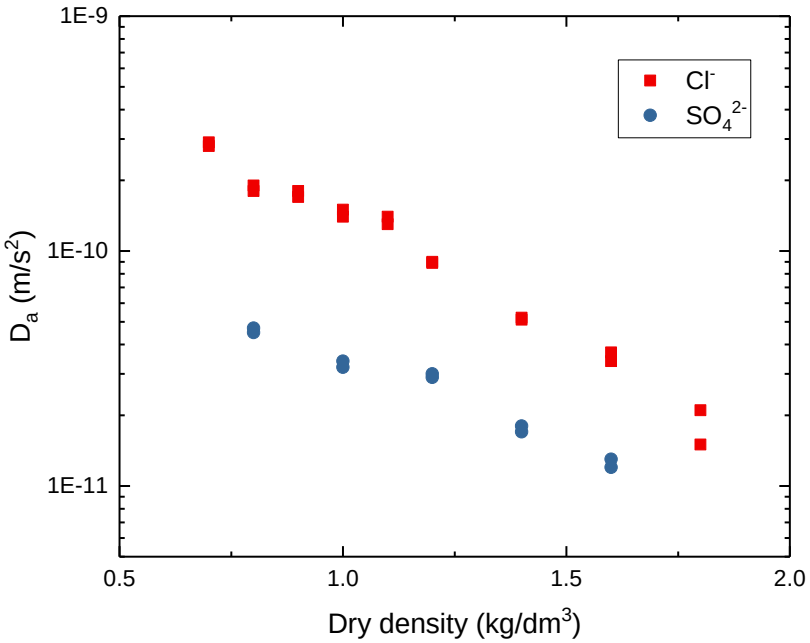

Figure 4-2. The D_a values of SO_4^{2-} (this study) and Cl^- ions [22,23] in water saturated compacted bentonite at 298 K as a function of dry density.

Figure 4-3 shows the temperature dependence of the D_a values of $^{35}SO_4^{2-}$ ions under different NaCl concentrations in compacted bentonite at dry density of 1 kg/dm^3. The D_a values at each temperature increased as the NaCl increased from 0 to 0.3 M. When the NaCl concentration further increases from 0.3 to 0.5 M, however, the increase of D_a became relatively small or almost zero.

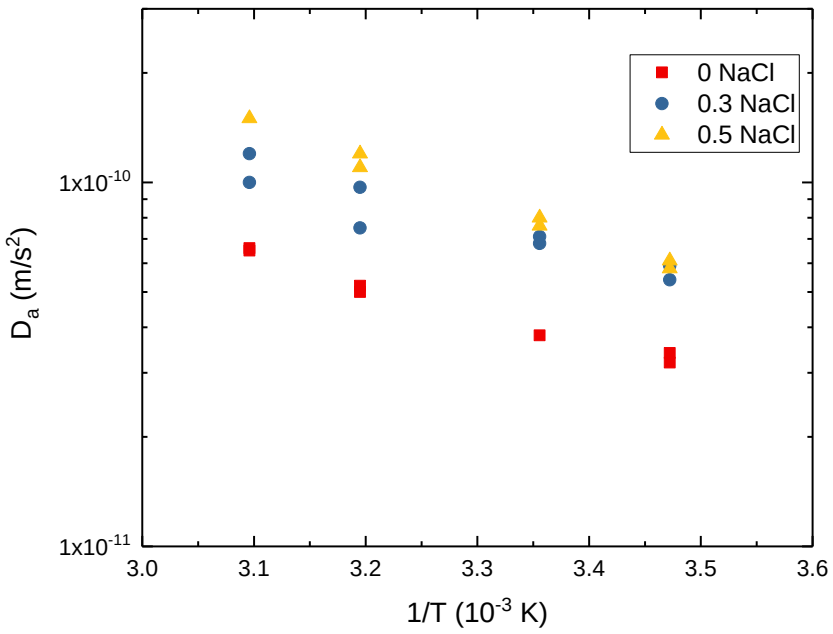

Figure 4-3. The temperature dependence of the D_a values of SO_4^{2-} in compacted bentonite at dry density of 1 kg/dm^3 under various NaCl concentrations.

4.3.2. E_a values of $^{35}SO_4^{2-}$ in compacted bentonite

Figure 4-4 shows the E_a values of $^{35}SO_4^{2-}$ ions in compacted bentonite as a function of dry density, together with those obtained at dry density of 1 kg/dm^3 under different NaCl concentrations. The E_a value of $^{35}SO_4^{2-}$ ions at dry density of 0.8 kg/dm^3 was found to be the same as the E_a value in free water, 20 kJ/mol (dash line in the figure) [42]. However, the E_a value decreased as the dry density increased to 1.2 kg/dm^3, and then slightly increased as the dry density further increased from 1.2 to 1.6 kg/dm^3. It should be noted that the standard error of E_a value at dry density of 1.6 kg/dm^3 is high and overlap with the E_a value in free water. At the dry density of 1.0 kg/dm^3, the E_a did not change when the NaCl concentration increased from 0 to 0.3 M, whereas it increased to become equal to that in free water as the NaCl concentration further increased from 0.3 to 0.5 M.

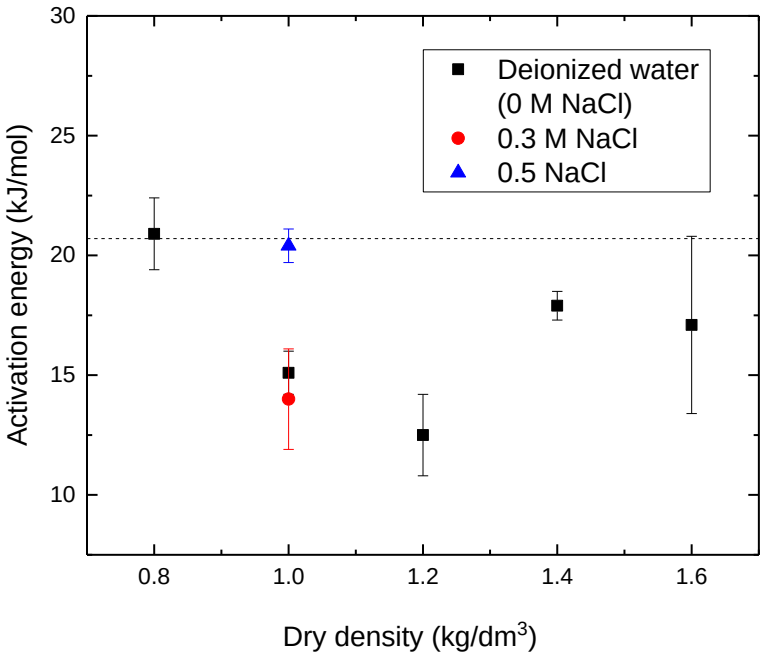

Figure 4-4. E_a values of $^{35}SO_4^{2-}$ ions in compacted bentonite as a function of dry density and NaCl concentration. The horizontal dash line is the E_a value of SO_4^{2-} ions in free water (20.7 kJ/mol [42]).

4.4. Discussion

4.4.1. *Effect of dry density on the diffusion of $^{35}SO_4^{2-}$ ions*

There are at least three possible diffusion pathways as above mentioned in Section 4.1, and also been discussed from the E_a values elsewhere [19,20]. According to the concept of diffusion pathways, the same E_a value of $^{35}SO_4^{2-}$ ions in compacted bentonite at dry density of 0.8 kg/dm^3 to that in free water suggests that the diffusion of $^{35}SO_4^{2-}$ ions occurs predominantly through the porewater at this dry density. The same predominant porewater diffusion has also been reported for Cl^- ions albeit at lower dry density of 0.7 kg/dm^3 as shown in Figure 4-5 [23]. This predominantly porewater diffusion for anions at low dry density is reasonable because of the high porosity of compacted bentonite at this dry density. The porewater fraction accounts for more than 55% at the dry density of bentonite lower than 1 kg/dm^3.

At dry density of 1 kg/dm^3 and higher, the E_a values became smaller than that in free water. This decrease of E_a can be attributed to the change of diffusion mechanism from predominantly through porewater to another. Surface diffusion is possible alternative pathway for cations, but not for anions. This surface diffusion can be contradictive to EDL theory, such as Stern and Gouy-Chapman, which expected anions are completely excluded from the negatively charged surface of bentonite. Kozaki *et al.* [23] pointed out that surface diffusion can be predominant if the structure of EDL follows the Grahame model. This result, nonetheless, suggests that the diffusion of $^{35}SO_4^{2-}$ ions in compacted bentonite at dry density higher than 1 kg/dm^3 cannot be explained solely by the porewater diffusion.

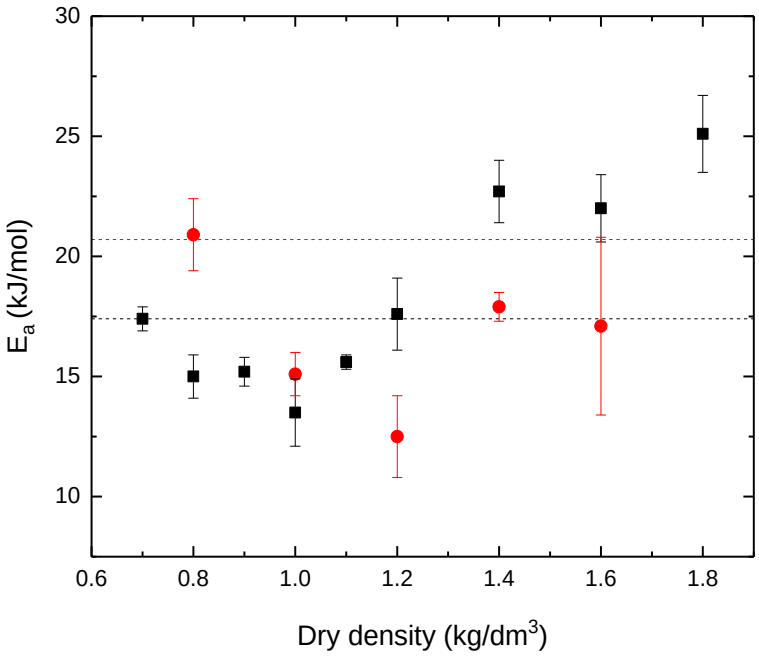

Figure 4-5. The E_a of $^{35}SO_4^{2-}$ (present study) and Cl^- [22,23] ions in compacted bentonite at different dry densities. The horizontal dash line is the E_a in free water (20.7 and 17.4 kJ/mol for SO_4^{2-} and Cl^- ions, respectively [42].

4.4.2. *Effect of salinity on the diffusion of $^{35}SO_4^{2-}$ ions*

The EDL developed on the surface of bentonite (montmorillonite) can eventually affect the diffusion mechanism of ions. As pointed out before, very thick EDL can be developed in the interparticle spaces of compacted bentonite saturated with deionized water. However, it would shrink in the presence of high concentration of NaCl in the porewater. The EDL thickness related to the ionic strength of the porewater is commonly expressed by reciprocal of the Debye length κ^{-1}:

$$\kappa^{-1} = \sqrt{\frac{\varepsilon RT}{2(N_a q_e)^2}\frac{1}{I}} \qquad (4-3)$$

where ε is the permittivity (6.95×10^{-10} F/m), R is the gas constant (8.314 J/Kmol), T is the absolute temperature (K), N_a is the Avogadro number (6.022×10^{-23} /mol), q_e is the elementary charge (1.6×10^{-19} C), and I is the ionic strength (mol/dm^3).

According to equation 4-3, the thickness of EDL on the bentonite surface at 0.3 M NaCl concentration is approximately 0.6 nm. This value is significantly smaller than the average width of the interparticle spaces which was estimated to be 15.9 nm [23]. Consequently, the free porewater fraction become dominant in the interparticle spaces at high ionic strength. In such conditions, SO_4^{2-} ions can diffuse predominantly in the free porewater. However, it is remarkable that the E_a value of SO_4^{2-} ions in compacted bentonite at 0 and 0.3 M NaCl concentration is smaller than that value in free water, suggesting that the porewater diffusion is not predominant. This contradicts to the prediction based on the shrinkage of the EDL. Conversely, the change of predominant diffusion pathway to porewater occurs when the ionic strength of the porewater increased up to 0.5 M, which can accompany the shrinkage of the EDL. These results suggest that

other factors than the fraction of porewater may influence the diffusion mechanism of $^{35}SO_4^{2-}$ ions in compacted bentonite.

Previous study on diffusion of Cl^- ions suggested that their diffusion behavior might be affected by charge compensation mechanism with Na^+ ions [23]. Indeed, when anions or cations diffuse in one direction, other chemical species with the opposite charge should follow to preserve electroneutrality. If this is the case, the diffusion behavior of Na^+ ions, which are the most possible cations to play important role in the charge compensation mechanism, should be considered as the pair ions for $^{35}SO_4^{2-}$ ions. Interestingly, diffusion behavior of Na^+ ions was reported to have similar dependency on NaCl concentration as SO_4^{2-} ions. The diffusion of Na^+ ions was suggested to be predominantly through interlayer in the range of 0.1 to 0.3 M NaCl concentration, and changed to porewater diffusion at the NaCl concentration higher than 0.3 M [9]. Therefore, the dependency of diffusion of $^{35}SO_4^{2-}$ ions on NaCl concentration might be explained by the charge compensation process, although the evidence to support the interaction between SO_4^{2-} and Na^+ ions is limited. In spite of that, we can conclude that the free porewater is not the solely possible predominant pathway for diffusion of $^{35}SO_4^{2-}$ ions.

4.5. Conclusion

Back-to-back diffusion experiments of $^{35}SO_4^{2-}$ ions in Na- bentonite were carried out to obtain their D_a and E_a values at various dry densities and NaCl concentrations. The D_a values decrease as the dry density of bentonite increases. The E_a values in water saturated compacted bentonite at dry density of 0.8, 1.0, 1.2, 1.4, and 1.6 kg/dm^3 were 20.9, 15.1, 12.5, 17.9, and 17.1 kJ/mol, respectively. The values at dry density of 1 kg/dm^3 with 0.3 and 0.5 M NaCl concentrations were 14.0 and 20.4 kJ/mol, respectively. These experimental data suggest that porewater diffusion is predominant in water saturated compacted bentonite at dry density of 0.8 kg/dm^3 and at dry density of 1 kg/dm^3 with NaCl concentration higher than 0.5 M. However, in water saturated compacted bentonite at dry density higher than 1 kg/dm^3 and at dry density of 1 kg/dm^3 with NaCl concentration lower than 0.3 M, the smaller E_a values than that in free water cannot be explained by the porewater diffusion process. This finding suggests dominant diffusion pathways for anions in compacted bentonite can be affected by salinity, indicating the possible involvement of the EDL on montmorillonite surface.

4.6. References

[1] Japan Nuclear Cycle Development Institute. H12: Project to Establish Technical Basis for HLW Disposal in Japan, Project Overview Report. JNC TN1410 2000-001. Tokai: JNC; 2000. (JNC TN1410 2000-001).

[2] Altmann S. 'Geo'chemical research: A key building block for nuclear waste disposal safety cases. J. Contam. Hydrol. 2008;102(3–4):174–179.

[3] Chapman N, Hooper A. The disposal of radioactive wastes underground. Proc. Geol. Assoc. 2012;123(1):46–63.

[4] International Atomic Energy Agency. Disposal of radioactive waste: Specific safety requirements. Vienna: IAEA; 2011. (IAEA Safety Standards Series No. SSR-5).

[5] Pusch R. Chapter 11.4 Clays and nuclear waste management. In: Bergaya F, Theng BKG, Lagaly G, editors. Handbook of clay science. Amsterdam: Elsevier; 2006.p.703–716.

[6] Sellin P, Leupin OX. The use of clay as an engineered barrier in radioactive-waste management - A review. Clays Clay Miner. 2014;61(6):477–498.

[7] Altmann S, Tournassat C, Goutelard F, et al. Diffusion-driven transport in clayrock formations. Appl. Geochemistry. 2012;27(2):463–478.

[8] Leroy P, Revil A, Coelho D. Diffusion of ionic species in bentonite. J. Colloid Interface Sci. 2006;296(1):248–255.

[9] Kozaki T, Liu J, Sato S. Diffusion mechanism of sodium ions in compacted montmorillonite under different NaCl concentration. Phys. Chem. Earth, Parts A/B/C. 2008;33(14–16):957–961.

[10] Shackelford CD, Moore SM. Fickian diffusion of radionuclides for engineered containment barriers: Diffusion coefficients, Porosities, And complicating issues. Eng. Geol. 2013;152(1):133–147.

[11] Bradbury MH, Baeyens B. Porewater chemistry in compacted re-saturated MX-80 bentonite. J. Contam. Hydrol. 2003;61(1–4):329–338.

[12] Bergaya F, Lagaly G. Chapter 1 General introduction: Clays, clay minerals, and clay science. In: Bergaya F, Theng BKG, Lagaly G, editors. Handbook of clay science. Elsevier; 2006.p.1–18.

[13] Tournassat C, Bourg IC, Steefel CI, et al. Chapter 1 - Surface Properties of Clay Minerals. In: Tournassat C, Steefel CI, Bourg IC, et al., editors. Natural and Engineered Clay Barriers. Elsevier; 2015.p.5–31.

[14] Appelo CAJ, Wersin P. Multicomponent diffusion modeling in clay systems with application to the diffusion of tritium, iodide, and sodium in Opalinus Clay. Environ. Sci. Technol. 2007;41(14):5002–5007.

[15] Appelo CAJ, Van Loon LR, Wersin P. Multicomponent diffusion of a suite of tracers (HTO, Cl, Br, I, Na, Sr, Cs) in a single sample of Opalinus Clay. Geochim. Cosmochim. Acta. 2010;74(4):1201–1219.

[16] Van Loon LR, Mibus J. A modified version of Archie's law to estimate effective diffusion coefficients of radionuclides in argillaceous rocks and its application in safety analysis studies. Appl. Geochemistry. 2015;59:85–94.

[17] Chagneau A, Tournassat C, Steefel CI, et al. Complete restriction of $^{36}Cl^-$ diffusion by celestite precipitation in densely compacted illite. Environ. Sci. Technol. Lett. 2015;2(5):139–143.

[18] Wigger C, Van Loon LR. Importance of interlayer equivalent pores for anion diffusion in clay-rich sedimentary rocks. Environ. Sci. Technol. 2017;51(4):1998–2006.

[19] Kozaki T, Sato H, Fujishima A, et al. Effect of dry density on activation energy for diffusion of strontium in compacted sodium montmorillonite. Material Resources Symposium Proceeding Volume 465 (Symposium II – Scienfific Basis for Nuclear Waste Management XX). 1997.p.893–900.

[20] Kozaki T, Sato H, Sato S, et al. Diffusion mechanism of cesium ions in compacted montmorillonite. Eng. Geol. 1999;54:223–230.

[21] Grambow B. Mobile fission and activation products in nuclear waste disposal. J. Contam. Hydrol. 2008;102(3–4):180–186.

[22] Kozaki T, Saito N, Fujishima A, et al. Activation energy for diffusion of chloride ions in compacted sodium montmorillonite. J. Contam. Hydrol. 1998;35(1–3):67–75.

[23] Kozaki T, Inada K, Sato S, et al. Diffusion mechanism of chloride ions in sodium montmorillonite. J. Contam. Hydrol. 2001;47(2–4):159–170.

[24] Molera M, Eriksen T, Jansson M. Anion diffusion pathways in bentonite clay compacted to different dry densities. Appl. Clay Sci. 2003;23(1–4):69–76.

[25] Van Loon LR, Glaus MA, Müller W. Anion exclusion effects in compacted bentonites: Towards a better understanding of anion diffusion. Appl. Geochemistry. 2007;22(11):2536–2552.

[26] Oscarson DW, Hume HB, Sawatsky NG, et al. Diffusion of iodide in compacted bentonite. Soil Sci. Soc. Am. J. 1992;56(5):1400–1406.

[27] Yukio Tachi, Kenji Yotsuji, Yoshimi Seida MY. Diffusion of cesium and iodine in compacted sodium montmorillonite under different saline conditions. Scientific Basis for Nuclear Waste Management XXXIII. Materials Research Society Proceeding. 2009.p.542–552.

[28] Tian W, Li C, Liu X, et al. The effect of ionic strength on the diffusion of ^{125}I in Gaomiaozi bentonite. J. Radioanal. Nucl. Chem. 2013;295(2):1423–1430.

[29] Ishidera T, Miyamotoy S, Sato H. Effect of sodium nitrate on the diffusion of Cl- and I- in compacted bentonite. J. Nucl. Sci. Technol. 2008;45(7):610–616.

[30] Aldaba D, Glaus MA, Van Loon LR, et al. Diffusion of radiosulphate and radiocaesium in kaolinite clay (KGa-2): Testing the applicability of the pore water diffusion model. Appl. Geochemistry. 2017;86:84–91.

[31] Van Loon LR, Leupin OX, Cloet V. The diffusion of SO_4^{2-} in Opalinus Clay : Measurements of effective diffusion coefficients and evaluation of their importance in view of microbial mediated reactions in the near field of radioactive waste repositories. Appl. Geochemistry. 2018;95:19–24.

[32] Idemitsu K, Kozaki H, Yuhara M, et al. Diffusion behavior of selenite in purified bentonite. Prog. Nucl. Energy. 2016;92:279–285.

[33] Wigger C, Van Loon LR. Effect of the pore water composition on the diffusive anion transport in argillaceous, low permeability sedimentary rocks. J. Contam. Hydrol. 2018;213(September 2017):40–48.

[34] Wigger C, Kennell-Morrison L, Jensen M, et al. A comparative anion diffusion study on different argillaceous, low permeability sedimentary rocks with various pore waters. Appl. Geochemistry. 2018;92(September 2017):157–165.

[35] Standish T, Chen J, Jacklin R, et al. Corrosion of copper-coated steel high level nuclear waste containers under permanent disposal conditions. Electrochim. Acta. 2016;211:331–342.

[36] King F, Chen J, Qin Z, et al. Sulphide-transport control of the corrosion of copper canisters. Corros. Eng. Sci. Technol. 2017;52:210–216.

[37] Liu X, Fattahi M, Montavon G, et al. Selenide retention onto pyrite under reducing conditions. Radiochim. Acta. 2008;96(8):473–479.

[38] Bourg IC, Tournassat C. Chapter 6 - Self-Diffusion of Water and Ions in Clay Barriers. In: Tournassat C, Steefel CI, Bourg IC, et al., editors. Natural and Engineered Clay Barriers. Elsevier; 2015.p.189–226.

[39] Kozaki T, Fujishima A, Sato S, et al. Self-diffusion of sodium ions in compacted sodium montmorillonite. Nucl. Technol. 1998;121(1):63–69.

[40] Kozaki T, Sato Y, Nakajima M, et al. Effect of particle size on the diffusion behavior of some radionuclides in compacted bentonite. Nucl. Mater. 1999;270:265–272.

[41] Crank J. The mathematics of diffusion. 2nd ed. Oxford: Clarendon Press; 1975.

[42] Parsons R. Handbook of electrochemical constants. Academic Press; 1959.

5. Conclusion

For safety assessment of geological disposal, it is necessary to demonstrate the ability of compacted bentonite, which is considered to be one of the engineered barriers, in retaining/retarding migration of radionuclide for a long period of time. In this context, understanding the fate and transport of radionuclides in compacted bentonite is critical. Although extensive effort has been made to study the performance of compacted bentonite regarding its application in geological disposal, resulting in a significant progress and large experimental data, there are still many uncertainties. This study provides the insight into the porewater chemistry, as well as the mechanism of migration and reaction in a compacted bentonite system. The conclusions from this thesis are summarized as follows:

Chapter 1 reviewed the overall background for this thesis, including the background information on geological disposal of high-level radioactive waste, especially on the importance of gaining understanding on fate and transport of ions in compacted bentonite, porewater chemistry in compacted bentonite, and alternation of bentonite including precipitation of $CaCO_3$. The main objectives of this thesis were provided in this chapter.

Chapter 2 presented the estimation of the activity coefficients of dissolved ions in the porewater of compacted bentonite based on the experimental results of $CaCO_3$ precipitation in compacted bentonite using an electromigration method. Solutions containing 1 M $CaCl_2$ and 0.7M $NaHCO_3$ were introduced under electrical potential gradient from the opposite sides of the compacted Na-bentonite packed at the dry density of 1.0 kg/dm^3 and saturated with 0.7 M $NaHCO_3$. After the electromigration, the spatial distribution of chemical species along the compacted bentonite sample was determined.

A sequential extraction method was developed to determine the concentrations of different chemical species involved in $CaCO_3$ precipitation in compacted bentonite. The XRD analysis of $CaCO_3$ precipitates showed no peaks suggesting a possibility of the precipitate in amorphous phase. The mean activity coefficients were calculated from the concentrations of free Ca^{2+} and HCO_3^-/CO_3^{2-} ions at the zone where the precipitation reaction was occurring. The resulting values were compared to the theoretical approximation calculated using PHREEQC code assuming dilute-solution conditions with no electrostatic interactions between ions and bentonite surface. The activity coefficients of dissolved ions in compacted bentonite were determined to be smaller than the theoretical approximation in bulk water by at least a factor of three. The smaller activity coefficient suggests a higher solubility, thus a higher mobility of radionuclides in compacted bentonite.

Chapter 3 presented the migration behavior of Ca^{2+} and HCO_3^-/CO_3^{2-} ions in compacted Na-bentonite packed at the dry density of 1.0 kg/dm^3 under electrical potential gradient. Two kinds of electromigration experiments were carried out in this study. The first was the electromigration using thin layer source to obtain electromigration parameters of Ca^{2+} and HCO_3^-/CO_3^{2-} ions. The second was the same a in Chapter 2 but with the variation of electromigration time. The results showed that under the experimental conditions, the mobility of Ca^{2+} ions was approximately an order of magnitude faster compared to that of HCO_3^-/CO_3^{2-} ions. The reaction front of $CaCO_3$ precipitation under the experimental conditions was found to move from the anode side towards the cathode side. The velocity of this reaction front was obtained to be constant during the experiments, unaffected by the formation of $CaCO_3$. The results suggest that major migration pathways of cations in compacted bentonite may be the interlayers,

whereas the precipitates are formed in inter-particle pores, thus the migration of cationic radionuclides may be unaffected by precipitate formation.

Chapter 4 presented the mechanisms of anions diffusion from the diffusion experiments of $^{35}SO_4^{2-}$ ions in Na-bentonite at various dry densities, diffusion temperatures, and NaCl concentrations. Back-to-back diffusion experiments were conducted to obtain the D_a values. The E_a values were calculated from the experimental D_a values as a function of temperature using Arrhenius equation. The E_a value of SO_4^{2-} ions in water saturated compacted bentonite at dry density of 0.8 kg/dm^3 was close to that in free water, suggesting that the porewater diffusion is predominant. This E_a value decreased to become lower than that in free water when the dry densities of compacted bentonite were higher than 1.0 kg/dm^3, showing that the porewater diffusion process may not be able to explain the dominant diffusion process. The E_a value increased to be equal to that in free water when salinity was increased up to 0.5 M at the dry density of 1.0 kg/dm^3, suggesting the increased pore space produced by the higher salinity may have made the pore diffusion dominant again. This finding suggests porewater diffusion may not be the dominant pathway for anions at high dry densities. It also suggests that dominant diffusion pathways for anions in compacted bentonite can be affected by salinity, indicating the possible involvement of the EDL on montmorillonite surface.

This thesis focused on the compacted bentonite system, which will be used as an engineered barrier in geological disposal. Major findings include estimation of activity coefficient, dominant migration pathways of cations and anions, and effects of precipitate formation on ion migration in the compacted bentonite system. These findings are expected to contribute to improvements of accuracy and confidence in safety assessment of geological disposal by enhancing the scientific understanding of the system.

Acknowledgement

I would like to express my sincere gratitude to my supervisor, Prof. Tamotsu Kozaki for his countless support and guidance throughout my study. My gratitude also goes to Associate Prof. Naoko Watanabe for her kind help and discussion, not only in study and research but also in daily life. My grateful thanks also to Assistant Prof. Shingo Tanaka for sharing his knowledge and helping in the experiment.

I would also like to thank to Prof. Michitsugu Mori, Prof. Takashi Kamiyama, and Associate Prof. Ryoko Fujiyoshi for their valuable comments that improved the contents of this thesis. My appreciation goes to all members in Laboratory of Nuclear and Environmental Materials: laboratory secretary Keiyaki-san, Carlos, Mizukami, Kitazawa, Kubota, Takenaka, Hiroaki, Sato, Kimoto, Akiyama, Ishii, Senga, and others who have graduated that I cannot mentioned here for their help and the pleasant atmosphere at the laboratory. The help from E^3 Program for the administration of my study is also greatly appreciated.

The experiment with radiotracer was performed at the Central Institute of Isotope Science, Hokkaido University. The SEM/EDS analysis was conducted at the High Voltage Electron Microscope Laboratory, Center for Advanced Research of Energy and Materials, Hokkaido University. Powder X-ray diffraction experiment was carried out in Material Analysis and Material Analysis and Structure Analysis Open Unit (MASAOU), Hokkaido University.

My grateful acknowledgement goes to Radioactive Waste Technology Center, National Nuclear Energy Agency of Indonesia (PTLR-BATAN), my direct supervisor Pak Yayak, and Head of the Center Pak Husen. The administration for my temporary leave for study is supported by Pusdiklat-BATAN. Financial support for my study is

provided by Ministry of Research, Technology and Higher Education of Indonesia (Kemenristekdikti) through RISET-Pro program.

I am grateful to my children Zikri and Harumi, and their mother Reni for their support and understanding. Finally, to my parents, there are no words to sufficiently express my gratitude.